

R89-927162-1

AD-A206 713

INVESTIGATION OF PLASMA PROCESSES IN ELECTRONIC TRANSITION LASERS

Final Report
February 28, 1989

Sponsored by The Office of Naval Research
Contract: N00014-85-C-0259

APPROVED FOR PUBLIC RELEASE
DISTRIBUTION UNLIMITED

S DTIC
ELECTE **D**
14 MAR 1989
CE



89 0 14 047

R89-927162-1

Investigation Of Plasma Processes In Electronic
Transition Lasers

Final Report
February 28, 1989

Sponsored by The Office of Naval Research
Contract: N00014-85-C-0259

Approved For Public Release
Distribution Unlimited

Unclassified

SECURITY CLASSIFICATION OF THIS PAGE

REPORT DOCUMENTATION PAGE				Form Approved OMB No. 0704-0188	
1a. REPORT SECURITY CLASSIFICATION Unclassified			1b. RESTRICTIVE MARKINGS		
2a. SECURITY CLASSIFICATION AUTHORITY		3. DISTRIBUTION AVAILABILITY OF REPORT Approved for public release; distribution unlimited.			
2b. DECLASSIFICATION/DOWNGRADING SCHEDULE					
4. PERFORMING ORGANIZATION REPORT NUMBER(S) R89-927162-1			5. MONITORING ORGANIZATION REPORT NUMBER(S)		
6a. NAME OF PERFORMING ORGANIZATION United Technologies Research Center		6b. OFFICE SYMBOL (if applicable)	7a. NAME OF MONITORING ORGANIZATION Office of Naval Research		
6c. ADDRESS (City, State, and ZIP Code) Silver Lane East Hartford, CT 06108			7b. ADDRESS (City, State, and ZIP Code) Physics Program Office (Code 1112LO) 800 N. Quincy St., Arlington, VA 22217-5000		
8a. NAME OF FUNDING/SPONSORING ORGANIZATION		8b. OFFICE SYMBOL (if applicable)	9. PROCUREMENT INSTRUMENT IDENTIFICATION NUMBER N00014-85-C-0259		
8c. ADDRESS (City, State, and ZIP Code)			10. SOURCE OF FUNDING NUMBERS		
		PROGRAM ELEMENT NO. 61153N	PROJECT NO. RR011-07	TASK NO. RR011-07-01	WORK UNIT ACCESSION NO. NR395-026
11. TITLE (Include Security Classification) Investigation of Plasma Processes in Electronic Transition Lasers (U)					
12. PERSONAL AUTHOR(S) William L. Nighan					
13a. TYPE OF REPORT Final Report		13b. TIME COVERED FROM 1/1/85 to 12/31/88	14. DATE OF REPORT (Year, Month, Day) 89/2/28		15. PAGE COUNT 99
16. SUPPLEMENTARY NOTATION					
17. COSATI CODES			18. SUBJECT TERMS (Continue on reverse if necessary and identify by block number)		
FIELD	GROUP	SUB-GROUP	XeF(C→A) laser; e-beam excited XeF(C→A) laser, rare gas-halide lasers; blue-green lasers; visible lasers; transient absorption in the visible region; rare gas-halide mixture synthesis, tunable blue-green laser.		
19. ABSTRACT (Continue on reverse if necessary and identify by block number)					
United Technologies Research Center has conducted an investigation of the fundamental processes affecting the operation, performance and application of electrically excited lasers having potential utility in a variety of areas of importance to the Navy. Particular attention was focused on the broadband XeF(C→A) laser, which has the potential for efficient, tunable operation throughout the blue-green spectral region. The research at UTRC has been coordinated with a complementary ONR-supported experimental program conducted at Rice University. This Final Report summarizes the results of this investigation, and includes reprints of published papers in which specific results and conclusions of the research are described in detail.					
20. DISTRIBUTION/AVAILABILITY OF ABSTRACT <input type="checkbox"/> UNCLASSIFIED/UNLIMITED <input checked="" type="checkbox"/> SAME AS RPT. <input type="checkbox"/> DTIC USERS			21. ABSTRACT SECURITY CLASSIFICATION Unclassified		
22a. NAME OF RESPONSIBLE INDIVIDUAL H. S. Pilloff		22b. TELEPHONE (Include Area Code) 202-696-4223		22c. OFFICE SYMBOL code 1112	

Investigation of Plasma Processes in Electronic Transition Lasers

TABLE OF CONTENTS

	<u>Page</u>
FOREWORD	i
I. HISTORICAL OVERVIEW	1-1
II. REPRINTS OF PUBLISHED PAPERS	II-1
• Kinetic Processes in Electron-Beam Excited XeF(C→A) Laser Media	II-2
• Kinetically Tailored Properties of Electron-Beam Excited XeF(C→A) and XeF(B→X) Laser Media Using an Ar-Kr Buffer	II-56
• Performance Characteristics of an Injection Controlled Electron Beam Pumped XeF(C→A) Laser System	II-64
• Injection Controlled Tuning of an Electron Beam Excited XeF(C→A) Laser	II-72
• Efficient Narrow Spectral Output in the Blue-Green Region from an Injection Controlled Electron Beam Excited XeF(C→A) Laser	II-78
• Simultaneous Multiwavelength Operation of a Commercial Rare Gas Halide Laser	II-82
• Simultaneous UV/Visible Laser Oscillation on the B→X and C→A XeF Excimer Transitions	II-86
III. LIST OF PATENTS	III-1

DISTRIBUTION LIST

Accession For	
NTIS GRA&I	<input checked="" type="checkbox"/>
DTIC TAB	<input type="checkbox"/>
Unannounced	<input type="checkbox"/>
Justification	
By _____	
Distribution/	
Availability Codes	
Dist	Avail and/or Special
A-1	



FOREWORD

United Technologies Research Center has conducted an investigation of the fundamental processes affecting the operation, performance and application of electrically excited lasers having potential utility in a variety of areas of importance to the Navy. Particular attention in this investigation was focused on the broadband XeF(C→A) laser, which has the potential for efficient, tunable operation throughout the blue-green spectral region. The research at UTRC has been closely coordinated with a complementary ONR-supported experimental program being conducted at Rice University.

This Final Report covers the period 1 January 85 through 31 December 88, and contains reprints of published papers in which specific results and conclusions of the research are described in detail.

I. HISTORICAL OVERVIEW

Rice University - United Technologies Research Center XeF(C-A) Laser Research -- Brief Summary

The XeF excimer laser operating on the C-A transition in the blue-green spectral region is a cousin of the well known UV rare gas halide lasers such as KrF(248 nm), XeCl(308 nm) and XeF(351 nm). In addition to the fact that the wavelength of the XeF(C-A) laser is in the visible region, this laser is continuously tunable throughout the blue-green region, a unique feature having importance for many applications.

Although laser oscillation on the C-A transition was demonstrated in the late 1970s shortly after the UV rare gas halide lasers were discovered, the operating efficiency of the XeF(C-A) laser was much too low for practical applications. This problem was the result of very low gain due to the combination of a stimulated emission cross section more than an order-of-magnitude smaller than that of the UV rare gas halide lasers, and a high level of transient absorption. Many thought that these characteristics represented fundamental limitations to successful exploitation of the special properties of the XeF(C-A) laser.

In the early 1980s Rice University and United Technologies Research Center joined forces in an effort to improve the performance of the 'C-A' laser. With support from the Office of Naval Research, this university-industry team identified the primary transient species in the laser gas mixture that were absorbing radiation at the laser wavelength. Based on the insight gained from this work, the team devised and patented special gas mixtures containing up to five constituents. Use of these mixtures significantly reduced the transient absorption resulting in a large increase in the net gain on the XeF(C-A) laser transition.

The laser performance improvement resulting from the higher gain was found to be dramatic. With excitation provided by a high current density electron beam having a temporal duration of 10 ns, XeF(C-A) laser energy density and intrinsic efficiency in excess of 1 Joule/liter and 1 % were demonstrated, values that for the first time were comparable to those typical of UV rare gas halide lasers (1). Subsequently, efficient injection controlled tuning was demonstrated, resulting in laser wavelengths with a spectral width less than 1 nm tuned over a 30 nm range centered at 485 nm (2).

Recently the Rice - United Technologies team set out to show that the impressive XeF(C-A) laser performance that had been obtained in a relatively small experiment could be scaled to a practically significant size. With the help of Maxwell Laboratories, a scaled electron beam system was designed and constructed permitting an optical path length of 50 cm and an active volume of one half liter. With the scaled laser configured as an injection controlled regenerative amplifier, laser pulse energy and power of 0.6 Joules and 60 MW were obtained. The laser wavelength was 486.8 nm with a spectral width of 0.01 nm. The pulse energy demonstrated in the first tests of the scaled XeF(C-A) laser corresponds to an energy density and efficiency values in excess of 1 Joule/liter and 1 %, respect-

ively, thereby confirming the promise of early small scale experiments. In addition, repetitive pulse operation at a PRF value of 1 Hz was demonstrated.

Additional experiments are now underway in order to fully characterize the behavior of the scaled laser system. However, the initial Rice - United Technologies tests show that the XeF(C-A) laser has impressive potential for development as an efficient, tunable blue-green laser source for applications requiring high energy and power.

-
1. 'Synthesis of rare gas halide mixtures resulting in efficient XeF(C-A) laser oscillation', W.L.Nighan, F.K.Tittel, W.L.Wilson, Jr., N.Y.Zhu, and R.Sauerbrey, Applied Physics Letters, vol. 45, pp. 947-949, 1984.
 2. 'Performance characteristics of an injection controlled electron beam pumped XeF(C-A) laser system', N.Hamada, R.Sauerbray, W.L.Wilson, Jr., F.K.Tittel and W.L.Nighan, IEEE Journal of Quantum Electronics, vol. 24, pp. 1571-1578, 1988.

II. PREPRINTS OF PUBLISHED PAPERS

- Kinetic Processes in Electron-Beam Excited XeF(C→A) Laser Media, W. L. Nighan and M. C. Fowler, *IEEE Journal of Quantum Electronics*, April 1989.
- Kinetically Tailored Properties of Electron-Beam Excited XeF(C→A) and XeF(B→X) Laser Media Using an Ar-Kr Buffer, W. L. Nighan, R. A. Sauerbrey, Y. Zhu, F. K. Tittel and W. L. Wilson, Jr. *IEEE Journal of Quantum Electronics*, Vol. QE-23, pp. 253-260, February 1987.
- Performance Characteristics of an Injection Controlled Electron Beam Pumped XeF(C→A) Laser System, N. Hamada, R. A. Sauerbrey, W. L. Wilson, Jr., F. K. Tittel and W. L. Nighan, *IEEE Journal of Quantum Electronics*, Vol. 24, pp. 1571-1578, August 1988.
- Injection Controlled Tuning of an Electron Beam Excited XeF(C→A) Laser, F. K. Tittel, G. Marowsky, W. L. Nighan, Y. Zhu, R. A. Sauerbrey and W. L. Wilson, Jr., *IEEE Journal of Quantum Electronics*, Vol. QE-22, pp. 2168-2173, November 1986.
- Efficient Narrow Spectral Output in the Blue-Green Region from an Injection Controlled Electron Beam Excited XeF(C→A) Laser, G. Merowsky, N. Nishida, H. Stiegler, F. K. Tittel, W. L. Wilson, Jr., Y. Zhu and W. L. Nighan, *Applied Physics Letters*, Vol. 47, pp. 657-660, October 1985.
- Simultaneous Multiwavelength Operation of a Commercial Rare Gas Halide Laser, R. A. Sauerbrey, W. L. Nighan, F. K. Tittel, W. L. Wilson, Jr., and J. Kinross-Wright, *IEEE Journal of Quantum Electronics*, Vol. QE-22, pp. 230-233, February 1986.
- Simultaneous UV/Visible Laser Oscillation on the B→X and C→A XeF Excimer Transitions, R. A. Sauerbrey, Y. Zhu, F. K. Tittel, W. L. Wilson, Jr., N. Nishida, F. Emmert and W. L. Nighan, *IEEE Journal of Quantum Electronics*, Vol. QE-21, pp. 418-420, May 1985.

Kinetic Processes in Electron-Beam-Excited XeF(C→A) Laser Media*

by

William L. Nighan and Michael C. Fowler

ABSTRACT

Fundamental processes affecting the operation and performance of electron-beam excited XeF(C→A) laser media have been analyzed and modeled. Emphasis has been placed on conditions typical of high current density ($\sim 250 \text{ A cm}^{-2}$), short pulse ($\sim 10 \text{ ns FWHM}$) e-beam excitation of high pressure ($\sim 6 \text{ atm}$) multi-component mixtures comprised of Ar-Kr-Xe-NF₃-F₂. Computation of the temporal evolution of excited and ionized species for such circumstances has permitted identification of the factors controlling XeF(C) formation and loss, and has resulted in the identification of the primary transient species that absorb radiation in the blue-green spectral region. The data so obtained serve to explain measured XeF(C→A) properties, particularly net gain, under conditions for which the C→A laser energy density and efficiency values are comparable to those of the UV XeF(B→X) laser.

*This work was supported by the Office of Naval Research.

I. INTRODUCTION

Over the past few years the performance of the electron-beam excited XeF(C→A) laser has improved significantly. The broadband C→A transition of XeF is centered at 480 nm in the blue-green region and, in marked contrast with the UV B→X transition, has a spectral width of nearly 100 nm. Thus, the XeF(C→A) laser has great potential as an optical source tunable over a broad bandwidth. Recently, extracted energy density and intrinsic efficiency values of 1-2 J/liter and 1-2%, respectively, have been demonstrated [1],[2], representing a level of performance approaching that typical of UV XeF(B→X) lasers [3],[4]. The improved XeF(C→A) laser performance results from the use of a high pressure (~6 atm) multi-component gas mixture comprised of Ar-Kr-Xe-NF₃-F₂, [2], excited by a high current density (~250 Acm⁻²) electron-beam of short temporal duration (~10 ns FWHM). For these conditions the (C→A) gain has a maximum value of approximately 3% cm⁻¹ and a duration of about 35 ns (FWHM) [1],[2], properties permitting efficient energy extraction using either a free running oscillator [1], or an injection controlled amplifier [2].

The multi-component mixtures resulting in the best XeF(C→A) laser performance represent a particularly complex kinetics problem for a number of reasons. (1) Use of a high pressure, two-component buffer comprised of heavy rare gas species (Ar+Kr) introduces numerous reactions not usually important for rare gas halide B→X lasers, a circumstance exacerbated by weaknesses in the data base of fundamental reaction rate coefficients. (2) Because the stimulated emission cross section for the XeF C→A transition is ~30 times smaller than that of the B→X transition, transient absorption is of exceptional importance. Thus, identification and quantitative modelling of absorbing excited and ionized species is an even more compelling requirement

than is the case for the B→X rare gas halide lasers. Additionally, consideration of XeF B and C state collisional transfer, and quantitative calculation of both state population densities is necessary.

In a prior work [5] a comprehensive spectroscopic investigation of XeF(C→A) laser mixtures was carried out, focusing particularly on the role of Kr. As part of that activity, a qualitative analysis of the effect of Kr on transient absorption and on XeF formation and loss was conducted. This paper reports the results of an analysis of XeF(C→A) laser medium properties in which the kinetics of the (Ar+Kr)-Xe-(NF₃+F₂) mixture are modelled in detail. The pertinent features of the kinetics model are discussed in Section II, in which particular attention is focused on those aspects of the problem found to be of particular importance: 1) Ar₂⁺ ↔ Ar₃⁺ quasi-equilibrium reactions, 2) halogen-rare gas excited state reactions and products, 3) neutral reactions affecting the populations of high energy rare gas excited states, and 4) transient absorption in the blue-green spectral region. The properties of an XeF(C→A) gain medium excited by a high current density electron-beam of short duration are presented in Section III, where a comparison is made with experimental results. Therein, factors controlling net gain on the C→A transition are emphasized, and the effects of Kr and the processes dominating XeF formation and loss are discussed. Additionally, Section III presents a brief discussion of XeF(C→A) gain medium properties when the excitation is provided by a low current density electron-beam pulse having a temporal duration on the order of 1 μsec.

II. KINETICS

Over the past ten years kinetic processes controlling the rare gas halide population in laser media have been the subject of considerable attention.

Consequently, relatively complete rate coefficient data are available for most processes of importance to the present investigation, including:

- i. XeF(B,C) formation processes such as positive ion-negative ion recombination [6],[7],[8] and halogen reactive quenching of rare gas metastable states [9],[10];
- ii. mixing and quenching of low vibrational levels of the XeF B and C states [11],[12];
- iii. two-body [13],[14] and three-body [15],[16] [17] rare gas molecular ion charge exchange and rearrangement [18];
- iv. excited state processes in rare gases and their mixtures [19],[20],[21];
- v. electron-halogen dissociative attachment [22]; and dissociative electron-ion recombination [23],[24],[25].

The body of data for these and related processes continues to grow, albeit slowly, in response to the importance of rare gas-halide lasers and other similar applications. In the present investigation, data from such sources [6]-[25] have been used in a self-consistent model of XeF(B,C) processes for the experimental conditions described in our previous work [2],[5].

Analytical and numerical procedures of the type utilized are well developed [26],[27],[28], [29]. Thus, the discussion to follow will concentrate only on those aspects of the kinetics and modelling having special significance in the present context, with little emphasis on general methods and procedures, and/or on processes that are well understood for which data are readily available in the literature.

A. Ionized and Excited Species

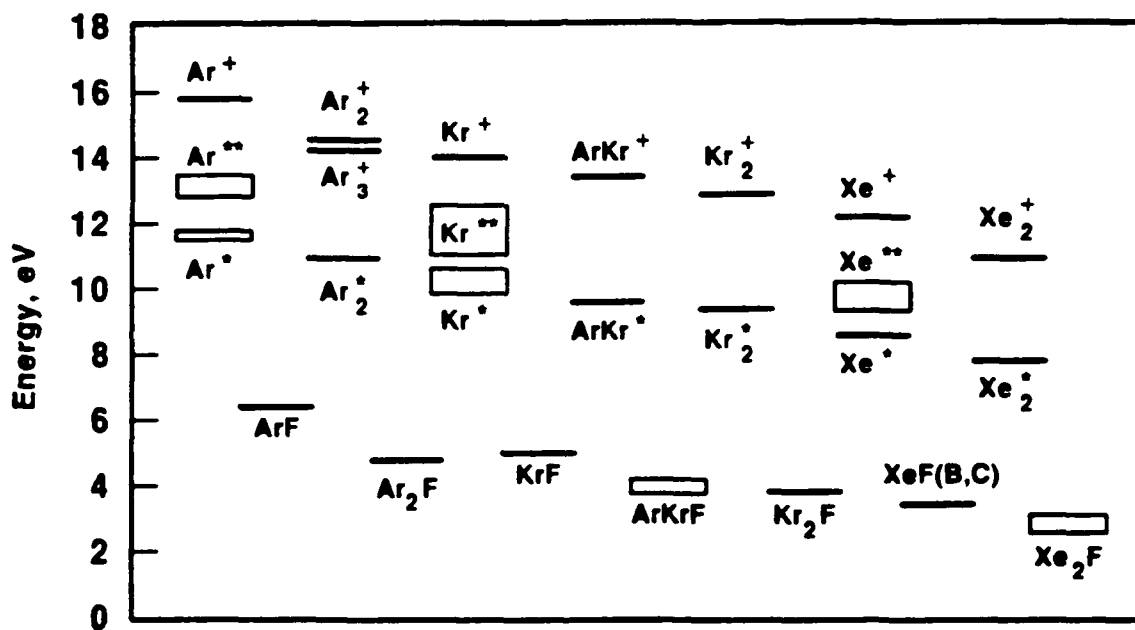
Presented in Fig. 1 are the energy-ordered positive ions and excited species that, on the basis of our prior investigations, we conclude are important to the problem at hand. The indicated species, along with electrons, F^- , and the neutral halogens, comprise the present model. We compute the temporal evolution of the concentrations of the indicated species in response to high current density ($\sim 250 \text{ Acm}^{-2}$) e-beam excitation ($\sim 10 \text{ ns FWHM}$) of a gas mixture typically comprised of Ar(6.1 atm) -Kr(300 Torr) -Xe(8 Torr) - NF_3 (8 Torr) - F_2 (1 Torr). These mixture conditions have been found to be optimum for the XeF(C+A) laser e-beam excitation scheme utilized, and result in an energy deposition of 100-150 J/liter in the optically active region [2].

The rare gas excited states are represented as two groups of coupled levels (Fig. 1); RG^* referring to the lowest energy s states (e.g., Ar($4\underline{s}, 4\underline{s}'$)), and RG^{**} referring to all higher energy states, but primarily the p states (e.g., Ar($4\underline{p}$)). The "boxes" in Fig. 1 indicate the approximate energy spread of the four low lying s states and several of the lowest energy p states. Specific details of rare gas excited state reactions are discussed in a section to follow.

B. Positive Ion Kinetics

1) $\text{Ar}_2^+ \rightleftharpoons \text{Ar}_3^+$ Quasi-equilibrium: Electron-beam excitation of laser mixtures using several atmospheres of argon as the buffer result in the production of Ar^+ which is converted to Ar_2^+ on a sub-nanosecond time scale, the latter usually thought to be the only argon molecular ion of consequence. However, for pressures $> 1 \text{ atm}$ formation of the weakly bound ($D_e \sim 0.2 \text{ eV}$)

FIG. 1



DAJ0377E.910

Ionized and excited species which, along with electrons, F⁻, and the neutral halogens, are considered in the XeF(C→A) laser model.

trimer ion Ar_3^+ [30] becomes appreciable, and its effect can be significant as regards photo absorption in $\text{XeF}(\text{C}\rightarrow\text{A})$ laser media [31]. In this work we have used the $\text{Ar}_2^+ \rightleftharpoons \text{Ar}_3^+$ forward and reverse rate coefficients reported by Turner and Conway [32]. Those data indicate that for a pressure of only one atmosphere at equilibrium, approximately 20% of the Ar_2^+ ions are converted to Ar_3^+ . Here we are interested in pressures of ~ 6 atm.

Based on the work of MacDonald, Biondi and Johnsen [33] showing that the rate coefficient for electron recombination with Ne_3^+ is five times larger than that of Ne_2^+ , we have assumed that the electron recombination coefficients for Ar_2^+ [23] and Ar_3^+ are in the same ratio. As regards the more important charge transfer and positive ion-negative ion recombination reactions, there are no data available for Ar_3^+ . For that reason we have assumed that the rate coefficients for Ar_3^+ are the same as those for Ar_2^+ .

2) Charge Exchange: The two-body charge exchange reactions $\text{Ar}_2^+ + \text{Kr} \rightarrow \text{Kr}^+ + 2\text{Ar}$, and $\text{Ar}_2^+ + \text{Xe} \rightarrow \text{Xe}^+ + 2\text{Ar}$ are very important for the $\text{XeF}(\text{C}\rightarrow\text{A})$ mixtures under consideration. The rate coefficients for these reactions are large ($\sim 5 \times 10^{-10} \text{ s}^{-1} \text{ cm}^3$), [13],[14]. In addition, rate coefficients for the termolecular reactions $\text{Ar}_2^+ + \text{Kr} + \text{M} \rightarrow \text{products}$, and $\text{Ar}_2^+ + \text{Xe} + \text{M} \rightarrow \text{products}$ have been found to be $\geq 10^{-30} \text{ s}^{-1} \text{ cm}^6$ [15]. Thus, for pressures typical of rare gas halide lasers, the effective two-body rate coefficients for the indicated three body reactions are comparable to those of the corresponding two-body charge exchange reactions. The effect of such termolecular reactions is not usually considered in rare gas halide laser modelling.

Unfortunately, the products of the indicated termolecular reactions have not been identified. In the present work we have assumed that the products of the two and three-body molecular ion reactions are the same, and that the corresponding rate coefficients for Kr molecular ions, for which there are little or no data, are the same as the corresponding Ar molecular ion reactions.

The dominant processes affecting $\text{Ar}_2^+ \rightleftharpoons \text{Ar}_3^+$ quasi-equilibrium and related Ar molecular ion reactions are summarized in Table I along with the corresponding rate coefficients used in our model.

C. Halogen Kinetics

1) Dissociative Attachment: It has been shown that use of an optimized combination of NF_3 and F_2 results in $\text{XeF}(\text{C}\rightarrow\text{A})$ laser performance that is better than that obtained using either F_2 or NF_3 individually [1],[5],[34]. Since the rate coefficients for electron dissociative attachment of NF_3 and F_2 differ significantly, each exhibiting a strong dependence on electron energy [22], combination of these two chemically compatible fluorine donors permits optimization of the attachment process (F^- production) over a broad range of electron energy, and also provides an added degree of control over the electron density.

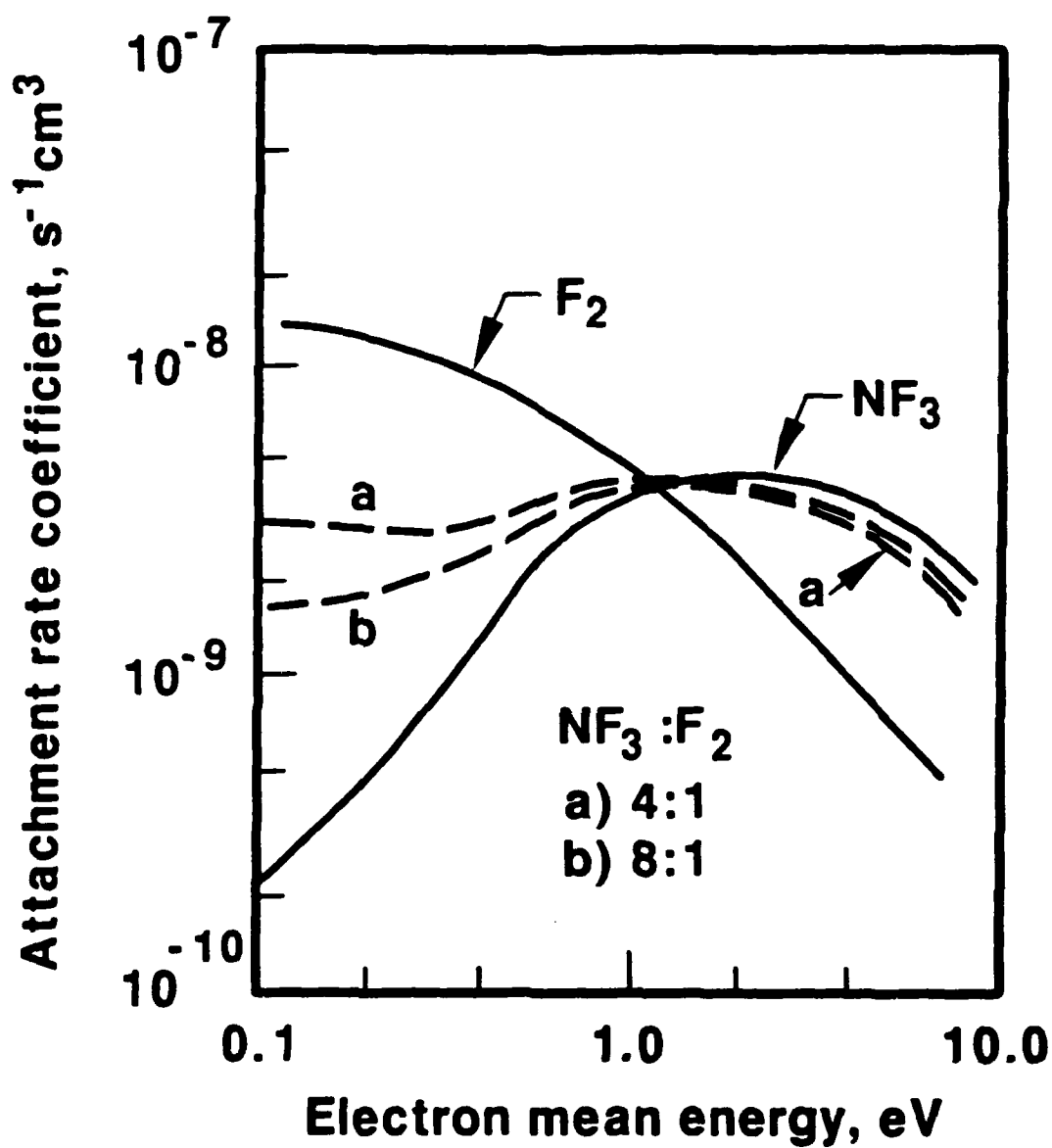
Presented in Fig. 2 are the electron rate coefficients for dissociative attachment of NF_3 and F_2 ; F^- is the negative ion product in both cases [22]. Also, shown for comparison is the effective rate coefficient for mixtures of NF_3 and F_2 combined in the ratios 8:1 and 4:1. During the e-beam excitation pulse (10 ns for the conditions of present interest) the secondary electron energy is a few eV, relaxing rapidly toward the translational temperature of the neutrals upon termination of the e-beam [35], [36]. The data of Fig. 2

TABLE I
Argon Molecular Ion Processes

Reaction ^a	Rate Coefficient ^b	Reference
1. $\text{Ar}_2^+ + 2\text{Ar} \rightleftharpoons \text{Ar}_3^+ + \text{Ar}$	7.0(-32), 9.0(-12)	32
2. $\text{Ar}_2^+ + e \rightarrow \text{Ar}^{**} + \text{Ar}$	6.5(-8)	23
3. $\text{Ar}_3^+ + e \rightarrow \text{Ar}^{**} + 2\text{Ar}$	3.25(-7)	see text
4. $\text{Ar}_2^+ + \text{F}^- \rightarrow \text{ArF} + \text{Ar}$	1.5(-6)	7,8
5. $\text{Ar}_2^+ + \text{Kr} \rightarrow \text{Kr}^+ + 2\text{Ar}$	7.5(-10)	13
6. $\text{Ar}_2^+ + \text{Kr} + \text{Ar} \rightarrow \text{Kr}^+ + 3\text{Ar}$	1.7(-30)	15
7. $\text{Ar}_2^+ + \text{Xe} \rightarrow \text{Xe}^+ + 2\text{Ar}$	7.5(-10)	14,15
8. $\text{Ar}_2^+ + \text{Xe} + \text{Ar} \rightarrow \text{Xe}^+ + 2\text{Ar}$	5.0(-30)	15

- a. For the Ar_3^+ reactions corresponding to 4→8 the indicated Ar_2^+ rate coefficients were used.
- b. The units for two-body and three-body rate coefficients are $\text{s}^{-1} \text{cm}^3$ and $\text{s}^{-1} \text{cm}^6$, respectively.

FIG. 2



Rate coefficients for electron dissociative attachment of NF_3 and F_2 adapted from the work of Chantry [22]. Also shown are the effective rate coefficients for NF_3 and F_2 mixtures having the indicated $\text{NF}_3 : \text{F}_2$ proportions.

show that for certain $\text{NF}_3\text{-F}_2$ combinations the effective attachment coefficient for the mixture is large ($>10^{-9} \text{ s}^{-1} \text{ cm}^3$) over the entire energy range of the secondary (i.e., low energy) electrons produced by the electron beam. Therefore, since dissociative attachment results in production of F^- and loss of electrons, the production of F^- , a primary XeF precursor, and the loss of electrons, which quench XeF , will both be large and essentially independent of electron energy throughout the temporal duration of the e-beam excitation pulse (~ 10 nsec FWHM) and the much longer afterglow ($\sim 50\text{-}100$ nsec), [2],[5],[31].

2) Reactive Quenching: The reactive quenching of rare gas excited states by NF_3 and F_2 and the branching to XeF are of particular importance. The rate coefficients and branching fractions for the rare gas metastable levels have been measured for practically all useful rare gas halide halogen donors [10]. The data obtained for the metastable levels are usually used in the modelling of higher energy rare gas excited states. However, the measurements of Ku and Setser [37] show that the halogen quenching rate coefficients for the $\text{Xe}(6p)$ states are significantly larger than for the $\text{Xe}(6s)$ metastable state, and that the differences between the individual levels of the $\text{Xe}(6p)$ manifold are also large. Table II shows an adaptation of the NF_3 and F_2 data of Ku and Setser, for which we have averaged their measurements of the individual $\text{Xe}(6p)$ levels. The average rate constant for $\text{Xe}(6p)$ quenching by NF_3 is about an order-of-magnitude larger than that for $\text{Xe}(6s)$. Even the rate constant for F_2 as the reagent is increased by nearly 30%.

In our modeling we have used the data of Table II and have assumed that the NF_3 and F_2 quenching rate constants of the higher excited states of argon and krypton (Ar^{**} and Kr^{**} in Figs. 1 and 3) are larger than those of the metastable levels of those species by the same factors indicated by the Xe data of Table II.

TABLE II

Total Quenching Rate Constants and XeF Branching Fractions

	Xe ^{*a}		Xe ^{**a}	
	k_Q^b	Γ_{XeF}	k_Q^b	Γ_{XeF}
NF ₃	0.9(-10)	0.27	8.9(-10)	0.35
F ₂	7.5(-10)	1.0	9.6(-10)	1.0

- a. Xe^{*} and Xe^{**} refer to the species designations shown in Figs. 1 and 3 and described in Sec. II-D.
- b. The rate constants (units of s⁻¹ cm³) and branching fractions indicated for Xe^{*} refer to values measured for the Xe(6s[3/2]₂) metastable state [9],[10], while those shown for Xe^{**} are averages of values measured for the Xe 6p[1/2]₀, 6p[3/2]₂ and 6p[5/2]₂ states as reported in [37]. The relative differences between the Xe^{*} and Xe^{**} rate coefficients and branching fractions for NF₃ and F₂ as the reagents were applied to the corresponding reactions involving Ar and Kr excited states.

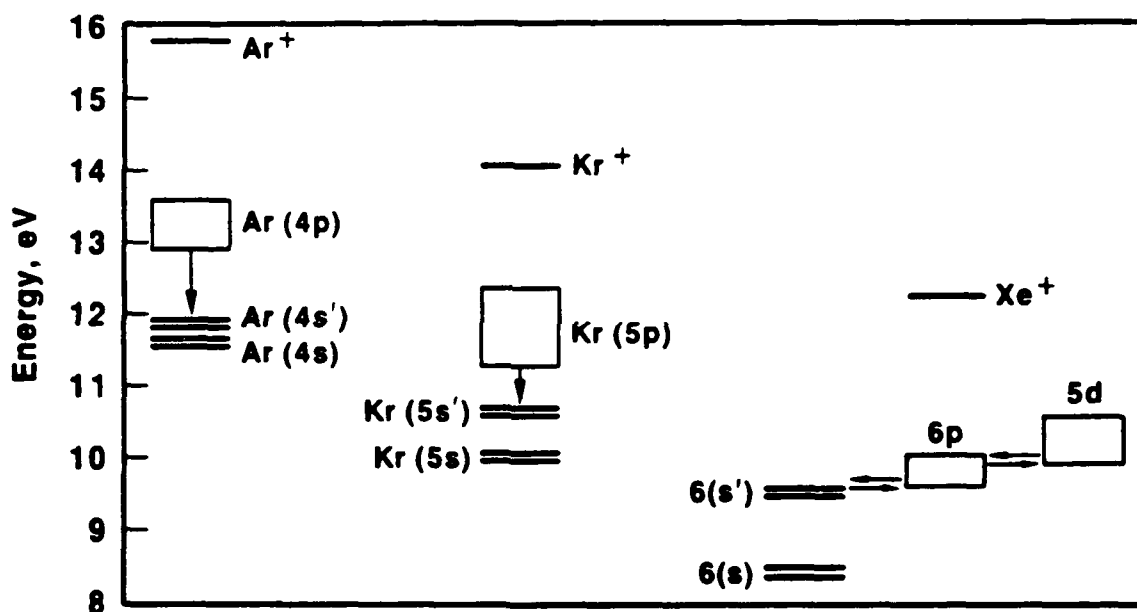
D. RG^*-RG^{**} Kinetics

In addition to their role as rare gas-halide precursors, the higher excited rare gas states exhibit broadband absorption extending throughout the UV/visible spectral region [38]. Knowledge and control of broadband transient absorption is important for B→X rare gas halide laser applications and is absolutely essential for the XeF(C→A) laser which typically will have a smaller gain.

1) Ar and Kr Excited States: Figure 3 shows in more detail those elements of Fig. 1 relevant to the present treatment of RG^*-RG^{**} kinetics. In our model we consider Ar^* to be comprised of the four Ar $4s$ and $4s'$ states, and Kr^* to be comprised of the corresponding Kr $5s$ and $5s'$ states. The species designation Ar^{**} refers to ten Ar $4p$ levels, the energy range of which is illustrated by the box in Fig. 3, and all higher energy argon excited states. For the pressures of interest (~ 6 atm), the latter can be expected to relax to the Ar p -state manifold with a sub-nanosecond time constant. The species Kr^{**} is defined in a similar way, and the statements made about Ar are also applicable.

When e-beam excitation is used the energy flow is, for the most part, downward toward the p states; and the collisional coupling between the p and s manifolds becomes an important issue, particularly as regards transient absorption by the p states [31]. While there is considerable energy overlap among the higher energy rare gas excited states, a factor facilitating relaxation, the energy gap between p and s' states is rather large, i.e., ~ 1 eV, for Ar and ~ 0.5 eV for Kr (Fig. 3). Nevertheless, Setser and co-workers have shown for Ar and Kr that $p \rightarrow s$ intermultiplet relaxation proceeds at a rapid rate by way of complex mechanisms involving curve crossings, in

FIG. 3



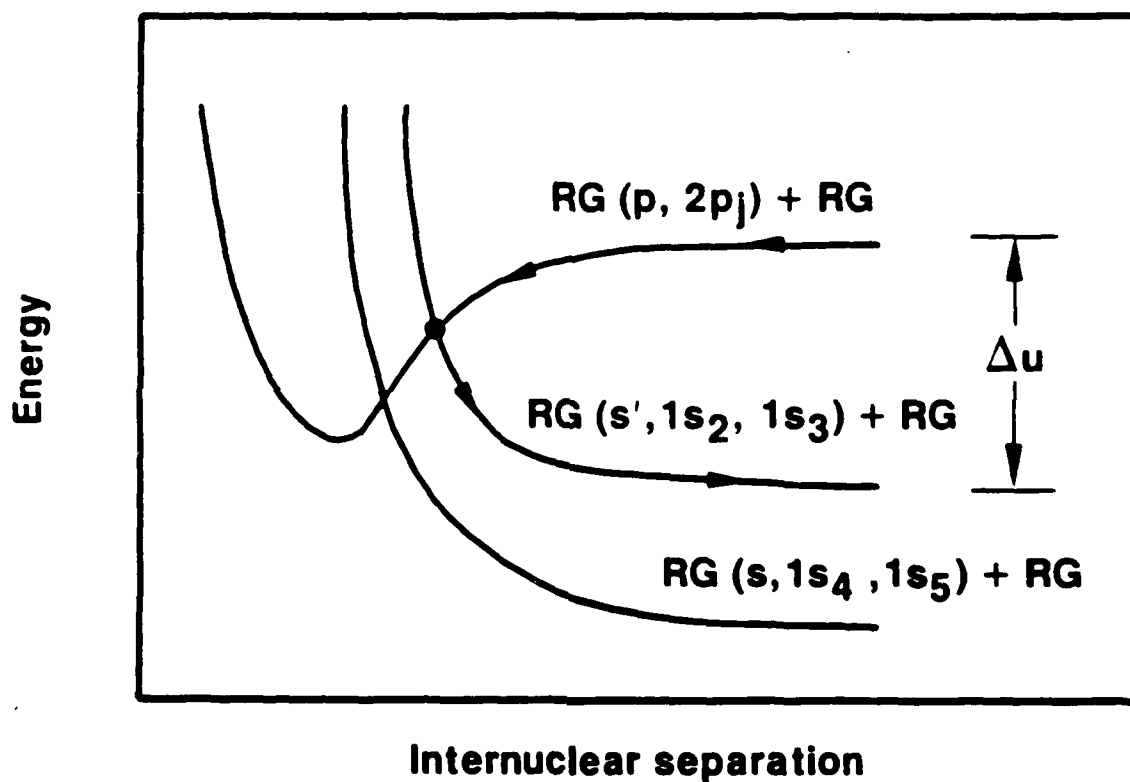
RA2627X 017

Rare gas excited states considered in the present model. In this work the designation Ar^* and Kr^* refers to the indicated s and s' states while Ar^{**} and Kr^{**} refer to the p and higher energy states. In contrast, Xe^* refers only to the Xe(6s) states, while Xe^{**} refers to the coupled 6s', 6p, and 5d (and higher energy) states as described in the text.

which attractive bound RG_2^{**} potential curves from $RG(p)$ and RG interact with the repulsive curves from $RG(s')$ and RG and $RG(s)$ and RG [39],[40].

This sequence of events is illustrated in simplified form by Fig. 4. For Ar, the average two body rate coefficient for intermultiplet relaxation between the ten p levels and s',s ($Ar^{**} \rightarrow Ar^*$, Fig. 3) is $\sim 3 \times 10^{-11} \text{sec}^{-1} \text{cm}^3$, with practically all $Ar(4p)$ levels participating [39]. Relaxation of the $Kr(5p)$ manifold in Ar proceeds in the same general way, except that quenching of only a few low energy levels of $Kr(5p)$, particularly $2p_{10}$, results in intermultiplet transfer to $Kr(5s',5s)$ [40]. Since our treatment of Kr^{**} refers to the entire $Kr(5p)$ manifold (and higher energy states as well), we have used a level-weighted value of $2.0 \times 10^{-11} \text{s}^{-1} \text{cm}^3$ for $Kr^{**} \rightarrow Kr^*$ two body quenching, a value significantly less than the $1.2 \times 10^{-10} \text{s}^{-1} \text{cm}^3$ measured for the $Kr(2p_{10})$ level alone. Thus, for either Ar^{**} or Kr^{**} relaxing to Ar^* or Kr^* in an Ar buffer at a pressure of several atm, the time constant is ≤ 1 nsec.

2) Xe Excited States: Xenon excited state relaxation differs from that of either Ar or Kr, and we believe substantially so. The illustration of Fig. 4 indicates that two-body relaxation of $RG(p)$ results in the formation of $RG(s')$ rather than $RG(s)$. As far as Ar and Kr are concerned, it doesn't matter whether the s' or s state is the exit channel for p state relaxation (Fig. 4), because both the s' and s levels lie ≥ 0.5 eV below the $2p_{10}$ level of the p state manifold. Thus, once relaxation has occurred the p states cannot be repopulated by neutral collisions. However, in Xe the upper $6s'$ level ($1s_2$) is nearly coincident in energy with the $2p_{10}$ level of the p state manifold. Experimental evidence [41],[42] [43] indicates that the primary product of intermultiplet relaxation of the $Xe(2p_5 + 2p_{10})$ levels is $Xe(6s')$, i.e., $1s_2$ and $1s_3$), as illustrated in Fig. 4, with little or no coupling to



0A26377E 016

Potential energy diagram illustrating two-body rare gas p→s' collisional deactivation, where RG refers to Ar, Kr or Xe.

the low lying Xe(6s) states. The energy coincidence of Xe(6s') and lower Xe(6p) levels, combined with the energy overlap between the Xe(6p) and Xe(5d) manifolds, results in an energy pool, the levels of which can be mixed by neutral collisions. For this reason, the relaxation mechanism that effectively depopulates the p (and higher) states of Ar and Kr (Fig. 4), is relatively ineffective at collisional deactivation of the coupled Xe 6s', 6p and 5d energy reservoir. The result is that the concentration of higher energy Xe excited states is typically much larger and longer lived than is typical of either Ar or Kr under similar circumstances, the consequences of which have been discussed in detail previously [31] and will be summarized in subsequent paragraphs.

For these reasons, in the present model we take Xe* to mean the two 6s levels, with Xe** referring to the collisionally coupled 6s', 6p and 5d manifolds of states. Reflecting this grouping of excited states, we assume that Xe** is not coupled to Xe* by collisions with neutrals (i.e., Ar).

The dominant collision processes coupling RG** and RG* are summarized in Table III along with corresponding rate coefficients.

E. Broadband Absorption

It is well known that broadband transient absorption has a significant adverse effect on the optical extraction efficiency of the UV rare gas halide B→X lasers, usually limiting extraction efficiency to a value $\leq 50\%$ of the intrinsic rare gas halide formation efficiency. For the XeF(C→A) laser, absorption is an even more important issue because the stimulated emission cross section for the C→A transition is approximately thirty times smaller than that of the B→X transition. Thus, transient absorption can be of the same order as the gain resulting from the XeF(C) molecule, with the result

TABLE III

 $RG^* \rightleftharpoons RG^{**}$ Processes

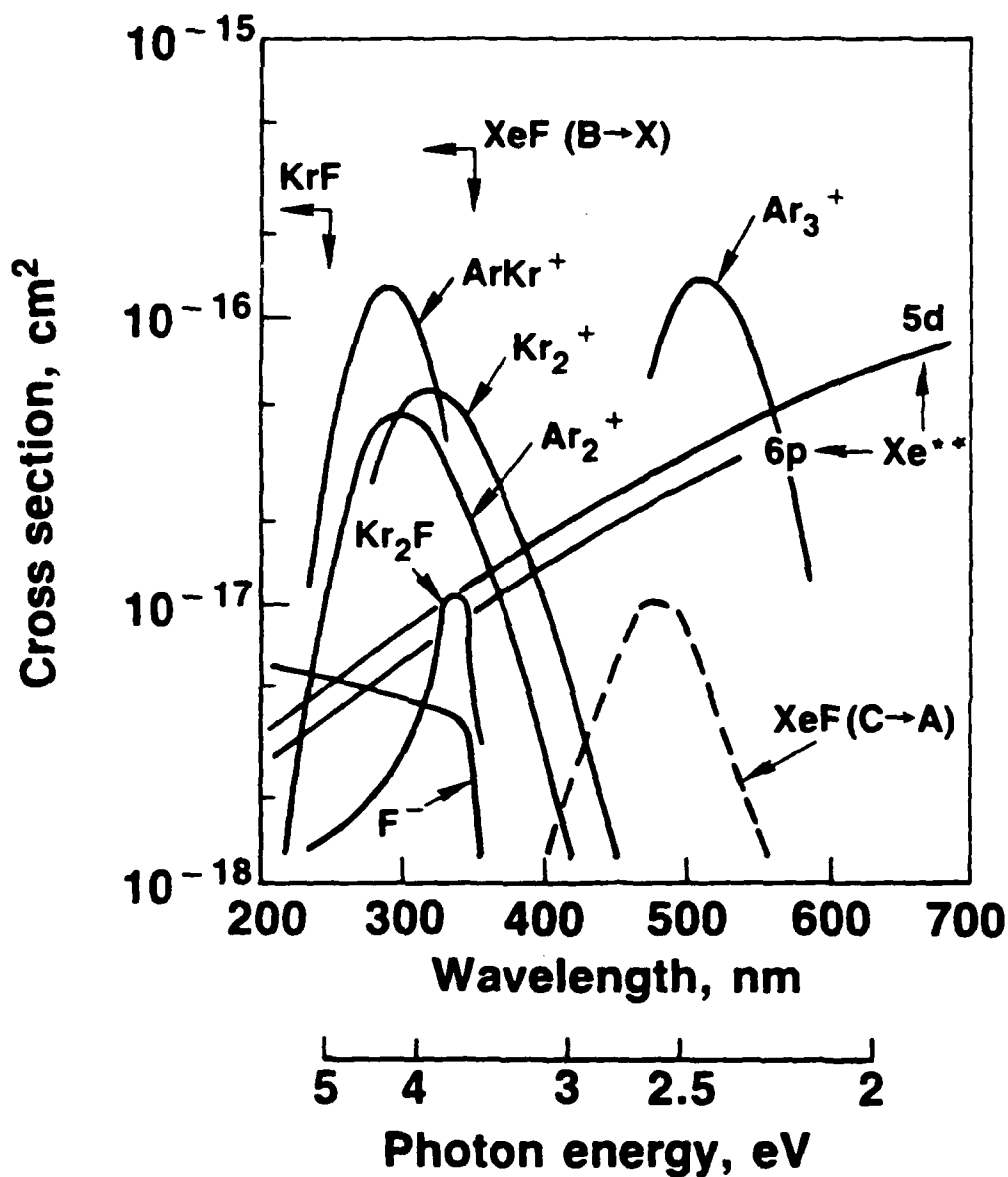
	Reaction	Rate Coefficient ^a	Reference
1.	$Ar^{**} + Ar \rightarrow Ar^* + Ar$	3.0(-11)	39
2.	$Kr^{**} + Ar \rightarrow Kr^* + Ar$	2.0(-11)	40
3.	$Xe^{**} + Ar \rightarrow Xe^* + Ar$	nil	see text
4.	$RG^{**} \rightarrow RG^* + h\nu$	3.0(7)	39,40,41,42
5.	$RG^* + e \rightarrow RG^{**} + e$	5.0(-7)	26
6.	$RG^{**} + e \rightarrow RG^* + e$	1.4(-6)	26

- a. The units for two-body rate coefficients are $s^{-1}cm^3$ and for radiative transitions the units are s^{-1} .

that the net gain usually is significantly less than the simple product of the C→A gain cross section and the C state population [31]. Indeed, identification of the transient species absorbing in the blue-green spectral region and control of their concentration by way of mixture optimization are responsible for the dramatic improvement in XeF(C→A) laser performance [1],[2],[5],[31],[34].

1) UV/Visible Photoabsorption Cross Sections: Presented in Fig. 5 are the broadband absorption cross sections [38],[44],[45],[46],[47],[48] for the species known to be important absorbers of UV and visible radiation for rare gas halide laser conditions. Also, shown for comparison are the stimulated emission cross sections for the B→X transitions of KrF and XeF and the XeF(C→A) transition [49].

Figure 5 shows that broadband absorption in the UV region is more complex than in the blue-green region, largely a reflection of the higher photon energy. Of significance is the fact that photoionization of the rare gas excited states [38] (our RG** species, Fig. 1) is important throughout the entire UV/visible spectral region. That process will be shown to dominate transient absorption for the XeF(C→A) laser conditions under investigation. Also of importance is the fact that the recently measured [44] Kr₂F absorption cross section has a magnitude and shape very different from that of Kr₂⁺ [45], contrary to earlier expectations [50]. Evidence of an Ar₂F absorption cross section much less than Ar₂⁺ is also becoming available; there are no data available for ArKrF. The concentrations of such rare gas halide trimers can be very large for XeF(C→A) laser conditions. Except for Kr₂F, they do not affect the C→A laser directly; but their presence can have a very significant effect on gain in the UV [5].



Photoabsorption cross sections for species known to be broadband transient absorbers for typical rare gas halide laser conditions: Xe^{**} [38]; Kr₂F [44]; Ar₂⁺ and Kr₂⁺ [45]; ArKr⁺ [46]; Ar₃⁺ [47]; F⁻ [48]. The photoabsorption cross sections for Ar^{**} and Kr^{**} [38] are not shown for the sake of clarity, but are very similar to those of Xe^{**}. Also shown for comparison are the stimulated emission cross sections for the B→X transition of KrF and for the XeF(C→A) transition [49].

86-6-44-1

2) Ar₃⁺ photoabsorption: Recently Lineberger and co-workers [47]

measured the magnitude and spectral shape of the Ar₃⁺ photoabsorption cross section (Fig. 5). Over the 440-520 nm effective tuning range [2] of the C→A laser, the measured Ar₃⁺ photoabsorption cross section is very large, confirming our earlier conclusion [31] that Ar₃⁺ is an important absorber in Ar-buffered XeF(C→A) laser mixtures not containing Kr.

3) Absorber Bleaching in the Blue-Green Region: It is important to note that because the blue-green photo-absorption cross sections for the primary absorbing species are significantly larger than the XeF(C→A) stimulated emission cross section (Fig. 5), the saturation fluxes for broadband transient absorbers such as Ar^{**}, Kr^{**}, and particularly Xe^{**}, are comparable to those of the C→A laser transition, in striking contrast to the situation typical of the B→X lasers. Thus, optical bleaching of transient absorption can be significant in XeF(C→A) lasers [31],[51], particularly when the laser is tuned off the peak of the gain cross section or at wavelengths for which narrow discrete absorption is known to occur [2]. We are unaware of any significant non-saturable absorption in the blue-green region under the conditions for which good XeF(C→A) laser performance has been obtained. Thus, although the low C→A gain cross section results in a lower net gain than is possible for the B→X transitions, higher energy extraction efficiency may be possible for optimized XeF(C→A) lasers.

III. XeF(C→A) LASER MEDIUM PROPERTIES

As mentioned previously, the primary focus of our analysis is short pulse (10 ns FWHM), electron-beam excitation of high pressure multi-component XeF(C→A) laser mixtures. Specific experimental conditions and a complete

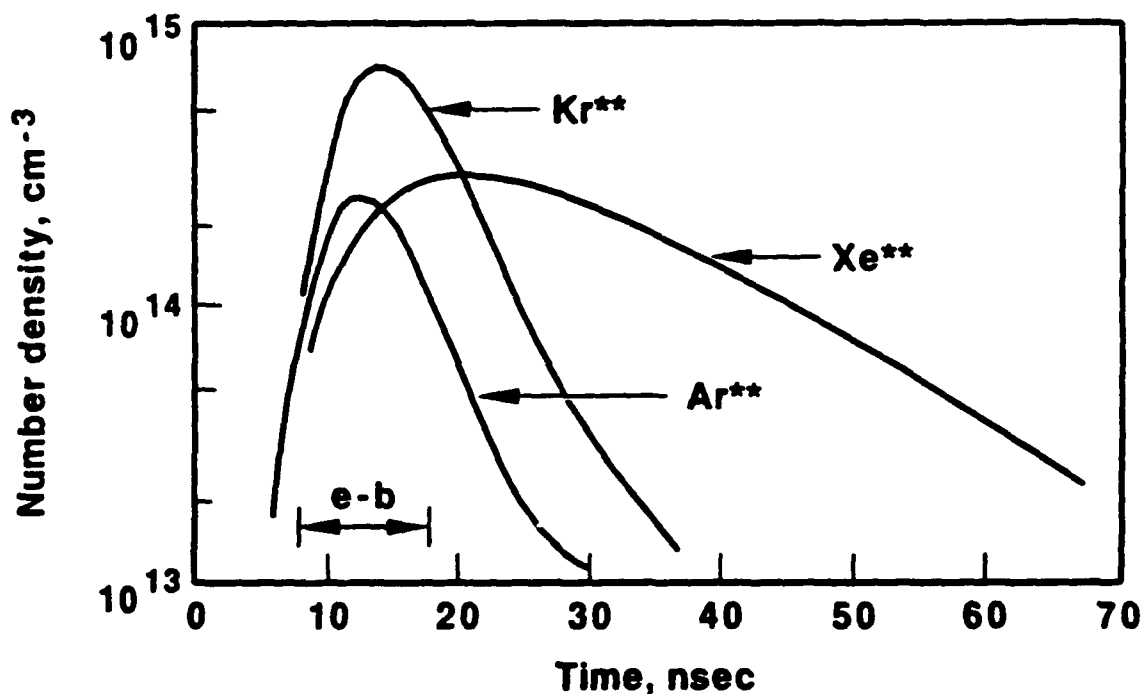
description of the laser cell used are reported elsewhere [2]. For those conditions, the energy deposition on the optical axis was on in the 100-150 J/liter range ($\sim 12.5 \text{ MW cm}^{-3}$). To first order the energy deposition is proportional to the Ar pressure. Since the gain is sensitive to energy deposition, changes in the Ar pressure are very significant. With the Ar pressure fixed at ~ 6 atm, the other constituent fractions have been optimized to maximize the gain. However, both experiment and theory show that the following constituent variations have only a small effect on the gain and laser performance: Kr-300 Torr ± 75 Torr; Xe-8 Torr ± 2 Torr; NF_3 -8 Torr ± 4 Torr; F_2 -1 Torr ± 0.5 Torr. Although the following discussion will focus on the specific mixture of Ref. [2], the indicated allowable variations should be understood.

A. Species Concentrations

Presented in Figs. 6-8 is the computed temporal variation of selected species concentrations. The rare gas species Ar^{**} , Kr^{**} and Xe^{**} (Fig. 6) will be shown to be the dominant source of broadband absorption in the blue-green region. Each of these species contributes significantly to absorption during the e-beam excitation pulse, but Xe^{**} absorption persists for a much longer time reflecting the relatively long time required for collisional deactivation of Xe^{**} as described in Section II-D.

As expected, the XeF(C) population (Fig. 7) is the largest by far and, were it not for absorption, would result in a gain of about $4\% \text{ cm}^{-1}$ for a wavelength of $\sim 480 \text{ nm}$ at the $\sim 10^{-17} \text{ cm}^2$ maximum of the C+A gain cross section [49], Fig. 5. The KrF and XeF(B) populations are also substantial for a short time, and the computed peak gain at 248 nm, and 351/353 nm is on the

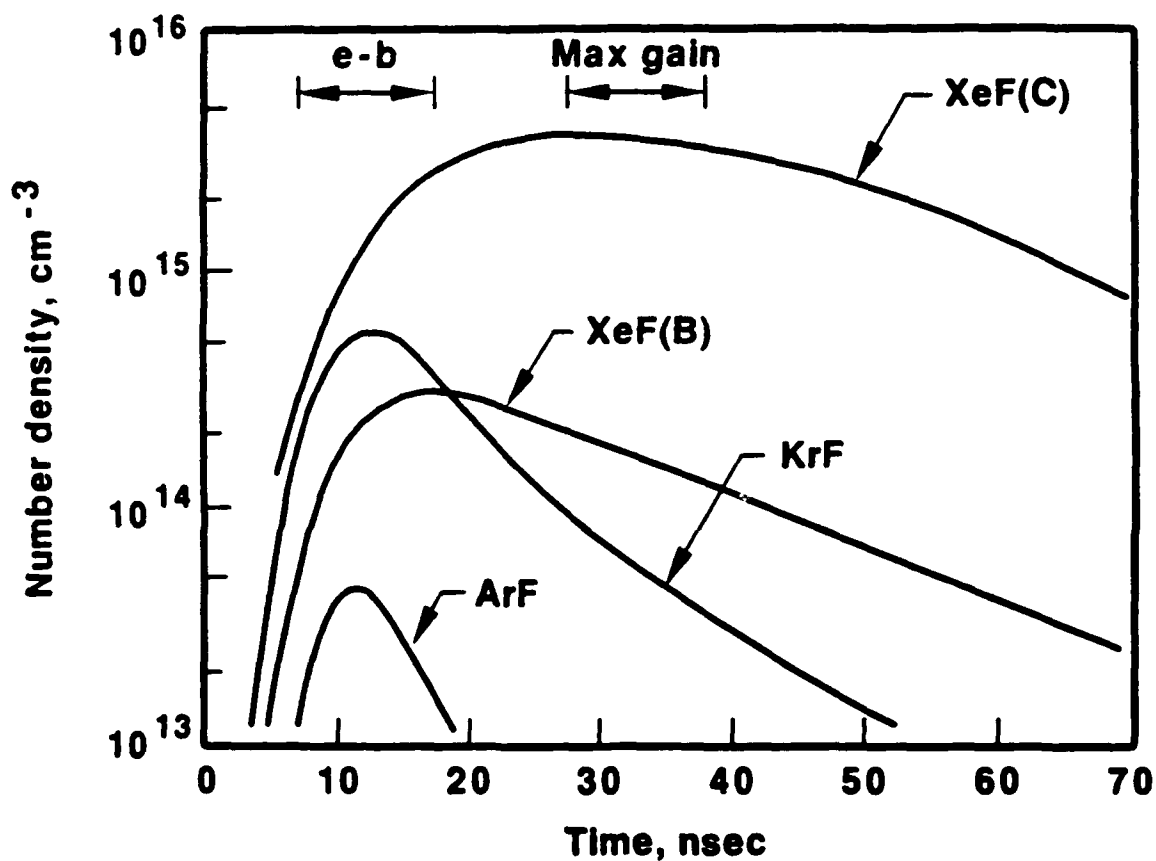
FIG. 6



RA2837X.004

Computed temporal variation of Ar**, Kr** and Xe** for a mixture comprised of Ar (6 atm)-Kr(300 Torr)-Xe(8 Torr)-NF₃(8 Torr)-F₂(1 Torr), excited by a ~1 MeV electron beam pulse having a duration of 10 nsec (FWHM) and a peak current density of ~250 Acm⁻². For these conditions the volumetric energy deposition is ~130 J/liter (13 MWcm⁻³).

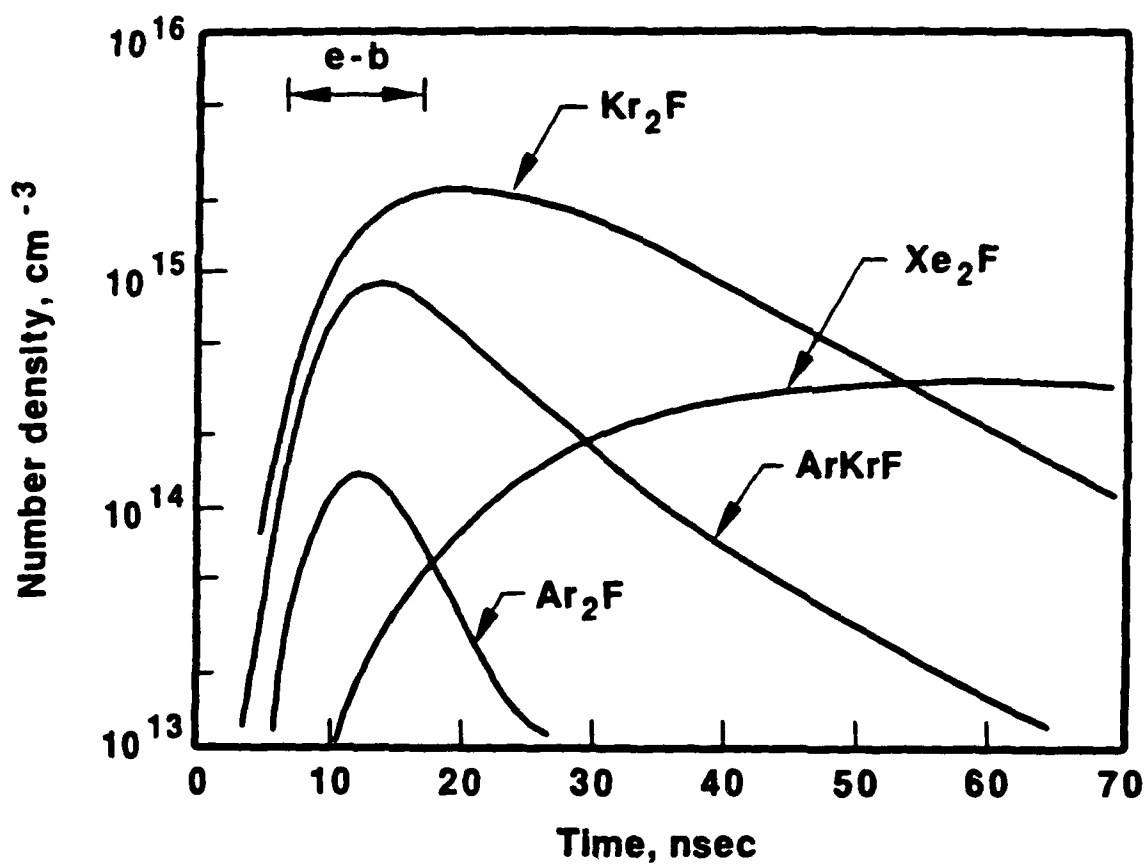
FIG. 7



RA26377X.005

Computed temporal variation of ArF, KrF, XeF(B) and XeF(C) for the conditions of Fig. 6. The temporal region of maximum XeF(C→A) net gain is indicated.

FIG. 8



RA2637TX.006

Computed temporal variation of Ar_2F , $ArKrF$, Kr_2F and Xe_2F for the conditions of Fig. 6.

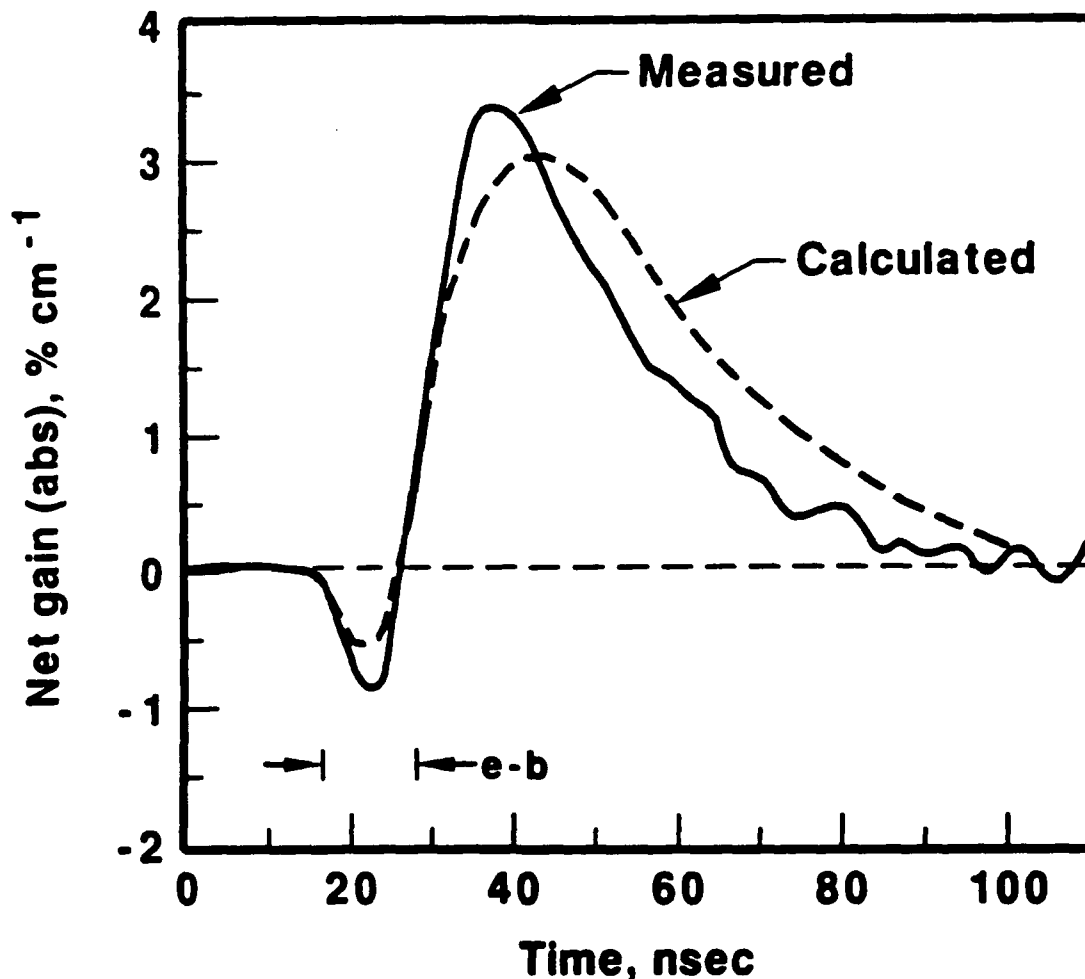
order of a few percent per cm. Indeed, relatively efficient simultaneous laser oscillation on the B→X and C→A transitions of XeF has been demonstrated for a gas mixture similar to that of Fig. 6 using a special cavity design [5].

1) Kr₂F: Of the rare gas halide trimers shown in Fig. 8, the populations of ArKrF and Kr₂F are very high, particularly the latter. In fact, except for the presence of Xe, the mixture conditions of Fig. 8 are very close to those found to be optimum for Kr₂F laser oscillation [52]. The presence of the Kr₂F trimer causes significant absorption at ~ 350 nm and, along with Kr^{**} and Kr₂⁺ (Fig. 5), tends to suppress oscillation on the XeF(B→X) transition [5]. In addition, Xe has been shown to be a very strong quencher of Kr₂F [5]. Based on our analysis of the dependence of the Kr₂F and XeF(C→A) fluorescence as Xe is added to the mixture, we infer a rate coefficient of $\sim 4.5 \times 10^{-10} \text{s}^{-1} \text{cm}^3$ for the reaction, $\text{Kr}_2\text{F} + \text{Xe} \rightarrow \text{XeF}(\text{B,C}) + 2\text{Kr}$. Because of the limited energy available (Fig. 1), XeF so formed must be in very low vibrational levels, in contrast to ion-ion recombination and harpooning reactions which result in rare gas halides in very high vibrational levels.

B. XeF(C→A) Net Gain

Presented in Fig. 9 are the measured [2] and computed C→A net gain at ~480 nm. The gain measurement is a spatial average of a double pass through a 10 cm long medium. Measurements of the e-beam energy deposition show it to be non-uniform [2], having a maximum value of ~150 J/liter in the center of the active region, tapering off in each direction along the optical axis. We have computed the gain as a function of energy deposition (position) along the optical axis and have analyzed the effect of the gain spatial nonuniformity on

FIG. 9



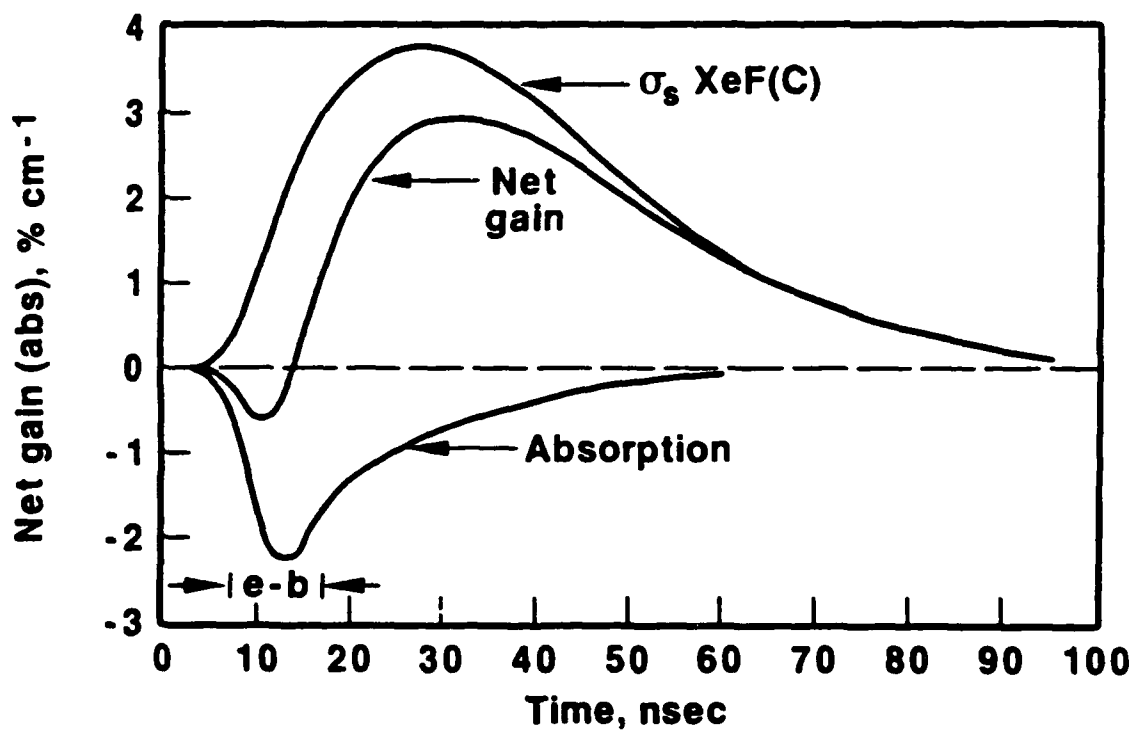
Measured [2] and computed XeF(C→A) net gain at ~480 nm, a wavelength corresponding to the maximum in the C→A gain cross section (Fig. 5). Measurements of e-beam energy deposition show it to be non-uniform along the optical axis, having a maximum value in the center of ~150 J/liter and an average value of ~100 J/liter [2]. As described in the text, analysis of the net gain measurement for these conditions shows that the effective energy deposition for a uniform medium would be ~130 J/liter. For this reason the comparison was made for the conditions of Fig. 6 (~130 J/liter deposited energy).

the measured average gain. The average value so measured corresponds to a uniform effective energy deposition value of ~ 130 J/liter, and the computed gain curve shown in Fig. 9 corresponds to that value. Considering the complexity of both the measurement and the kinetics model, the agreement between the measured and computed gain is considered to be good.

1) Broadband Transient Absorption: Presented in Fig. 10 is the computed net gain of Fig. 9, along with the individual contributions of XeF(C) and the total broadband transient absorption. During the period of initial absorption (~ 5 -15 nsec) both the XeF(C) gain and the transient absorption are comparable in magnitude and are significantly larger than the actual net absorption. Obviously, in that temporal region the demands on the accuracy of the kinetics model are severe as regards quantitative computation of the net absorption. After termination of the e-beam the absorption decays while the XeF(C) population continues to rise. In the temporal region for which the net gain maximum occurs, the XeF(C) contribution is ~ 6 times larger than the broadband absorption.

2) Rare Gas Excited State Absorption: Figure 11 shows the individual contributions to the broadband transient absorption at 480 nm. For these conditions our analysis indicates that the absorption in the blue-green region is dominated by photoionization [38] of the rare gas excited states Ar^{**} , Kr^{**} , Xe^{**} , the modelling of which is described in Sec. II-D.

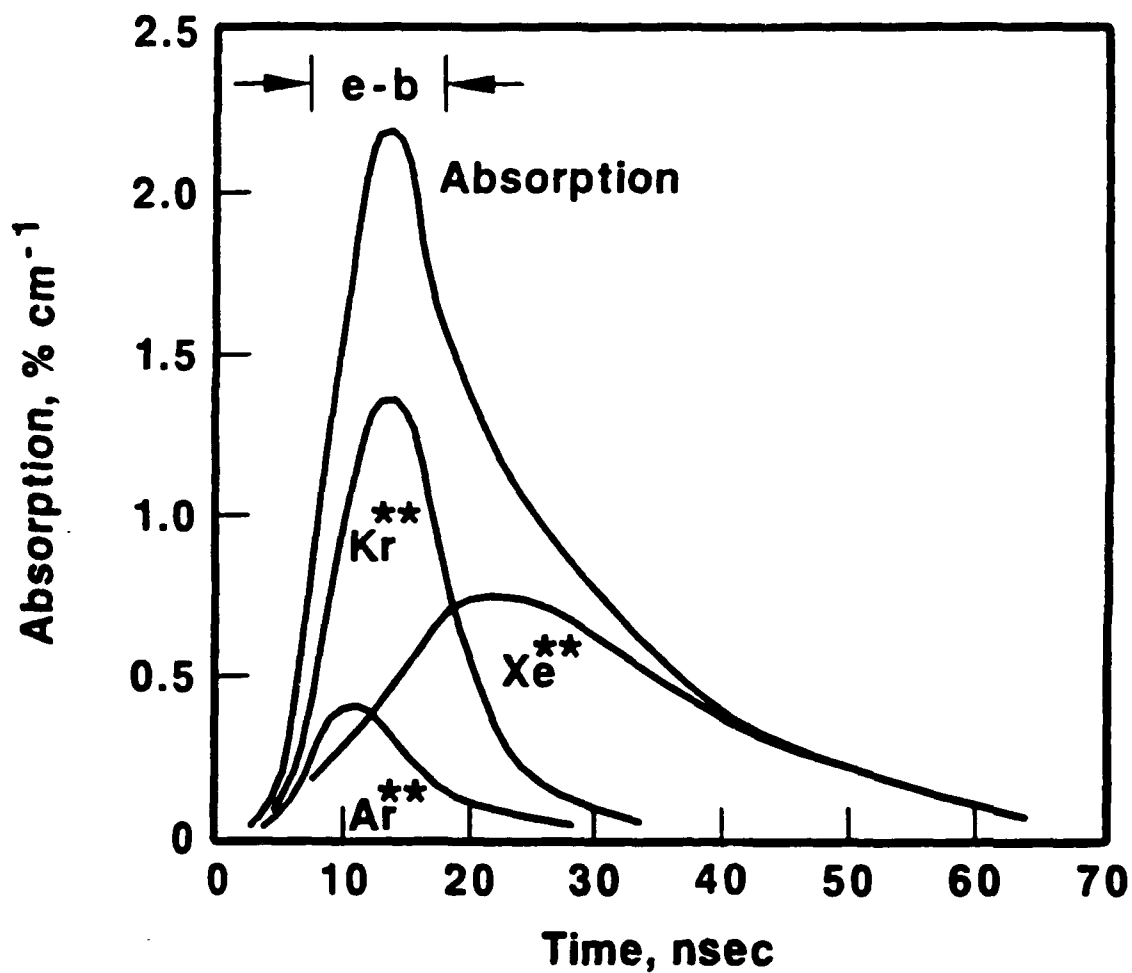
XeF(C+A) laser spectra always exhibit evidence of very narrow discrete absorption [2] attributable to bound-bound phototransitions between low energy rare gas excited states and Rydberg levels. Cross sections for these processes are not known. However, except when tuning the laser to a specific wavelength corresponding to a Rydberg transition, discrete absorption is insignificant



RA2637X.014

Computed net gain profile of Fig. 9, along with the individual contributions of XeF(C) and the total transient absorption.

FIG. 11



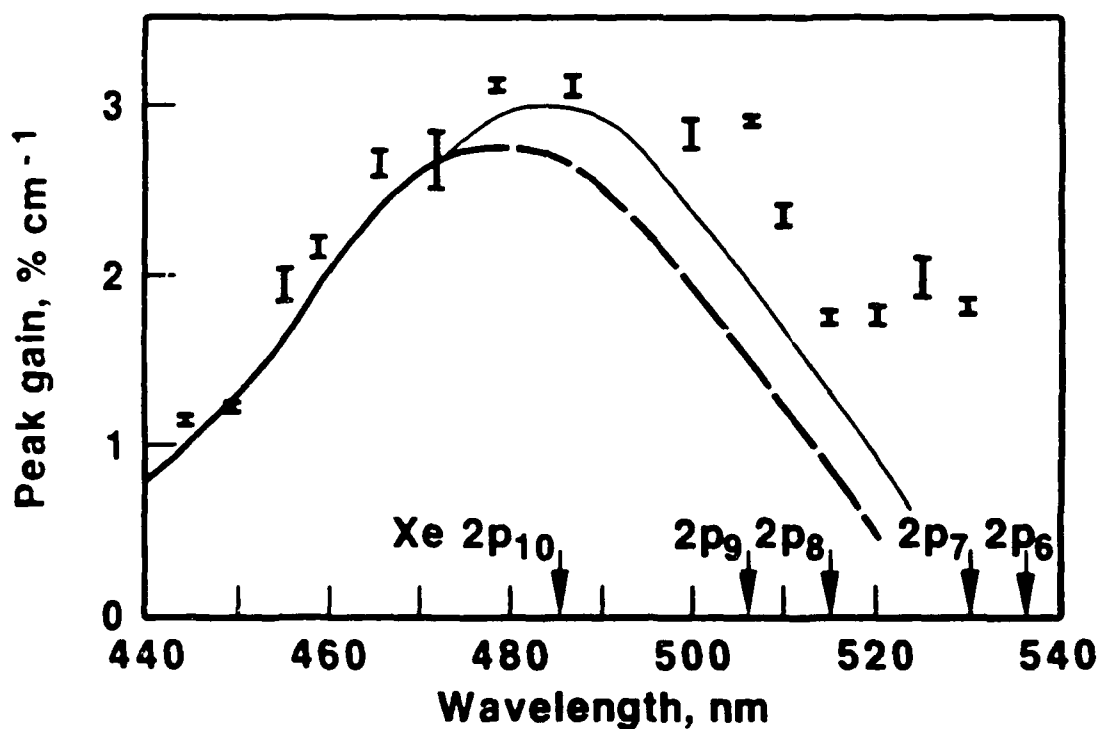
RA2637TX.010

Primary individual contributions to the transient absorption for the conditions of Figs. 9 and 10.

compared to broadband transient absorption. Thus, in the present analysis only broadband transient absorption processes have been considered.

3) Wavelength Dependence of Peak Gain: By far the most unique feature of the XeF(C→A) laser is its potential for continuous, broadband tunability. Indeed, this laser is the only UV/visible gas laser that is broadly tunable and scalable. Figure 12 shows the computed wavelength dependence of the maximum gain. Also shown for comparison are experimental data [53] obtained under similar but somewhat different conditions than those of Fig. 9. The data points shown correspond to wavelengths for which discrete absorption does not occur. Thus, the measured wavelength dependence of the peak gain can be compared directly with the computed curve. Referring to the calculated curve, the maximum gain exceeds $2\% \text{cm}^{-1}$ over a ~ 40 nm spectral range and it exceeds $1\% \text{cm}^{-1}$ over a ~ 70 nm range. Indeed, this laser has been tuned with efficient (1-1.5%) energy extraction between 470 and 500 nm with nearly constant output [2].

Although the agreement between the computed curve and the data points shown is satisfactory, the difference above ~ 490 nm is obviously larger than at other wavelengths and appears to be systematic. The difference may be real and due, at least in part, to the fact that the Xe($2p_{10}$) level, the lowest energy level of Xe($6p$) manifold, requires a photon energy of at least 2.5 eV (i.e., $\lambda < 490$ nm) for photoionization. The $2p_{10}$ level is the one in quasiequilibrium with Xe($1s_2$), the combination likely to be the dominant contributor to our Xe^{**}, particularly after termination of the e-beam excitation pulse. Thus, our procedure for modelling Xe^{**} is most likely semiquantitative at best as regards calculation of absorption for wavelengths ≥ 500 nm. In any case, the measured gain for wavelength > 500 nm suggests an even larger tuning range than the computed gain curve.



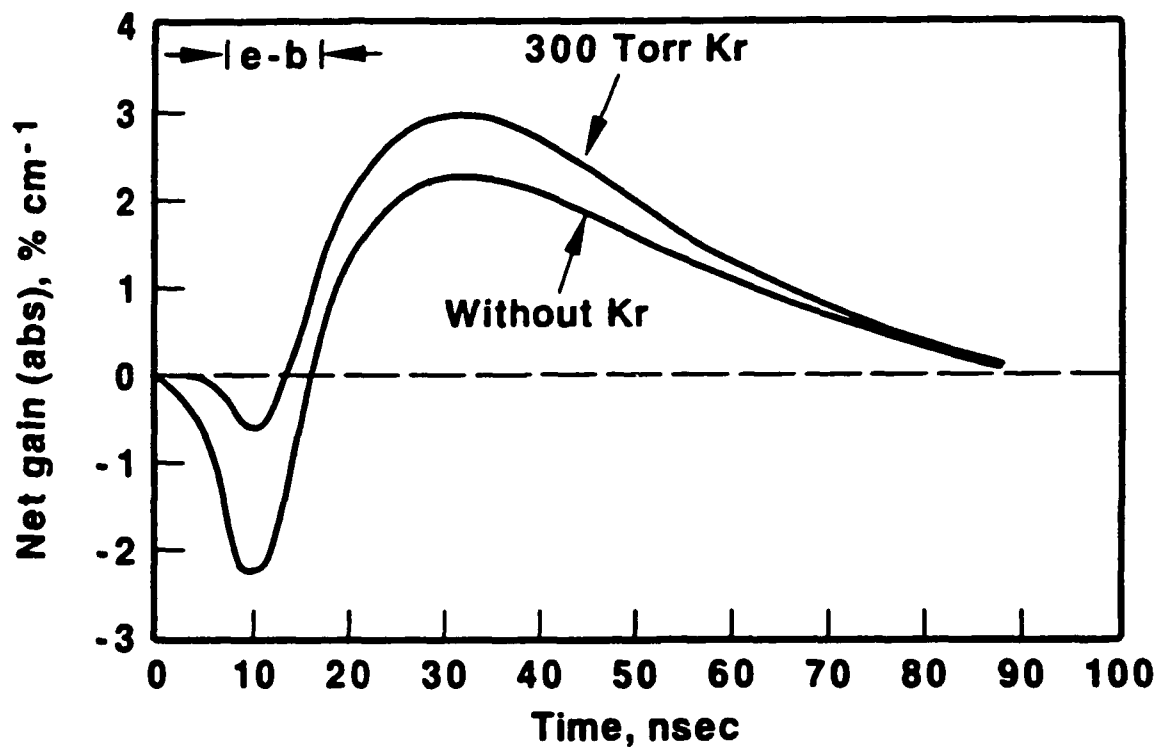
MB2676TX.001

Calculated wavelength dependence of the maximum XeF(C→A) net gain (occurring at ~30 ns, Figs. 9 and 10). Also shown for comparative purposes are experimental points obtained under generally similar conditions for wavelengths at which discrete absorption does not occur [53]. The upper curve ($\lambda \gtrsim 470$ nm) was obtained by subtracting the effect of absorption due to the Xe ($2P_6+2P_{10}$) states, having wavelength thresholds as indicated, see Sec 3-B.

C. Effect of Kr on Absorption

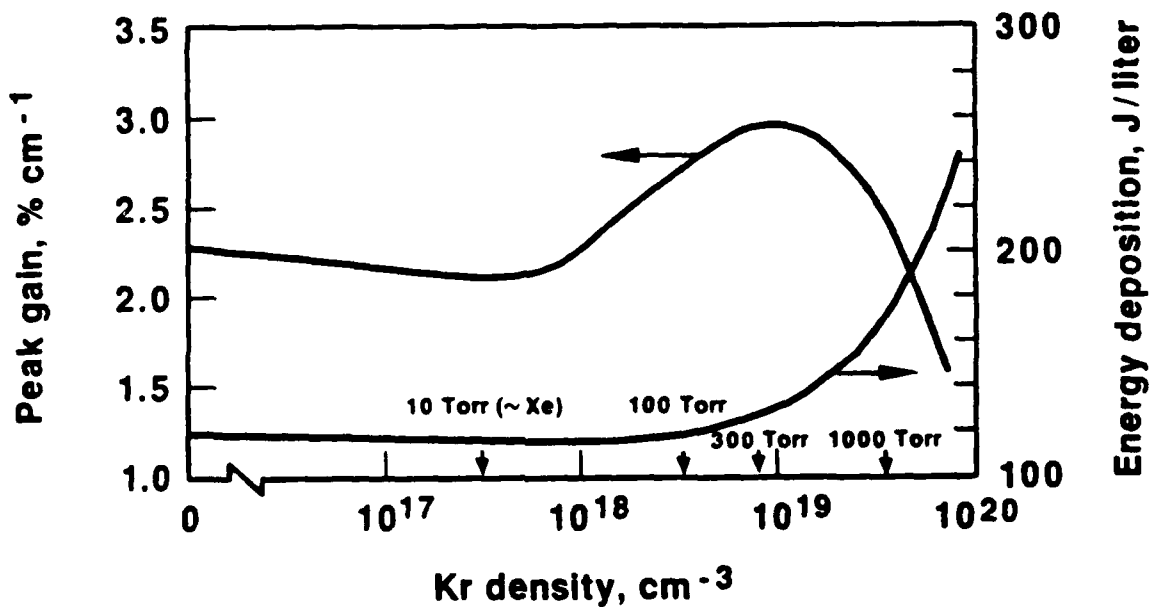
As reported previously [5] and discussed herein, the presence of Kr in the XeF(C→A) laser mixture affects practically all aspects of gas kinetics. However, the most striking effect, and the first observed [31], is a significant reduction in the transient absorption during the e-beam excitation pulse when Kr is added to the gas mixture. Presented in Fig. 13 is a comparison of the temporal gain profile discussed previously [Fig. 9] with a gain profile computed for exactly the same conditions, but with no Kr in the mixture. The much larger initial absorption when Kr is omitted is in very good agreement with experimental observations [53]. Analysis shows that the reduced absorption is due almost entirely to a reduced Ar_3^+ concentration, which is approximately an order-of-magnitude lower in the Ar-Kr buffered mixture, a reflection of the strong $\text{Ar}_2^+(\text{Ar}_3^+) + \text{Kr}^+$ charge exchange reactions (Table I). Figure 5 shows that the cross section for Ar_3^+ photoabsorption is exceptionally high for blue-green photons. Thus, the reduction in the population of Ar_2^+ and Ar_3^+ as a consequence of charge exchange with Kr results in a very significant decrease in the initial absorption when Kr is combined with Ar to form the buffer.

1) Kr variation: Figure 14 illustrates the effect of Kr variation on the peak XeF(C→A) gain, which occurs at the ~30 nsec point in Fig. 13. As Kr is added, initially there is a slight decrease in the C→A peak gain as the Kr and Xe compete. In fact, a slight gain minimum is observed when the Kr and Xe pressures are approximately equal. This is consistent with experimental observations which show that for $\text{Kr} \sim \text{Xe}$, the C→A laser output actually decreases [53]. However, as the Kr pressure is increased further ($\text{Kr} \gg \text{Xe}$), the C→A gain rises dramatically, reaching a broad maximum at a Kr pressure of ~300 Torr, a value shown by experiment to be optimum for the conditions of



RA2627TX.016

Comparison of the temporal gain profiles (480 nm) for the mixture of Fig. 6, and the same mixture without Kr.



RA2637TX.012

Effect of Kr variation on the maximum gain (480 nm), (occurring at ~30 nsec, Fig. 13), and on the volumetric e-beam energy deposition.

Fig. 9, [1], [2]. For Kr pressures above ~500 Torr the C→A gain decreases rapidly, even though the energy deposition is increasing, also in accord with experimental observations [1].

Throughout a four order-of-magnitude variation in Kr pressure (Fig. 14), the computed XeF(C) population changes by no more than ±20%, even though Kr significantly effects all aspects of the kinetics. This rather remarkable result is entirely consistent with the experimental observation that the time integrated C→A fluorescence is essentially independent of Kr pressure [5]. In fact, the undulating nature of the C→A gain for the conditions of Fig. 14 is due almost entirely to the effect of Kr on transient absorption. In the 30 to 300 Torr range of Kr pressure the concentrations of transient absorbers (Ar_3^+ in particular) decrease. Above 300 Torr, absorption due to Kr^{**} and Xe^{**} increases reflecting in part the increased energy deposition level. In that connection, it should be pointed out that for every value of total pressure and e-beam temporal duration there is an optimum combination of mixture constituents and e-beam pumping intensity. However, experimental constraints and/or procedures usually limit the range of accessible parameter space. Thus, the presentation of Fig. 14 reflects the usual experimental procedure [1] for which the total pressure, minority mixture fractions and e-beam parameters are fixed while the Kr pressure is varied.

D. XeF(B,C) Formation and Loss

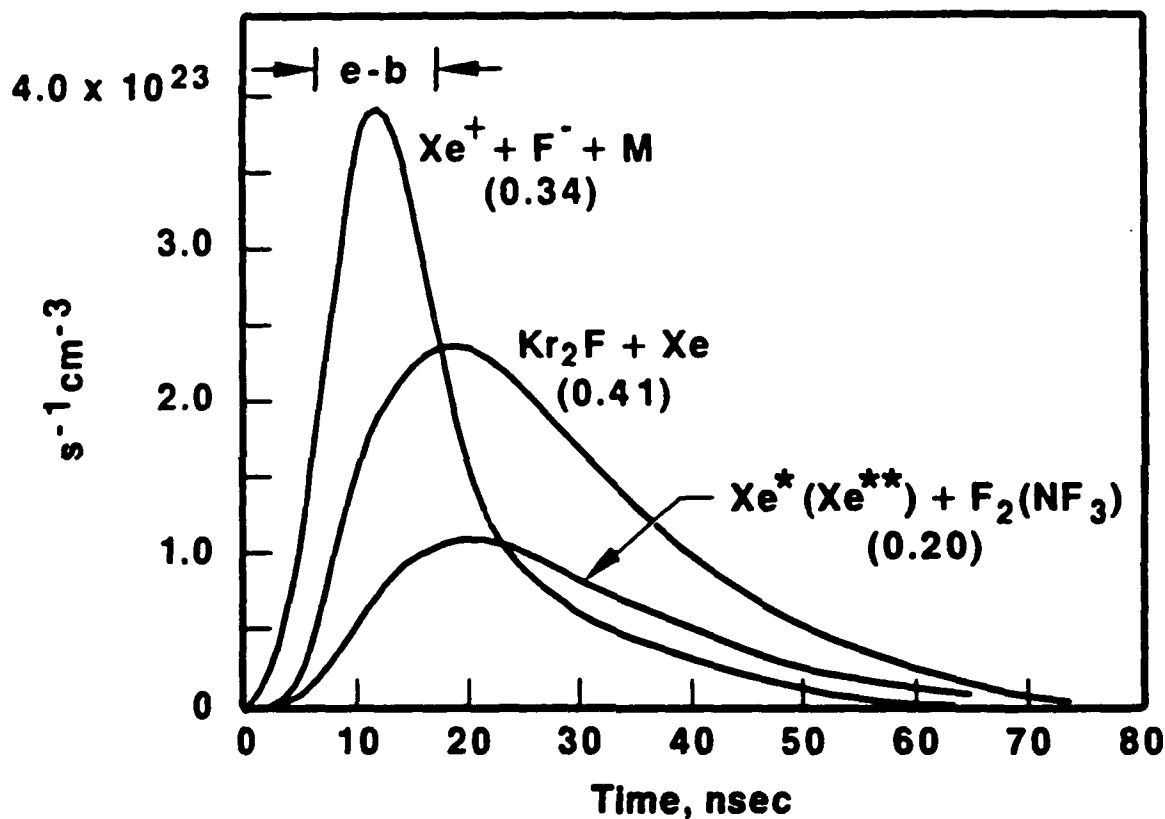
Figures 15 and 16 present the temporal variation of the primary individual contributions to XeF(B,C) formation and loss for the conditions of Figs. 6-14.

1) XeF Formation: As regards XeF formation, the indicated ion-ion recombination and harpooning reactions are more important at lower Kr

concentrations. However, the increasing importance of the $\text{Kr}_2\text{F} + \text{Xe} \rightarrow \text{XeF}$ displacement reaction as the Kr pressure is increased compensates for the decreasing importance of those reactions, with the result that the XeF formation rate is sensibly constant over a very large range of Kr pressure. As mentioned previously, we infer a value of $\sim 4.5 \times 10^{-10} \text{ s}^{-1} \text{ cm}^3$ for the indicated $\text{Kr}_2\text{F} - \text{Xe}$ displacement reaction. Displacement reactions involving ArF and/or KrF are not important sources of XeF because these species are rapidly converted to rare gas halide triatomics at a pressure of six atm and, therefore, are present in relatively low concentrations (Fig. 7).

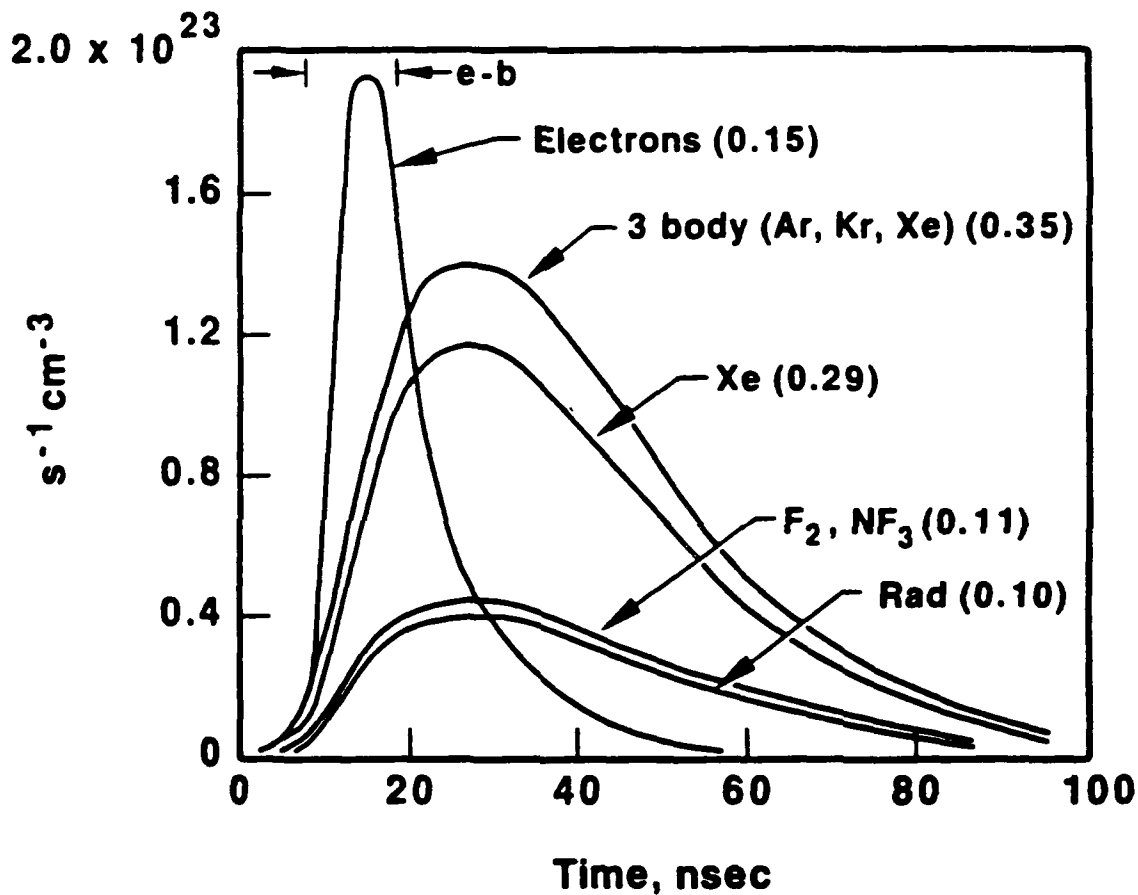
For the conditions of Fig. 15 the calculated XeF formation efficiency is $\sim 6\%$, a value which is affected by the $\sim 2.5 \text{ eV}$ photon energy of the C \rightarrow A transition. Numerical experimentation indicates that the XeF(C) formation efficiency may be as high as $\sim 10\%$ for certain combinations of pressure, mixture and e-beam pump intensity/duration.

2) **XeF Quenching:** Quenching of XeF is dominated by three-body processes, reflecting the 6 atm Ar buffer pressure, and by two-body collisions with Xe (Fig. 16). For the present conditions, Ar, Kr and Xe contribute approximately equally to three-body quenching of XeF. Our modelling shows that the peak gain increases slightly as the pressure is reduced below 6 atm, provided that the electron-beam current density is increased to maintain the pump energy density level constant. This trend is due to the reduced importance of three-body quenching of XeF (Fig. 16) as the pressure is reduced. Table IV shows the dominant XeF quenching processes considered in our model along with the corresponding rate coefficients.



RA2837TX.000

Temporal variations of the primary XeF(B,C) formation processes for the conditions of Fig. 6-13. The fractional contribution of each process on a time integrated basis is also indicated.



RA2637TX.007

Temporal variations of the primary XeF(B,C) loss processes for the conditions of Figs. 6-13. The fractional contribution of each process on a time integrated basis is also indicated.

TABLE IV
XeF Loss Processes

Reaction	Rate Coefficient ^a	Reference
XeF + 2Ar → products	7×10^{-34}	See Ref. 11
XeF + Xe + Ar → products	4×10^{-31}	12
XeF + Kr + Ar → products	$\sim 1.0 \times 10^{-32}$	this work
XeF + Xe → products	1.2×10^{-10}	12
XeF + F ₂ → products	2.0×10^{-10}	11
XeF + NF ₃ → products	2.0×10^{-11}	11
XeF(B) → XeF(X) + hν	7.7×10^7	11,49
XeF(C) → XeF(A) + Hν	1.0×10^7	11,49
XeF(B) + e → products	1.4×10^{-7}	see text
XeF(C) + e → products	4.0×10^{-8}	see text

a. The units for two- and three-body rate coefficients are $s^{-1}cm^3$ and $s^{-1}cm^6$, respectively, and for radiative transitions the units are s^{-1} .

3) Electron Quenching: Figure 16 shows that the effect of electron quenching is significant. Rate coefficients for electron quenching of rare gas halide diatomics and triatomics are highly uncertain. Such data are never determined directly, and their inference requires accurate knowledge of the halogen concentration, the electron density, the average electron energy, and possibly even specific details of the electron energy distribution [35]. The two latter properties are highly dependent on gas pressure and on the specific gas mixture. Thus, it is not surprising that there is almost an order-of-magnitude variation in reported values of electron quenching coefficients for rare gas halides. In this work we have used values of $1.4 \times 10^{-7} \text{ s}^{-1}\text{cm}^3$ and $4.0 \times 10^{-8} \text{ s}^{-1}\text{cm}^3$ for electron quenching of the B and C states of XeF. These values are twice those computed by Hazi, Rescigno and Orel [54] for super-elastic de-excitation of XeF by electrons, and are in reasonable agreement with values of total quenching coefficients reported by others. Numerical experimentation shows that an increase in the B and C state electron quenching coefficients by as much as a factor of three over the values used reduces the peak XeF(C) population by only $\sim 20\%$. Nonetheless, electron quenching has a significant influence on the variation of the peak gain as the electron beam energy deposition (pump power) is increased. For energy deposition values up to approximately 50 J/liter (5 MWcm^{-3} for our 10 ns excitation pulse) the peak gain is nearly proportional to pump energy/power. However, as the electron beam pumping level is increased above 50 J/liter, the increasing electron density and the resulting XeF(B,C) quenching by electrons limits the increase in the XeF(C) population. Indeed, our modelling shows that for the conditions of present interest the peak gain saturates for pumping levels of $\gtrsim 100$ J/liter (10 MWcm^{-3}). The computed variation of maximum XeF(C \rightarrow A) gain with electron beam pump energy is found to be in good agreement with experimental observations [2].

4) Rate Coefficient Sensitivity: Figures 15 and 16 show that no single process dominates either XeF formation or loss. For this reason our numerical experimentation with the various rate coefficients corresponding to the processes indicated in the figures shows that the maximum likely uncertainty in the computed XeF(C) population near the peak of the gain profile is $\pm 20\%$. Since the absorption is relatively small at the time the XeF(C) population reaches its maximum value (Fig. 10), the uncertainty in the computed net gain maximum is also estimated to be on the order of $\pm 20\%$.

E. Alternate Excitation Conditions

All of our work to date has focused on high current density e-beam excitation of short temporal duration. Such conditions result in the highest net gain on the XeF(C \rightarrow A) transition, a particularly important consideration when efficient, broadband, continuous tuning [2] is the primary objective. However, other excitation techniques such as soft e-beam pumping for times > 100 nsec and discharge excitation have considerable potential.

1) Long Pulse E-Beam Excitation: Shortly after laser oscillation on the XeF(C \rightarrow A) transition was first demonstrated, Campbell, Fisher and Center [55] achieved laser oscillation, albeit at very low efficiency, using a low current density (< 10 A/cm²) e-beam having a duration of 1 μ sec. Either Ar at a pressure of two atm or Kr at one atm was used as the buffer gas, and both F₂ and NF₃ (individually) were used as a source of fluorine. Although laser oscillation was demonstrated, the measured net gain at 488 nm was very low, $< 0.1\%$ cm⁻¹, resulting in an extraction energy density on the order of one mJ/liter when a stable resonator was utilized.

We have computed the net gain at 480 nm for the same conditions used by Campbell, et. al., and find it to be $\sim 0.1\%$ cm⁻¹. More important, however, the computed magnitudes of the contributions to the net gain of both XeF(C) and

transient absorption are both significantly larger than the net gain itself. Thus, relatively small changes in either the C state population or the absorption level will have a disproportionately large effect on the net gain. Accordingly, we re-computed the net gain at 480 nm for e-beam conditions generally similar to those of Ref. [55], i.e., two atm Ar buffer pressure, but with the Kr, Xe, NF_3 and F_2 pressures of Figs. 6-13. For these conditions, corresponding to an electron beam energy deposition of ~ 300 J/liter ($\sim 300 \text{ kWcm}^{-3}$) in 1 μsec , the computed net gain at 480 nm increased from $\sim 0.1\% \text{ cm}^{-1}$ to $\sim 0.5\% \text{ cm}^{-1}$. Although no attempt was made to optimize the mixture or the e-beam pumping level, it is clear that a net gain on the order of $0.5\% \text{ cm}^{-1}$ should be consistent with reasonably efficient energy extraction using a microsecond excitation pulse. Indeed, $\text{XeF}(\text{C}\rightarrow\text{A})$ laser output energy density and intrinsic efficiency values of ~ 1 J/liter and $\sim 1\%$ have been reported recently using a similar Ar, Kr, Xe, F_2 , NF_3 mixture excited by a ~ 0.7 μsec electron beam [56]. It should be pointed out, however, that the gain in the wings of the profile and at wavelengths for which discrete absorption occurs [2] will be considerably less than $0.5\% \text{ cm}^{-1}$, a factor that is significant as regards wavelength tuning off the gain maximum.

2) Discharge Excitation: For some applications discharge excitation of the $\text{XeF}(\text{C}\rightarrow\text{A})$ laser will have advantages over e-beam excitation. In the past discharge excitation of the C \rightarrow A has suffered from the same problem as long pulse e-beam excitation, i.e. low gain and therefore unacceptably low extraction energy/efficiency [57],[58]. Injection control [59] improved the situation, but use of a stable optical cavity severely limited the portion of the active volume from which energy could be extracted. Very recently [60],

injection control of a discharge excited C→A laser was accomplished injecting through a small hole in the large mirror of an unstable cavity. The latter served as a beam expanding telescope [2] permitting use of the entire active volume. With this arrangement extraction energy density and intrinsic efficiency values of approximately 0.1 J/liter and 0.1%, respectively, have been obtained, representing a significant improvement over prior results. In that work, the gas mixture found to be compatible with stable discharge operation was He buffered, and was essentially the same as that used for XeF(B→X) laser oscillation. Although we have not modeled the discharge excited C→A laser, it seems clear that the key issue is attainment of stable discharges in mixtures compatible with efficient XeF(C) formation and low transient absorption.

IV. SUMMARY

Through kinetics optimization using multi-component gas mixtures [1], [5], [34], the XeF(C→A) laser has emerged as one that is capable of extraction energy density and efficiency values comparable to those of the better developed rare gas halide B→X lasers when excited under generally similar conditions. Moreover, the C→A laser is the only excimer laser capable of wideband, continuous wavelength tuning. Indeed, efficient (~1%) tuning over a 30 nm bandwidth has already been demonstrated [2] using "short pulse" e-beam excitation as described herein, and an efficient tuning range approaching 100 nm is a distinct possibility.

In this work we have analyzed the fundamental processes affecting formation and loss of both the XeF excimer and the primary transient species that absorb in the blue-green spectral region. Agreement and consistency with

experimental observations [1],[2] is generally good for the high current density, short temporal duration e-beam conditions examined. Additionally, low current density, "soft" e-beam pumping for a duration on the order of 1.0 μ sec appears very promising [56]. Efficient energy extraction using discharge excitation is also on the horizon [60] if laser medium and discharge stability compatibility can be achieved.

Although the results of the present analysis/modeling indicate that XeF(C+A) laser kinetics are reasonably well understood, our investigation also reveals areas for which the fundamental data base is weak or incomplete. Examples of processes for which the data base of rate coefficients and reaction products could be significantly improved are as follows:

- i. two- and three-body charge exchange involving Ar, Kr and Xe homonuclear and heteronuclear molecular ions, particularly the latter;
- ii. formation and destruction of weakly bound (<0.5 eV) heteronuclear rare gas dimer ions and excited species;
- iii. halogen reactive quenching of higher excited states of the rare gases;
- iv. reactive quenching of rare gas excited states by halogen dissociation fragments;
- v. rare gas displacement reactions for rare gas halide diatomic and triatomic species;
- vi. electron quenching of rare gas halide diatomic and triatomic species.

Strengthening and expansion of the data base for reactions of the type indicated are important for applications involving all UV rare gas-halide lasers, the XeF(C+A) laser, and other lasers such as the atomic xenon laser [61], particularly as attempts are made to scale laser systems to large sizes.

ACKNOWLEDGMENT

It is a pleasure to acknowledge numerous helpful and informative conversations with our colleagues and collaborators at Rice University, particularly F. K. Tittel, R. A. Sauerbrey, W. L. Wilson, Jr., and N. Hamada. The insightful comments of D. W. Setser of Kansas State University concerning chemical reaction kinetics are very much appreciated.

REFERENCES

1. W. L. Nighan, F. K. Tittel, W. L. Wilson, Jr., N. Nishida, Y. Zhu, and R. Sauerbrey, "Synthesis of rare-gas halide mixtures resulting in efficient XeF(C→A) laser oscillation", Appl. Phys. Lett., Vol. 45, pp. 947-949, 1984.
2. N. Hamada, R. Sauerbrey, W. L. Wilson, Jr., F. K. Tittel, and W. L. Nighan, "Performance characteristics of an injection-controlled electron-beam pumped XeF(C→A) laser system", IEEE J. Quantum Electron, Vol. QE-24, pp. 1571-1578.
3. A. E. Mandl and H. A. Hyman, "XeF laser performance for F₂ and NF₃ fuels", IEEE J. Quantum Electron, Vol. QE-22, pp. 349-359, 1986.
4. A. E. Mandl and L. Litzemberger, "XeF laser at high electron beam pump rate", Appl. Phys. Lett., Vol. 51, pp. 955-957, 1987.
5. W. L. Nighan, R. A. Sauerbrey, Y. Zhu, F. K. Tittel, and W. L. Wilson, Jr., "Kinetically tailored properties of electron-beam excited XeF(C→A) and XeF(B→X) laser media using an Ar-Kr buffer mixture", IEEE J. Quantum Electron, Vol. QE-23, pp. 253-261, 1987.
6. M. R. Flannery and T. P. Tang, "Ionic recombination of rare gas atomic ions X⁺ and F⁻ in a dense gas X", Appl. Phys. Lett., Vol. 32, pp. 327-329, 1978.
7. M. R. Flannery and T. P. Tang, "Ionic recombination of rare gas molecular ions X₂⁺ with F⁻ in a dense gas X", Appl. Phys. Lett., Vol. 32, pp. 356-357, 1978.

8. M. R. Flannery, "Ion-ion recombination in high pressure plasmas", in Applied Atomic Collision Physics, Volume 3: Gas Lasers, edited by H. S. W. Massey, E. W. McDaniel and B. Bederson, Academic, New York, 1982, Chap. 5.
9. J. E. Velazco, J. H. Kolts, and D. W. Setser, "Rate constants and quenching mechanisms for the metastable states of argon, krypton and xenon", J. Chem. Phys., Vol. 69, pp. 4357-4373, 1978.
10. J. E. Velazco, J. H. Kolts, and D. W. Setser, "Quenching rate constants for metastable argon, krypton and xenon atoms by fluorine containing molecules and branching ratios for XeF^* and KrF^* formation", J. Chem. Phys., Vol. 65, pp. 3468-3480, 1976.
11. H. C. Brashears and D. W. Setser, "Transfer and quenching rate constants for $\text{XeF}(\text{B})$ and $\text{XeF}(\text{C})$ states in low vibrational levels", J. Chem. Phys., Vol. 76, pp. 4932-4946, 1982.
12. R. Sauerbrey, W. Walter, F. K. Tittel, and W. L. Wilson, Jr., "Kinetic processes of electron beam generated XeF^* and Xe_2F^* excimers", J. Chem. Phys., Vol. 76, pp. 735-747, 1983.
13. D. K. Bohme, N. G. Adams, M. Mosesman, D. B. Dunkin, and E. E. Ferguson, "Flowing afterglow studies of the reactions of the rare-gas molecular ions He_2^+ , Ne_2^+ and Ar_2^+ with molecules and rare gas atoms", J. Chem. Phys., Vol. 52, pp. 5094-5100, 1970.
14. R. J. Shul, R. Passarella, B. L. Upschulte, R. G. Keesee, and A. W. Castleman, Jr., "Thermal energy reactions involving Ar^+ monomer and dimer ions with N_2 , H_2 , Xe and Kr", J. Chem. Phys., Vol. 86, pp. 4446-4451, 1987.

15. C. B. Collins and F. W. Lee, "Measurement of the rate coefficients for the bimolecular and trimolecular ion-molecule reactions of Ar_2^+ with selected atomic and molecular species", J. Chem. Phys., Vol. 71, pp. 184-191, 1979.
16. C. B. Collins, Z. Chen, V. T. Gylys, H. R. Jahani, J. M. Pouvesle, and J. Stevefelt, "The importance of three-body processes to reaction kinetics at atmospheric pressures-I: Archetype reactions of the species with N_2 ", IEEE J. Quantum Electron., Vol. QE-22, pp. 38-46, 1986.
17. H. R. Jahani, V. T. Gylys, C. B. Collins, J. M. Pouvesle and J. Stevefelt, "The importance of three-body processes to reaction kinetics at atmospheric pressures III: Reactions of He_2^+ with selected atomic and molecular reactants", IEEE J. Quantum Electron., Vol. 24, pp. 568-572, 1988.
18. W. J. Wiegand, Jr., "High pressure ion kinetics", in Applied Atomic Collision Physics; Volume 3: Gas Lasers, edited by H. S. W. Massey, E. W. McDaniel, and B. Bederson, Academic, New York, 1982, Chap. 3 and references cited therein.
19. P. Millet, A. Birot, H. Brunet, H. Dijols, J. Galy, and Y. Salamero, "Spectroscopic and kinetic analysis of the VUV emissions of argon and argon-xenon mixtures: I. Study of pure argon", J. Phys. B: At. Mol. Phys., Vol. 15, pp. 2935-2944, 1982.
20. H. Brunet, A. Birot, H. Dijols, J. Galy, P. Millet, and Y. Salamero, "Spectroscopic and kinetic analysis of the VUV emissions of argon and argon-xenon mixtures: II. Energy transfer in Ar-Xe mixtures", J. Phys. B: At. Mol. Phys., Vol. 15, pp. 2945-2967, 1982.

21. Y. Salamero, A. Birot, H. Brunet, H. Dijols, J. Galy, P. Millet, and J. P. Montagne, "Energy transfer kinetics of the VUV emissions for Kr-Xe mixtures", J. Chem. Phys., Vol. 74, pp. 288-296, 1981.
22. P. J. Chantry, "Negative ion formation in gas lasers", in Applied Atomic Collision Physics; Volume 3: Gas Lasers, edited by H. S. W. Massey, E. W. McDaniel and B. Bederson, Academic, New York, 1982, Chap. 2.
23. Y-J Shiu and M. A. Biondi, "Dissociative recombination in argon: Dependence of the total rate coefficient and excited state production on electron temperature", Phys. Rev. A., Vol. 17, pp. 868-872, 1978.
24. Y-J Shiu and M. A. Biondi and D. P. Siples, "Dissociative recombination in Xenon: Variation of the total rate coefficient and excited state production with electron temperature", Phys. Rev. A., Vol. 15, pp. 494-498, 1977.
25. Y-J Shiu and M. A. Biondi, "Dissociative recombination in Krypton: Dependence of the total rate coefficient and excited state production on electron temperature", Phys. Rev. A., Vol. 16, pp. 1817-1820, 1977.
26. W. L. Nighan, "Plasma processes in electron-beam controlled rare gas halide lasers", IEEE J. Quantum Electron., Vol. QE-14, pp. 714-726, 1978.
27. A. Mandl, D. Klimek, and J. H. Parks, "KrF laser kinetics studies", J. Appl. Phys., Vol. 55, pp. 3940-3949, 1984.
28. T. T. Yang, J. A. Blauer, C. E. Turner, Jr., and D. A. Copeland, "Multiline model for the e-beam pumped XeF(B+X) laser", AIAA J., Vol. 23, pp. 741-748, 1985.

29. F. Kannari, M. Obara and T. Fujioka, "An advanced kinetic model of electron-beam-excited KrF lasers including the vibrational relaxation in KrF(B) and collisional mixing of KrF(B,C)", J. Appl. Phys., Vol. 57, pp. 4309-4322, 1985.
30. H. H. Michels and J. A. Montgomery, "Electronic structure and stability of the Ar_3^+ cluster ion", Chem. Phys. Lett. (in press).
31. Y. Nachshon, F. K. Tittel, W. L. Wilson, Jr., and W. L. Nighan, "Efficient XeF(C \rightarrow A) laser oscillation using electron beam excitation", J. Appl. Phys., Vol. 56, pp. 36-48, 1984.
32. D. L. Turner and D. C. Conway, "Study of the $2\text{Ar} + \text{Ar}_2^+ = \text{Ar} + \text{Ar}_3^+$ reaction", J. Chem. Phys., Vol. 71, pp. 1899-1901.
33. J. A. MacDonald, M. A. Biondi and R. Johnson, "Electron temperature dependence of the dissociative recombination of Ne_3^+ ions with electrons", J. Phys. B, Vol. 16, pp. 4273-4280, 1983.
34. W. L. Nighan, Y. Nachshon, F. K. Tittel, and W. L. Wilson, Jr., "Optimization of electrically excited XeF(C \rightarrow A) laser performance", Appl. Phys. Lett., Vol. 42, pp. 1006-1008, 1983.
35. Z. Rosenberg, M. Lando, and M. Rokni, "Direct measurement of the electron density in electron-beam-irradiated Ar-F₂ gas mixtures by time resolved interferometry", Phys. Rev. A, Vol. 35, pp. 4151-4159, 1987.
36. C. J. Elliott and A. E. Greene, "Electron energy distributions in e-beam generated Xe and Ar plasmas", J. Appl. Phys., Vol. 47, pp. 2946-2952, 1976.

37. J. K. Ku and D. W. Setser, "Significant enhancement of XeCl(B,C) and XeF(B,C) formation rate constants in reactions of Xe(5p⁵6p) atoms with halogen donors", Appl. Phys. Lett., Vol. 48, pp. 689-691, 1986.
38. C. Duzy and H. A. Hyman, "Photoionization of excited rare gas atoms", Phys. Rev. A, Vol. 22, pp. 1878-1883, 1980.
39. R. S. F. Chang and D. W. Setser, "Radiative lifetimes and two-body deactivation rate constants for Ar(3p⁵,4p) and Ar(3p⁵,4p') states", J. Chem. Phys., Vol. 69, pp. 3885-3897, 1978.
40. R. S. F. Chang, H. Horiguchi and D. W. Setser, "Radiative lifetimes and two-body collisional deactivation rate constants in argon for Kr(4p⁵5p) and Kr(4p⁵5p') states", J. Chem. Phys., Vol. 73, pp. 778-780, 1980.
41. G. Inoue, J. K. Ku, and D. W. Setser, "Laser induced fluorescence study of Xe(5p⁵6p, 5p⁵6p', 5p⁵7p and 5p⁵6d) states in Ne and Ar: Radiative lifetimes and collisional deactivation rate constants", J. Chem. Phys., Vol. 81, pp. 5760-5774, 1984.
42. J. K. Ku and D. W. Setser, "Collisional deactivation of Xe(5p⁵6p) states in Xe and Ar", J. Chem. Phys. Vol. 84, pp. 4304-4316, 1986.
43. J. Xu and D. W. Setser, "Collisional deactivation studies of the Xe(6p) states in Kr and Ar", J. Chem. Phys. (in press).
44. D. B. Geohegan and J. G. Eden, "Absorption spectrum of Kr₂F(4²Γ) in the near ultraviolet and visible (335 ≤ λ ≤ 600 nm): Comparison with Kr₂⁺(1(1/2)_u) measurements", J. Chem. Phys. (in press).

45. H. H. Michels, R. H. Hobbs, and L. A. Wright, "Electronic structure of the noble gas dimer ions. II. Theoretical absorption spectrum for the $A^2\Sigma_{v2u}^+ \rightarrow D^2\Sigma_{1/2g}^+$ system", J. Chem. Phys., Vol. 71, pp. 5053-5062, 1979.
46. C. F. Bender and N. W. Winter, "Theoretical absorption spectra of $ArKr^+$ ", Appl. Phys. Lett., Vol. 33, pp. 24-31, 1978.
47. N. E. Levinger, D. Ray, K. K. Murray, A. S. Mullin, C. P. Schulz, and W. C. Lineberger", "The visible photoabsorption spectrum of Ar_3^+ ", J. Chem. Phys., Vol. 89, pp. 71-74, 1988.
48. A. Mandl, "Electron photodetachment cross section of the negative ion of fluorine", Phs. Rev. A, Vol. 3, pp. 251-255, 1971.
49. W. K. Bischel, D. J. Eckstrom, H. C. Walker, Jr. and R. A. Tilton, "Photolytically pumped $XeF(C\rightarrow A)$ laser studies", J. Appl. Phys., Vol. 52, pp. 4429-4434, 1981.
50. W. R. Wadt and P. J. Hay, "Electronic States of Ar_2F and Kr_2F ", J. Chem Phys., Vol. 68, pp. 3850-3863, 1978.
51. Y. Nachshon and F. K. Tittel, "A new blue-green $XeF(C\rightarrow A)$ excimer laser amplifier concept", Appl. Phys.: B, Vol. 25, pp. 227-231, 1984.
52. F. K. Tittel, M. Smayling, W. L. Wilson, Jr. and G. Marowsky, "Blue laser action by the rare gas halide trimer Kr_2F ", Appl. Phys. Lett., Vol. 37, pp. 862-864, 1980.
53. R. A. Sauerbrey (private communication).

54. A. V. Hazi, T. N. Rescigno and A. E. Orel, "Theoretical study of the de-excitation of KrF and XeF excimers by low energy electrons", Appl. Phys. Lett., Vol. 35, pp. 477-479, 1979.
55. J. D. Campbell, C. H. Fisher, and R. E. Center, "Observations of gain and laser oscillation in the blue-green during direct pumping of XeF by microsecond electron beam pulses", Appl. Phys. Lett., Vol. 37, pp. 349-350, 1980.
56. A. E. Mandl and L. N. Litzenberger, "Efficient, long pulse XeF(C→A) laser at moderate electron-beam pump rates", Appl. Phys. Lett. (in press).
57. R. Burnham, "A discharge pumped laser on the C→A transition of XeF", Appl. Phys. Lett., Vol. 35, pp. 48-49, 1979.
58. C. H. Fisher, R. E. Center, G. J. Mullaney and J. P. McDaniel, "A 490 nm XeF electric discharge laser", Appl. Phys. Lett., Vol. 35, pp. 26-28, 1979.
59. C. H. Fisher, R. E. Center, G. J. Mullaney and J. P. McDaniel, "Multipass amplification and tuning of the blue-green XeF(C→A) laser", Appl. Phys. Lett., Vol. 35, pp. 901-903, 1979.
60. H. Voges and G. Marowsky, "Injection control of a multipass amplification of a discharge excited XeF(C→A) laser", IEEE J. Quantum Electron., Vol. QE-24, pp. 827-832, 1988..
61. N. G. Basov, V. V. Baranov, A. Y. Chugunov, V. A. Danilychev, A. Y. Dudin I. V. Kholin, N. N. Ustinovskii and D. A. Zayarnyi, "60 J quasistationary electroionization laser on Xe atomic metastables," IEEE J. Quantum Electron., Vol. QE-21, pp. 1756-1760, 1985.

Kinetically Tailored Properties of Electron-Beam Excited XeF($C \rightarrow A$) and XeF($B \rightarrow X$) Laser Media Using an Ar-Kr Buffer Mixture

WILLIAM L. NIGHAN, SENIOR MEMBER, IEEE, ROLAND A. SAUERBREY, MEMBER, IEEE, YUNPING ZHU, STUDENT MEMBER, IEEE, FRANK K. TITTEL, FELLOW, IEEE, AND WILLIAM L. WILSON, JR., MEMBER, IEEE

Abstract—Use of a two-component buffer gas comprised of Ar and Kr results in electron-beam excited XeF($C \rightarrow A$) laser pulse energy and intrinsic efficiency values comparable to those of UV rare gas-halide lasers. Herein we report measurements of transient absorption confirming that the primary effect of a buffer comprised of Ar and Kr is a significantly lower level of ionized and excited species that absorb in the blue-green spectral region. Spectral analysis of a variety of mixtures shows that the Ar-Kr buffer also benefits XeF($C \rightarrow A$) laser performance due to an increase in gain in the 400–450 nm region caused by the presence of the Kr₂F excimer. In addition, a large increase in absorption at ~351 nm, also due to Kr₂F, suppresses oscillation on the competitive XeF($B \rightarrow X$) transition and, for certain conditions, makes efficient simultaneous oscillation of the XeF($B \rightarrow X$) and XeF($C \rightarrow A$) laser transitions possible.

I. INTRODUCTION

ELECTRICALLY excited rare gas-halide laser mixtures typically are comprised of a high pressure (> 1 atm) rare gas background, or *buffer*, a second rare gas species at much lower pressure from which the rare gas-halide excimer molecule is comprised, and a halogen donor at a partial pressure of a few torr [1], [2]. Selection of a particular buffer species and its pressure is dictated by several requirements: 1) vibrational relaxation of the rare gas halide (RGH) excimer by the buffer must be fast compared to deactivation processes, 2) collisional quenching of the RGH by the buffer must be minimal, 3) transient absorption at the laser wavelength by buffer-related ionized and excited species must be held to an acceptable level, and 4) when electron-beam (*e*-beam) excitation is used the buffer gas must have a relatively high stopping power, while electric discharge excitation requires a buffer compatible with formation of a stable discharge. Additionally, each specific RGH laser often has one or more unique requirements affecting buffer gas selection, but they are generally of less importance than

those listed above. Thus, determination of the rare gas buffer species that is best for a particular situation is clearly a compromise involving several conflicting factors.

Based on several years of experimentation supplemented by analysis, the optimum buffer for the *e*-beam excited XeF(351 nm) laser has been found to be neon [1], [3], while helium is usually used when discharge excitation is employed [4]. The 308 nm XeCl laser uses either neon or helium as the buffer [4], [5], while the KrF (248 nm) laser usually uses helium when excitation is provided by a discharge [4] and argon when *e*-beam excitation is employed [6], [7]. Additionally, the best performance from the broad-band *e*-beam excited XeF($C \rightarrow A$) laser (450–510 nm) has been obtained using argon as the single buffer [8]. Recently, investigations have been carried out focused on evaluation of the merits of using *two* rare gas components to form the buffer gas [9]–[12]. Notable success has been realized using an Ar-Kr combination to form the high pressure buffer for an *e*-beam excited XeF($C \rightarrow A$) laser [11], [12]. This approach has resulted in a dramatic improvement in the net gain of the broad-band XeF($C \rightarrow A$) transition centered at ~480 nm. Indeed, laser pulse energy density and intrinsic efficiency values have been demonstrated that compare very favorably with those of the more highly developed UV RGH $B \rightarrow X$ lasers, by using the XeF($C \rightarrow A$) medium either as a broad-band oscillator [11], or as a wavelength selectable amplifier [12]. In addition, use of Ar-Kr buffer gas mixtures permits relatively efficient, simultaneous oscillation of the XeF $B \rightarrow X$ and $C \rightarrow A$ laser transitions [13]. Interpretation of these results led to the conclusion that the primary effect of Ar and Kr in combination was a significantly lower level of transient absorption in the blue-green spectral region [11]. Herein we report on recent work supporting this conclusion, along with evidence of additional factors that benefit XeF($C \rightarrow A$) laser performance, including: 1) faster mixing of the XeF B and C states, 2) a contribution to the net gain in the 400–450 nm region due to the presence of a high concentration of the Kr₂F excimer, and 3) a large increase in absorption at UV wavelengths, also due to Kr₂F, which suppresses oscillation on the competitive XeF($B \rightarrow X$) transition and, for certain

Manuscript received June 3, 1986. This work was supported in part by the Office of Naval Research, the National Science Foundation, and the Robert A. Welch Foundation.

W. L. Nighan is with the United Technologies Research Center, East Hartford, CT 06018.

R. A. Sauerbrey, Y. Zhu, F. K. Tittel, and W. L. Wilson, Jr., are with the Department of Electrical and Computer Engineering, Rice University, Houston, TX 77251.

IEEE Log Number 8611712.

conditions, makes possible relatively efficient, simultaneous oscillation of the $\text{XeF}(B \rightarrow X)$ and $\text{XeF}(C \rightarrow A)$ laser transitions.

The details of the experimental arrangement and related diagnostics used in this investigation are described in Section II. In Section III the effect of Kr as an additive to reduce transient blue-green absorption is treated. Spectroscopic data relevant to the role of Ar-Kr mixtures on mixing of $\text{XeF}(B, C)$, and on the influence of Kr_2F kinetics on $\text{XeF}(C \rightarrow A)$ laser performance are presented in Section IV, while a discussion of conditions for which simultaneous $\text{XeF } B \rightarrow X$ and $C \rightarrow A$ laser oscillation can be obtained is presented in Section V.

II. EXPERIMENT

A. Electron-Beam and Reaction Cell

The overall experimental arrangement used in this investigation is illustrated in Fig. 1. A Physics International Pulserad 110 electron-beam generator was used to transversely excite the high pressure gas mixtures [8], [12]. The electron beam energy was 1 MeV and the pump pulse duration was 10 ns (FWHM), producing a pump energy density of $\sim 135 \text{ J/l}$, as measured by a calorimeter and a Faraday cup probe. The excited region was the cylindrical 28 cm^3 volume defined by the clear aperture (1.9 cm diameter) and the pumped length (10 cm).

The stainless steel reaction cell was well passivated by prolonged exposure to F_2 prior to any experiments. High purity gas mixtures of research grade Ar, Xe, Kr, NF_3 , and F_2 were used, with the F_2 in a 10–90 F_2 -He mixture. Good mixing of the gas components was achieved by turbulent flow of the high pressure gas components into the reaction cell. A fresh gas mixture was used for each shot, although up to ten shots could be made before any significant deterioration of the mixture was observable.

B. Diagnostics

The temporal evolution of the fluorescence and the laser output were monitored by a fast vacuum photodiode detector [ITT-F4000(S5)]. Neutral density filters were used to avoid saturation of the photodiode, and interference and color glass filters were used to define the spectral regions of interest. Signals were recorded by a Tektronix R 7912 Transient Digitizer. The time resolution of the entire system was better than 2 ns. The temporally-integrated, spectrally-resolved fluorescence was recorded by an optical-multichannel-analyzer (OMA III), using a Jarrell-Ash 0.25 meter spectrometer having a spectral resolution of $\sim 0.3 \text{ nm}$. Data from the Transient Digitizer were processed using a PDP 11/23 minicomputer. The OMA III signals were recorded by an IBM PC-XT computer.

The spectrometer and the OMA III have a wavelength dependent sensitivity. In order to account for this, the spectral sensitivity of the system was determined by three different methods and the measured spectra were appropriately corrected. The first procedure utilized $\text{N}_2(C \rightarrow B)$ fluorescence emission lines [14]; the second method used a Xe flashlamp with a known spectral intensity dis-

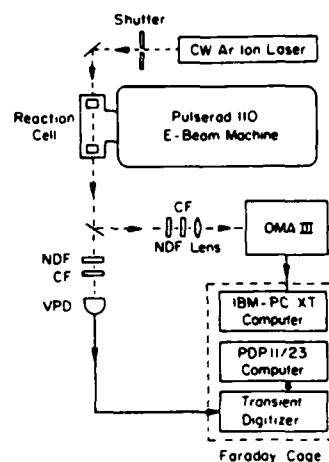


Fig. 1. Schematic illustration of the experimental apparatus and arrangement. NDF = neutral density filter, CF = color glass filter, VPD = vacuum photo diode, and OMA = optical multichannel analyzer.

tribution together with narrow frame interference filters to define the spectral sensitivity measurement regions; and the third utilized an Ar^+ laser with known power at each transition line. Using these techniques the wavelength response of the OMA III system was quantified for the 330–520 nm spectral region, and all experimental data were corrected to account for the spectral response of the detection system.

C. Gain / Absorption Measurement

A CW Ar-ion laser was used to measure gain at several blue-green wavelengths, concentrating on the $\sim 480 \text{ nm}$ region for which the $\text{XeF}(C \rightarrow A)$ gain is a maximum. Three passes of the probe beam through the cell were used in order to maximize the signal-to-noise ratio. The laser probe signal was focused on a Lasermetrics 3117 PIN diode through a narrow-band interference filter, a color-glass filter, and an iris located 10 m from the laser cell. The detector was located inside a Faraday cage to minimize electrical noise pickup and stray fluorescence. A mechanical shutter was used to produce a 4 ms laser probe pulse to avoid saturation of the detector. The electron beam pulse was synchronized to appear in the middle of the laser probe pulse. In the CW mode, the detector diode is linear with input power for output currents up to 4 mA. However, the time response of the detector for currents above 2 mA began to deteriorate. Therefore, the detector current was always maintained below 2 mA, for which the time response was better than 2 ns.

III. ABSORPTION IN THE BLUE-GREEN SPECTRAL REGION

A. Net Gain in $\text{XeF}(C \rightarrow A)$ Laser Mixtures

In order to compensate for a stimulated emission cross section [15] having a peak value of only $\sim 10^{-17} \text{ cm}^2$, intense pumping is required to produce adequate gain on the $\text{XeF}(C \rightarrow A)$ transition, a circumstance resulting in very high concentrations of excited and ionized species, many of which absorb at the laser wavelength [8]. Thus,

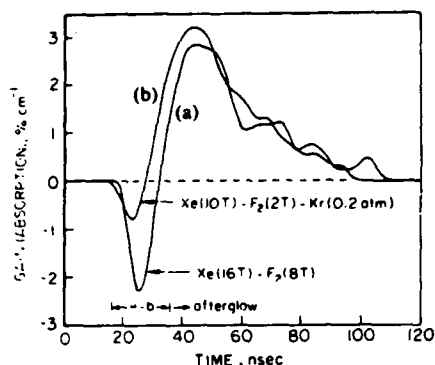


Fig. 2. Temporal evolution of the *e*-beam excited XeF(C → A) net gain profile measured at 488 nm using an Ar-ion probe laser for mixtures comprised of 6.5 atm Ar, 16 torr Xe, 8 torr NF₃ and 8 torr F₂. (a), and 6.5 atm Ar, 10 torr Xe, 8 torr NF₃, 2 torr F₂ and 150 torr Kr (b).

electrical excitation of the XeF(C → A) medium is usually characterized by a period of strong transient absorption during the excitation pulse, followed by development of net gain in the afterglow regime [8], [11]. Presented in Fig. 2 is the measured temporal evolution of the net gain for representative *e*-beam excited mixtures with and without Kr, vividly illustrating the significant reduction in the initial absorption occurring during the excitation pulse, and the increase in peak gain when an optimized Ar–Kr buffer mixture is used [11]. The results of Fig. 2 are typical of the wavelength region between 460–510 nm [12], and are found to be *relatively* insensitive to Kr pressure for values in the 0.1–1.0 atm range, although optimum gain is achieved for a Kr pressure of ~0.5 atm.

B. The Role of Kr

1) *Transient Absorption in Laser Mixtures*: Detailed modeling [8] of XeF(C → A) medium properties for the mixture of Fig. 2 that does *not* contain Kr provided evidence that the primary absorbing species during and after the *e*-beam excitation pulse are Ar₃⁺, Ar₂⁺, Ar*(4*p*, 3*d*) and Xe*(6*p*, 5*d*), with the latter being the dominant absorber and one having a particularly slow rate of decay. With a few tenths of an atmosphere of Kr present in the mixture, species such as Ar₃⁺ (and its precursor Ar₂⁺) and Ar₂⁺ are converted to Kr⁺ and Kr* on a nanosecond time scale, with the latter atomic species apparently replacing Ar-related molecular species as effective XeF(B, C) precursors. That is, we postulate that upon addition of Kr certain molecular XeF(B, C) precursors that exhibit *broad-band* absorption have been *partially* replaced by atomic precursors that do not. Moreover, Kr-related molecular species such as Kr₂⁺ or Kr₂^{*} that might also be expected to contribute to broad-band absorption at blue-green wavelengths are formed at a slow rate compared to corresponding Ar-related species since the Kr pressure is much less than that of Ar. Also, heteronuclear species such as ArKr⁺ or ArKr* are produced at a slow rate because their three-body formation rate coefficients are generally much less than those of similar homonuclear species [16]. For these reasons, in Ar–Kr buffered mixtures

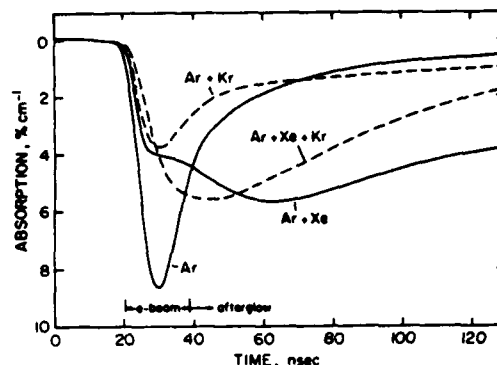


Fig. 3. Temporal evolution of the absorption measured at 488 nm in 6 atm Ar and in a mixture comprised of 6 atm Ar and 16 torr Xe (solid lines). The absorption measured for the same conditions but with 150 torr Kr added to each mixture is also shown (dashed lines).

it appears that the role of molecular absorbing species as XeF(B, C) precursors is reduced compared to the situation typical of Ar-buffered mixtures, and that the rate of decay of long lived absorbing species such as Xe*(6*p*) is increased.

2) *Absorption in Ar and Ar–Xe Mixtures*: The above interpretation is supported by measurements of absorption in Ar and Ar–Xe mixtures with and without addition of Kr. Presented in Fig. 3 is the time dependence of the measured transient absorption in such mixtures for conditions otherwise similar to those of Fig. 2. In this illustrative example, for Ar at 6 atm the peak absorption during the *e*-beam excitation pulse is reduced by about 50 percent with 0.2 atm Kr added, a change interpreted as due to reduced concentrations of Ar-related molecular absorbers as described above. The peak absorption occurring during the excitation pulse in the Ar–Xe mixture is affected only slightly with 0.2 atm Kr added, since in that case Xe plays a role similar to that of Kr as regards reduction in the concentration of Ar-related molecular species. However, Fig. 3 shows that the temporal decay of the absorption in the Ar–Xe mixture is exceptionally slow, extending far into the afterglow region. Modeling [8] has shown that the absorption in that case is due almost entirely to photoionization of Xe(6*p*) states for which there is no effective loss channel with Ar as the buffer. However, with Kr added to the Ar–Xe mixture the rate of absorption decay in the afterglow is increased significantly, indicative of the presence of more effective Xe(6*p*) exit channels [8] with Kr in the mixture.

3) *Quenching and Absorption in Kr-Containing Mixtures*: The fact that an Ar–Kr buffer mixture results in substantially less blue-green absorption than use of Ar alone suggests simple substitution of Kr for Ar rather than use of the two together. In order to explore this possibility, measurements [11] were carried out using Kr as the buffer for XeF(C → A) laser mixtures at pressures such that the *e*-beam energy deposition was essentially the same as for the mixtures of Fig. 2, i.e., Kr pressures of 3–4 atm. For these tests the partial pressure of *each* mixture constituent was reoptimized, a very important factor, yet

no conditions were found for which Kr-buffered laser mixtures performed as well as either Ar or Ar-Kr buffered mixtures similar to those of Fig. 2. Moreover, examination of the fluorescence and laser output as Kr pressure is increased above the optimum level for Kr-containing mixtures provides evidence of additional XeF quenching and/or blue-green absorption processes not observed in Ar buffered mixtures. Since the rate coefficients for two body quenching of XeF(*B*, *C*) by either Ar or Kr are small, as is the three-body coefficient for XeF quenching by Ar [17], we feel that the most probable additional quenching process is three-body quenching of XeF(*B*, *C*) by Kr with Ar acting as the third body. A rate coefficient value $\approx 10^{-32} \text{ s}^{-1} \text{ cm}^6$ for the reaction $\text{XeF}(\text{B}, \text{C}) + \text{Kr} + \text{Ar} \rightarrow \text{products}$ is consistent with our observations and with those of others as well [18]. Additionally, it is likely that Kr-related broad-band absorbing species are produced at high Kr pressures. Whether the observed effects are due to quenching, absorption, or some combination of the two, use of Kr as the *sole* buffer at pressures above approximately one atmosphere apparently introduces processes which, for the present conditions, offset the aforementioned advantages of reduced blue-green absorption in Ar-Kr buffered mixtures.¹

IV. SPECTRAL ANALYSIS

Although the primary effect of an XeF(*C* → *A*) buffer gas comprised of both Ar and Kr appears to be a reduction of absorption in the blue-green region, spectral analysis of laser mixtures has revealed other beneficial effects. Presented in Fig. 4 are time-integrated fluorescence spectra for an *e*-beam excited XeF(*C* → *A*) laser mixture for various values of Kr pressure. Aside from the expected appearance of the 248 nm KrF(*B* → *X*) fluorescence, examination of Fig. 4(a)-(d) reveals other interesting features. Upon addition of 50 Torr Kr, the XeF(*B* → *X*) fluorescence decreases significantly, but there is no measurable change in the value of the peak XeF(*C* → *A*) fluorescence near 480 nm. Certainly, Kr addition at the level indicated changes the XeF(*B*, *C*) precursors as described previously, and introduces the *possibility* of additional loss processes as well. However, for an Ar pressure of 6 atm the XeF *B* and *C* states are collisionally coupled and therefore their populations should either increase or decrease together in response to changes in XeF formation or loss processes due to the presence of Kr. One explanation for the decrease and then leveling off of the time integrated XeF(*B* → *X*) fluorescence as Kr is added (Fig. 4(a)-(d)) is enhanced *B*-*C* mixing. Since >95 percent of the XeF(*B*, *C*) population is in the *C* state for the condi-

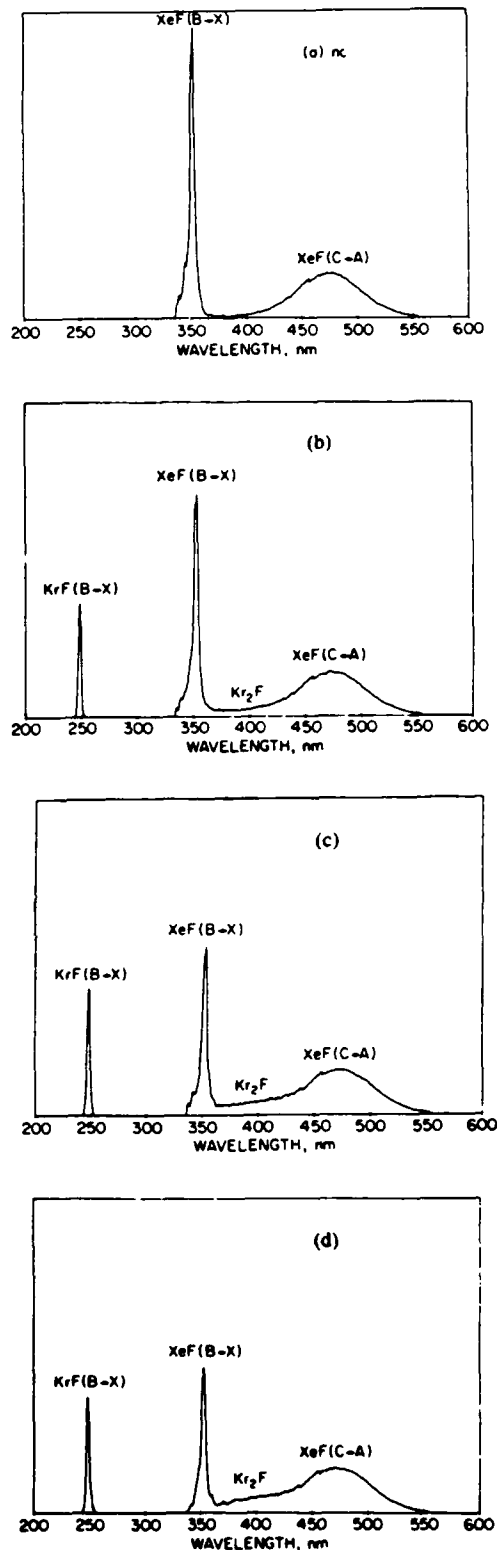


Fig. 4. Time integrated fluorescence spectra for *e*-beam excited mixtures comprised of 6 atm Ar, 8 torr Xe, 8 torr NF₃, and 1 torr F₂ (a), and the same mixture with 50 torr Kr added (b), 200 torr Kr (c), and 400 torr Kr (d). All spectra were corrected for the response of the detection system as described in the text. The Ar₂F concentration may be substantial for certain of these mixture conditions. However, the spectral sensitivity of the detection system is very low for wavelengths below ~350 nm, so that the intensity of the broad-band 280 nm Ar₂F fluorescence is on the order of the experimental noise. The Ar₂F fluorescence is clearly visible in high pressure Ar/F₂ mixtures [19].

¹J. D. Campbell, C. H. Fisher, and R. E. Center, *Appl. Phys. Lett.*, vol. 37, p. 348, 1980. The authors found that use of 1 atm Kr instead of 2 atm Ar as the buffer for an *e*-beam excited XeF(*C* → *A*) laser resulted in increased laser energy, an effect attributed to a lower level of broad-band absorption in the Kr-buffered mixture. However, in that work the *e*-beam current density was more than an order of magnitude less than that of the present work, and the duration of the *e*-beam pulse was about two orders of magnitude longer, factors resulting in medium characteristics very different and output energy levels very much less than those of the present investigation.

tions of Fig. 4, faster *B-C* mixing favoring the *C* state would be observed as a reduction in the *B* → *X* fluorescence intensity, with the XeF(*C*) fluorescence (population) remaining essentially unchanged. Krypton is known to be much more effective than Ar in driving the coupled XeF(*B*, *C*) manifolds towards equilibrium [17], and comparison of Fig. 4(a) and (b) suggests that this effect of Kr may be significant even for an Ar pressure of 6 atm and an Ar-Kr ratio of ~ 100 : 1.

A. Kr₂F Kinetics

Fig. 4 also shows a distinct change in the nature of the spectra between 375 and 425 nm as the Kr pressure is increased. This feature is not caused by a change in the XeF(*C* → *A*) spectra but, rather, results from the gradual development of broadband Kr₂F fluorescence centered at ~ 400 nm [19]. Presented in Fig. 5 are spectra for conditions similar to those of Fig. 4(c), but with the Xe pressure varied. In the absence of Xe the Kr₂F fluorescence is clearly apparent [Fig. 5(a)]. Indeed, the mixture of Fig. 5(a) is essentially the same as that found to be optimum for *e*-beam excitation of the Kr₂F laser [20]. However, addition of as little as 1 torr Xe [Fig. 5(b)] significantly alters the spectrum with the appearance of both 351 nm XeF(*B* → *X*) and XeF(*C* → *A*) fluorescence, the latter overlapping the Kr₂F fluorescence to produce a nearly constant spectral intensity extending from 375–500 nm. The significant decrease in the magnitude of the Kr₂F fluorescence when only 1 torr of Xe is added reflects the large rate coefficient ($> 10^{-10} \text{ s}^{-1} \text{ cm}^3$) for Kr₂F quenching by Xe [21]. Nonetheless, the Kr₂F number density is comparable to that of XeF(*C*) for optimum XeF(*C* → *A*) laser conditions [8], $\sim 5 \times 10^{15} \text{ cm}^{-3}$. Fig. 6 shows the dependence of the peak Kr₂F population on Kr pressure for conditions similar to those of Fig. 4, estimated on the basis of fluorescence data and assuming a 200 ns lifetime [19] for Kr₂F.

1) *Kr₃F Formation*: Very recent measurements [22] have shown that the four-atomic rare gas-halide exciplex Ar₃F is stable and is readily formed from Ar₂F in Ar-F₂ and Ar-NF₃ *e*-beam excited mixtures at pressures ≤ 1 atm. Since the binding energy of Kr₃⁺ is somewhat larger than that of Ar₃⁺ (0.22 eV), this new finding suggests that Kr₃F formation may have an important bearing on the Kr₂F population in the present experiment. Indeed, we believe that the leveling off of the Kr₂F number density as the Kr pressure is increased above ~ 100 torr (Fig. 6) is the result of three-body quenching of Kr₂F, probably resulting in the formation of Kr₃F. The trend exhibited by the data of Fig. 6 is consistent with a rate coefficient of $\sim 10^{-31} \text{ s}^{-1} \text{ cm}^6$ for the reaction, $\text{Kr}_2\text{F} + \text{Kr} + \text{Ar} \rightarrow \text{Kr}_3\text{F} + \text{Ar}$. Based on this interpretation, it seems likely that $\text{Rg}_2\text{X} \rightleftharpoons \text{Rg}_3\text{X}$ kinetics may play a significant role for conditions typical of many rare-gas halide lasers. Additionally, it appears that all prior measurements of Rg_2X rate coefficients, lifetimes and other phenomena dependent on interpretation of Rg_2X collision processes should be reexamined in light of this development.

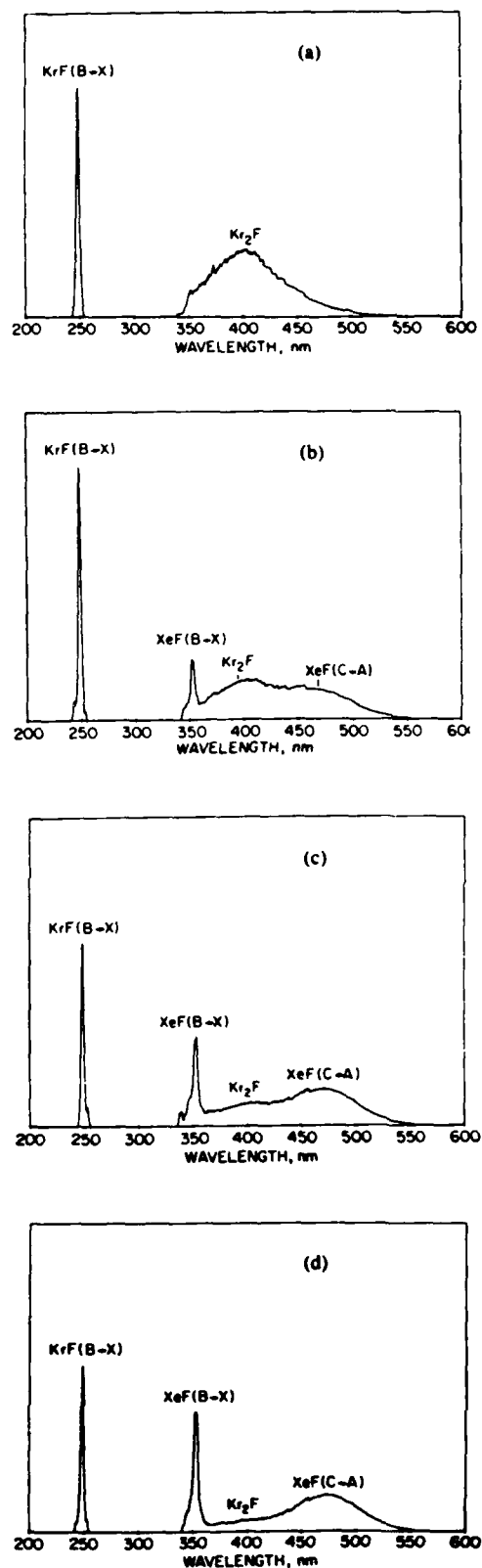


Fig. 5. Time-integrated fluorescence spectra for a mixture comprised of 6 atm Ar, 200 torr Kr, 8 torr NF₃, and 1 torr F₂ (a), and the same mixture with 1 torr Xe added (b), 3 torr Xe (c), and 8 torr Xe (d). Note that the relative intensities of the *B* → *X* KrF and XeF fluorescence should be the same in Fig. 4(c) and Fig. 5(d) for which the experimental conditions are the same. However, the calibration correction applied to the OMA data is very large in the UV so that the absolute KrF(*B* → *X*) intensity levels of Figs. 4 and 5 are rather uncertain.

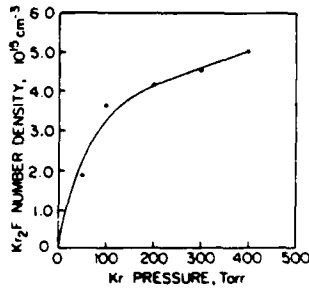


Fig. 6. Dependence of the peak Kr_2F population on Kr pressure estimated for conditions typical of those of Fig. 4.

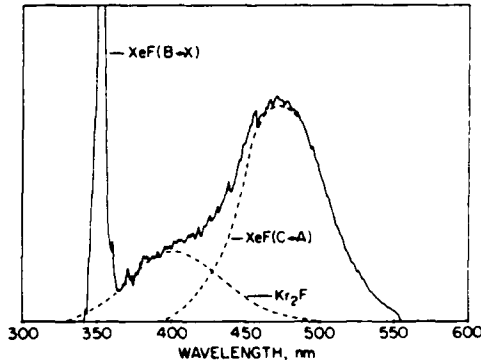


Fig. 7. Time-integrated fluorescence spectra for the conditions of Fig. 4(d) indicating the individual contributions of Kr_2F and $XeF(C \rightarrow A)$.

2) Kr_2F Effect on Blue-Green Gain: Presented in Fig. 7 is an enlarged version of Fig. 4(d) in which are indicated the Kr_2F and $XeF(C \rightarrow A)$ contributions to the time-integrated fluorescence in the 300–600 nm region. The fact that the $XeF(C)$ and Kr_2F populations are comparable in $XeF(C \rightarrow A)$ mixtures containing Kr suggests that Kr_2F may be making a contribution to the gain on the short wavelength side of the laser spectrum. However, the broader spectral width, longer natural lifetime, and shorter wavelength of Kr_2F compared to $XeF(C \rightarrow A)$ results in a stimulated emission cross section that we estimate to be only $\sim 2.5 \times 10^{-18} \text{ cm}^2$ at its peak at 400 nm, a value approximately one fourth that of the $XeF(C \rightarrow A)$ transition. Thus, any influence of Kr_2F on the gain for the wavelengths $\leq 480 \text{ nm}$ must be quite small.

Other factors also have to be considered, however. Fig. 8 presents the temporal evolution of both the Kr_2F and $XeF(C \rightarrow A)$ fluorescence spectra, showing that the peak in the Kr_2F fluorescence precedes that of $XeF(C \rightarrow A)$ by 15–20 ns. Therefore, even though its stimulated emission cross section is small, a large Kr_2F population favors an earlier buildup of gain for wavelengths to the short wavelength side of the $XeF(C \rightarrow A)$ gain maximum. For example, based on the data of Figs. 7 and 8 we estimate that the Kr_2F contribution to the peak gain at $\sim 450 \text{ nm}$ could be as high as 10 percent. Such an effect could be significant when the $C \rightarrow A$ gain medium is used as a wavelength tuned amplifier [12], [23]. This line of reasoning suggests that any increase in the gain of the $XeF(C \rightarrow A)$ laser medium due to the presence of Kr_2F should be ob-

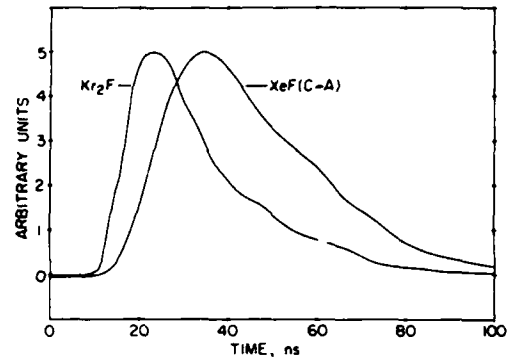


Fig. 8. Normalized temporal evolution of the Kr_2F and $XeF(C \rightarrow A)$ fluorescence spectra for the conditions of Fig. 4(d) and Fig. 7.

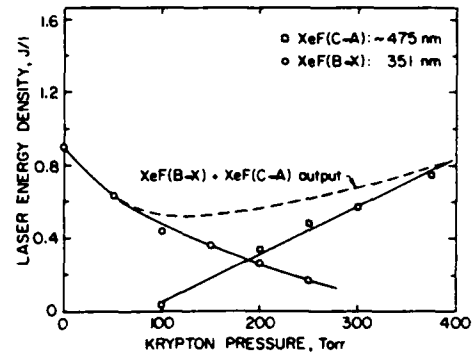


Fig. 9. Measured laser pulse energy density for the simultaneously occurring $B \rightarrow X$ and $C \rightarrow A$ XeF excimer transitions in an e -beam excited mixture comprised of 6.5 atm Ar, 8 torr Xe, 8 torr NF_3 , 1 torr F_2 , and variable Kr pressure. The e -beam energy deposition was approximately 135 J/l.

servable only on the short wavelength side of the laser spectrum. In fact, comparison of free-running laser spectra for Ar and Ar-Kr buffered mixtures shows a ~ 50 percent greater increase in the $XeF(C \rightarrow A)$ laser intensity around 470 nm than at 490 nm when Kr is added [11].

V. SIMULTANEOUS UV/VISIBLE LASER OSCILLATION

Although more than 95 percent of the total $XeF(B, C)$ population resides in the C state for the conditions of primary interest to us, since the stimulated emission cross section [1] for $XeF(B \rightarrow X)$ is $3\text{--}4 \times 10^{-16} \text{ cm}^2$, the intense pumping required to produce adequate $XeF(C \rightarrow A)$ net gain usually results in even larger transient gain at the $XeF(B \rightarrow X)$ 351 nm wavelength. Thus, even though steps can be taken in the design of the $C \rightarrow A$ cavity to minimize the possibility of $B \rightarrow X$ oscillation, the $B \rightarrow X$ gain is frequently so high that amplified stimulated emission of the $B \rightarrow X$ transition occurs thereby depleting the gain on the desired $C \rightarrow A$ transition.

In earlier work [24] we took advantage of this characteristic in order to demonstrate the feasibility of simultaneous UV/visible laser oscillation on both the $B \rightarrow X$ and $C \rightarrow A$ transitions of the XeF excimer. However, the dual wavelength cavity used was far from optimum so that very low levels of laser energy and efficiency were obtained. Recently [13], these dual wavelength laser experiments

were repeated with two important differences: 1) a cavity optimized for laser oscillation at 351 nm and at 480 nm was used, and 2) Kr was added to Ar to form a two component buffer mixture as in the work described herein. The cavity was comprised of a mirror having nearly total reflectivity in the UV and blue-green regions, and a multiple coating out-coupler having a transmission of 20 percent at ~ 350 nm and 10 percent between 460 and 510 nm. Fig. 9 presents the measured laser pulse energy densities for the UV and blue-green transitions of XeF as a function of Kr pressure, obtained using this dual wavelength cavity for conditions otherwise similar to those of Figs. 3-8. With no Kr in the mixture and using a $C \rightarrow A$ cavity alone, previously these conditions resulted in $C \rightarrow A$ laser pulses having an energy density of approximately 1 J/l [11]. However, Fig. 9 shows that when the optimized dual-wavelength cavity is used, no $C \rightarrow A$ laser oscillation is observed in the absence of Kr, but the $B \rightarrow X$ transition oscillates with an output pulse energy density of ~ 1 J/l, a relatively high energy density level considering that the mixture used is very different from that found to be optimum for the XeF ($B \rightarrow X$) laser, [3], [25]. Addition of Kr results in an immediate decrease in $B \rightarrow X$ output, followed by simultaneous oscillation of the UV and visible transitions, and eventually $C \rightarrow A$ oscillation alone for Kr pressures above ~ 300 torr.

A. UV Absorption

The decrease in $B \rightarrow X$ laser energy (Fig. 9) upon addition of Kr is the result of a reduction in the XeF(B) population relative to that of XeF(C) as discussed previously [Fig. 4(a)-4(d)] and, perhaps more significantly, because of the likelihood of a strong increase in absorption at ~ 351 nm due to the presence of Kr₂F. Calculations of the low-lying states of Ar₂F and Kr₂F have shown that the presence of F⁻ has a negligible effect on the states of Ar₂⁺ and Kr₂⁺, respectively [26]. For this reason, the strong near UV absorption of the rare gas dimer ions [27] should carry over directly to the triatomic rare gas-halides. Since the dominant absorption of Kr₂⁺ has a cross section of $\sim 4 \times 10^{-17}$ cm² at the 351 nm wavelength of the XeF($B \rightarrow X$) transition [27], the Kr₂F population estimates of Fig. 6 indicate that a Kr partial pressure as low as 50 torr is likely to result in a very significant Kr₂F contribution to absorption at 351 nm. We feel that this is the primary cause of the decrease in XeF($B \rightarrow X$) laser output as Kr is added (Fig. 9). This trend continues as Kr pressure is increased and for Kr pressures above about 150 torr, for which the presence of Kr results in a reduction in absorption in the blue-green region, significant laser output is obtained from the $C \rightarrow A$ transition. For Kr pressure between about 150-250 torr combined UV/visible output in excess of 0.5 J/l is obtained using the cavity optimized at both the $B \rightarrow X$ and $C \rightarrow A$ wavelengths, corresponding to an intrinsic efficiency of ~ 0.4 percent. However, as the Kr pressure is increased above ~ 300 torr, for which optimum $C \rightarrow A$ performance has been demonstrated [11], the $B \rightarrow X$ output decreases to a very

very low level. For this condition the beneficial influence of Kr on $C \rightarrow A$ laser performance is at its maximum, while the peak absorption at 351 nm due to Kr₂F is estimated on the basis of the Kr₂⁺ absorption cross section to be on the order of 10 percent cm⁻¹. In view of the fact that the cavity used for this demonstration was specifically designed to support XeF($B \rightarrow X$) oscillation (Fig. 9), we interpret these results as evidence that the two component Ar-Kr buffer used to optimize XeF($C \rightarrow A$) laser performance alone, when used with $C \rightarrow A$ optics, significantly reduces the possibility of competitive oscillation on the parasitic $B \rightarrow X$ transition, a particularly important consideration for the design of efficient XeF($C \rightarrow A$) lasers.

VI. SUMMARY

The findings of this investigation show that use of Ar and Kr together to form synthesized rare gas buffer properties results in unique XeF($C \rightarrow A$) laser medium characteristics not attainable using either species alone. All aspects of the medium are affected by the two-component buffer, including: XeF(B, C) formation and quenching; B, C state vibrational relaxation and mixing; and transient absorption in both the UV and blue-green spectral regions. For this reason use of two rare gas components to form the buffer introduces an extra element of flexibility and control as regards optimization of laser medium characteristics, with no penalty in the area of system complexity. Indeed, *e*-beam excited XeF($C \rightarrow A$) media optimized on the basis of the two-component buffer described herein have resulted in levels of blue-green laser pulse energy density and intrinsic efficiency rivaling those of UV RGH lasers, with the added element of broad-band tunability [11], [12], [23].

Although the present work is focused on *e*-beam excited XeF($C \rightarrow A$) laser media, there is no apparent reason why other RGH lasers using either *e*-beam or discharge excitation cannot be improved by increasing the number of mixture constituents beyond the usual three. Preliminary evidence supporting this conclusion is provided by our recent demonstration [28] of simultaneous laser oscillation on the KrF (248 nm) and XeF(351) RGH transitions and on the ArF(193 nm) and KrF (248 nm) transitions using discharge excitation of nonoptimized mixtures comprised of He, Kr, Xe, and F₂, and He, Ar, Kr, and F₂, respectively. In that work XeF $B \rightarrow X$ laser oscillation at 351 and KrF oscillation at 248 nm were demonstrated separately at pulse energy levels only slightly less than the highest obtainable using optimized three component mixtures in the same device. Thus, considering the complexity of the kinetics of these systems and the fact that no attempt was made to optimize the four component mixtures, there is reason to believe that the efficiency of UV RGH lasers may be further improved through use of four (or more) component gas mixtures once optimum mixtures and complementary pumping levels and cavity properties are identified.

ACKNOWLEDGMENT

The skillful experimental assistance of B. Zook, J. Kinross-Wright, and J. Hooten is gratefully acknowledged.

REFERENCES

- [1] M. Rokni and J. H. Jacob, "Rare gas halide lasers," in *Applied Atomic Collision Physics: Volume 3, Gas Lasers*, H. S. W. Massey, E. W. McDaniel, and B. Bederson, Eds. New York: Academic, 1982, ch. 10.
- [2] C. Brau, "Rare gas halogen excimers," in *Topics in Applied Physics: Volume 30, Excimer Lasers*, 2nd ed., by C. K. Rhodes, Ed. New York: Springer-Verlag, 1984, ch. 4.
- [3] A. E. Mandl and H. A. Hyman, "XeF laser performance for F₂ and NF₃ fuels," *IEEE J. Quantum Electron.*, vol. QE-22, pp. 349-359, Feb. 1986.
- [4] H. Pummer, "The excimer laser: 10 years of fast growth," *Photon. Spectra.*, vol. 19, pp. 73-82, 1985.
- [5] W. H. Long, Jr., M. J. Plummer, and E. A. Stappaerts, "Efficient discharge pumping of an XeCl laser using a high-voltage prepulse," *Appl. Phys. Lett.*, vol. 43, pp. 735-737, 1983.
- [6] D. E. Klimek, J. C. Hsia, J. H. Jacob, D. W. Trainor, C. Duzy, and H. A. Hyman, "Kinetic issues for short-pulse KrF laser operation," *IEEE J. Quantum Electron.*, vol. QE-17, pp. 1847-1855, 1981.
- [7] F. Kannari, A. Suda, M. Obara, and T. Fujioka, "Theoretical evaluation of electron-beam-excited KrF lasers using argon-free mixtures of one atmosphere," *Appl. Phys. Lett.*, vol. 45, pp. 305-307, 1984.
- [8] Y. Nachshon, F. K. Tittel, W. L. Wilson, Jr., and W. L. Nighan, "Efficient XeF(C → A) laser oscillation using electron-beam excitation," *J. Appl. Phys.*, vol. 56, pp. 36-48, 1984.
- [9] T. Gerber, P. J. M. Peters, H. M. J. Bastiaens, and W. J. Witteman, "Enhancement of the specific output energy of an electron-beam pumped KrF laser by using Ne as the main buffer gas," *Appl. Phys. Lett.*, vol. 45, pp. 356-357, 1984.
- [10] B. M. H. H. Kleikamp, P. J. M. Peters, and W. J. Witteman, "An investigation of the role of Ne, Ar, and Kr as buffer gas in a coaxial e-beam pumped KrF laser," *IEEE J. Quantum Electron.*, vol. QE-22, pp. 219-222, Feb. 1986.
- [11] W. L. Nighan, F. K. Tittel, W. L. Wilson, Jr., N. Nishida, Y. Zhu, and R. A. Sauerbrey, "Synthesis of rare gas-halide mixtures resulting in efficient XeF(C → A) laser oscillation," *Appl. Phys. Lett.*, vol. 45, pp. 947-948, 1984.
- [12] F. K. Tittel, G. Marowsky, W. L. Nighan, Y. Zhu, R. A. Sauerbrey, and W. L. Wilson, Jr., "Injection controlled tuning of an electron-beam excited XeF(C → A) laser," *IEEE J. Quantum Electron.*, vol. QE-22, pp. 2168-2173, Nov. 1986.
- [13] R. A. Sauerbrey, F. K. Tittel, W. L. Wilson, Jr., Y. Zhu, N. Nishida, and W. L. Nighan, "Efficient simultaneous multiwavelength UV/visible operation of excimer lasers," presented at CLEO 1985, Baltimore, MD.
- [14] L. A. Gundel, D. W. Setser, M. A. A. Clyne, J. A. Coxon, and W. Nip, "Rate constants for specific product channels from metastable Ar(³P_{2,0}) reactions and spectrometer calibration in the vacuum ultraviolet," *J. Chem. Phys.*, vol. 64, pp. 4390-4410, 1976.
- [15] W. K. Bischel, D. J. Eckstrom, H. C. Walker, Jr., and R. A. Tilton, "Photolytically pumped XeF(C → A) laser studies," *J. Appl. Phys.*, vol. 52, pp. 4429-4434, 1981.
- [16] J. H. Kolts and D. W. Setser, "Decay rates of Ar(4s, ³P₂), Ar(4s, ³P₀), Kr(5s, ³P₂), and Xe(6s, ³P₂) atoms in argon," *J. Chem. Phys.*, vol. 68, pp. 4848-4859, 1978.
- [17] H. C. Brashears, Jr. and D. W. Setser, "Transfer and quenching rate constants for XeF(B) and XeF(C) states in low vibrational levels," *J. Chem. Phys.*, vol. 76, pp. 4932-4946, 1982.
- [18] H. C. Brashears, Jr., D. W. Setser, and Y. C. Yu, "Emission spectra of KrXeCl*, KrXeBr*, KrXeI*, ArKrF*, and ArKrCl*," *J. Chem. Phys.*, vol. 74, pp. 10-17, 1981.
- [19] D. L. Huestis, G. Marowsky, and F. K. Tittel, "Triatomic rare-gas-halide excimers," in *Topics in Applied Physics: Volume 30, Excimer Lasers*, 2nd ed., C. K. Rhodes, Ed. New York: Springer-Verlag, 1986, ch. 6.
- [20] F. K. Tittel, M. Smayling, W. L. Wilson, Jr., and G. Marowsky, "Blue laser action by the rare gas halide trimer Kr₃F," *Appl. Phys. Lett.*, vol. 37, pp. 862-864, 1980.
- [21] R. A. Sauerbrey, F. K. Tittel, W. L. Wilson, Jr., and Y. Zhu, "The α₂ placement reactions of the triatomic rare gas halide excimers," *J. Chem. Phys.*, vol. 82, pp. 2507-2508, 1985.
- [22] R. A. Sauerbrey, Y. Zhu, F. K. Tittel, and W. L. Wilson, Jr., "Optical emission and kinetic reactions of a four-atomic rare gas halide excimer: Ar₄F," *J. Chem. Phys.*, vol. 85, pp. 1299-1302, 1986.
- [23] G. Marowsky, N. Nishida, H. Stiegler, F. K. Tittel, W. L. Wilson, Jr., Y. Zhu, and W. L. Nighan, "Efficient narrow spectral output in the blue-green region from an injection-controlled electron-beam excited XeF(C → A) laser," *Appl. Phys. Lett.*, vol. 41, pp. 657-660, 1985.
- [24] R. A. Sauerbrey, Y. Zhu, F. K. Tittel, W. L. Wilson, Jr., N. Nishida, F. Emmert, and W. L. Nighan, "Simultaneous UV/visible laser oscillation on the B → X and C → A XeF excimer transitions," *IEEE J. Quantum Electron.*, vol. QE-21, pp. 418-420, May 1985.
- [25] J. C. Hsia, J. A. Mangano, J. H. Jacob, and M. Rokni, "Improvement in XeF laser efficiency at elevated temperatures," *Appl. Phys. Lett.*, vol. 34, pp. 208-210, 1979.
- [26] W. R. Wadt and P. J. Hay, "Electronic states of Ar₂F and Kr₂F," *J. Chem. Phys.*, vol. 68, pp. 3850-3863, 1978.
- [27] H. H. Michels, R. H. Hobbs, and L. A. Wright, "Visible photoabsorption by noble-gas trimer ions," *Appl. Phys. Lett.*, vol. 35, pp. 153-155, 1979.
- [28] R. A. Sauerbrey, W. L. Nighan, F. K. Tittel, W. L. Wilson, Jr., and J. Kinross-Wright, "Simultaneous multiwavelength operation of a commercial rare gas halide laser," *IEEE J. Quantum Electron.*, vol. QE-22, pp. 230-233, Feb. 1986.

Performance Characteristics of an Injection-Controlled Electron-Beam Pumped XeF($C \rightarrow A$) Laser System

NAOYA HAMADA, ROLAND SAUERBREY, MEMBER, IEEE,
WILLIAM L. WILSON, JR., SENIOR MEMBER, IEEE,
FRANK K. TITTEL, FELLOW, IEEE, AND
WILLIAM L. NIGHAN, SENIOR MEMBER, IEEE

Abstract—Characteristics of an injection-controlled electron-beam pumped XeF($C \rightarrow A$) laser have been investigated with emphasis on *efficient* wide-band tuning and scaling issues. Using a quasi-CW dye laser as an injection source, data were obtained that describe the laser characteristics over a wide parameter range. A high Z electron-beam backscattering reflector inside the laser reaction cell improved the electron-beam energy deposition by 40 percent, resulting in an increase of the amplified laser output by more than a factor of four. *Efficient* and *continuous* wavelength tuning between 470 and 500 nm has been achieved with an output energy density of ~ 1 J/l, and an intrinsic efficiency of ~ 1 percent throughout the entire tuning region.

I. INTRODUCTON

A wide-band and continuous wavelength tuning characteristics in the visible spectral region is a desirable optical source for many diverse applications ranging from optical communications to laser spectroscopy. The XeF($C \rightarrow A$) excimer transition exhibits an exceptionally broad-band fluorescence spectrum in the blue-green, and has the potential to meet such laser requirements. Free-running stable laser oscillators operating on the XeF($C \rightarrow A$) transition typically exhibit a broad laser spectrum (~ 20 nm, FWHM) centered near 485 nm [1]. Such an XeF($C \rightarrow A$) laser has also been tuned from about 450 to 510 nm with a spectral width on the order of a few nanometers, albeit with very low efficiency [2]–[4]. More recently, *efficient* and narrow spectral width (0.001–0.01 nm) operation of the XeF($C \rightarrow A$) laser has been achieved for wavelengths near 480 nm by using injection-control [5], [6]. In that work, the tuning was neither continuous nor *efficient*, due in part to the presence of transient absorbing species [7] which give rise to broadband absorption and to narrow line absorption corresponding to transitions in the rare-gas atoms. The very high saturation intensity ($>$

10^6 W/cm²) of the XeF($C \rightarrow A$) transition, due primarily to its small stimulated emission cross section ($\sim 10^{-17}$ cm²), indicated, however, that the transient absorption might be saturable through the use of a strong injection photon flux [8].

Our previous work [6] was hampered by a limited database because of the uncertainty between the timing of the injection laser pulse and the electron-beam pulse, each having a temporal duration of approximately 10 ns, a value less than the inherent jitter of the electron-beam generator (~ 50 ns). Also, in those studies, the electron-beam energy deposition in the laser cell was kept constant. Thus, the relationship among excitation rate, small-signal gain, and laser output was not completely characterized. It is important that these relationships be understood in order to realize higher output energy levels and/or higher efficiency through system scaling.

This paper describes the following new experimental results: 1) injection control of an XeF($C \rightarrow A$) laser using a long pulse quasi-CW injection source, 2) *efficient* and *continuous* tuning over a 30 nm wavelength range, 3) scaling of the injection-controlled XeF($C \rightarrow A$) laser performance with pumping power, and 4) initial geometric scaling of the XeF($C \rightarrow A$) laser.

The details of the experimental arrangement and related diagnostics are described in Section II. In Section III, experimental results are presented along with a discussion of prospects for further improvement in XeF($C \rightarrow A$) laser performance.

II. EXPERIMENT

A. Electron-Beam Excitation System and Reaction Cell

The experimental setup used in this study is shown in Fig. 1. A Physics International Pulserad 110 electron-beam generator was used to transversely excite the high-pressure laser gas mixture through a metal foil. The electron-beam energy was 1 MeV, and the excitation pulse duration was 10 ns (FWHM). In order to obtain a maximum foil lifetime, a stainless steel wire mesh was mounted as an anode between the electron-beam cathode and the foil. The electron-beam cathode length used for most of the experiments was 7.6 cm. A 15.2 cm long

Manuscript received January 4, 1988. This work was supported in part by the Office of Naval Research, the National Science Foundation and the Welch Foundation. The work of N. Hamada was supported by the Nippon Steel Corporation.

N. Hamada, R. Sauerbrey, W. L. Wilson, Jr., and F. K. Tittel are with the Department of Electrical and Computer Engineering, Rice University, Houston, TX 77251.

W. L. Nighan is with United Technologies Research Center, East Hartford, CT 06108.

IEEE Log Number 8821712.

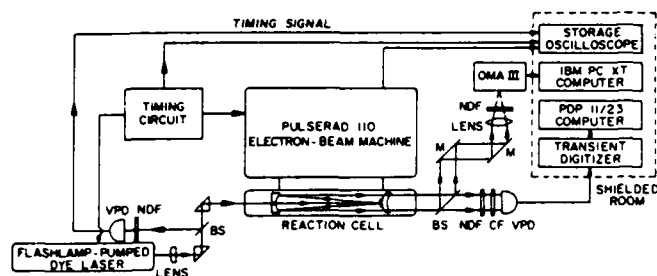


Fig. 1. Schematic illustration of the experimental setup, showing the unstable cavity optics inside the reaction cell, the tunable injection laser, and the timing and data acquisition systems. OMA: optical multichannel analyzer, VPD: vacuum photodiode, CF: color glass filter, NDF: neutral density filter, BS: beam splitter, M: total reflection mirror.

cathode was used in order to investigate the scaling of the laser output with increased pumping length. To vary the electron-beam excitation level of the laser gas mixture, various foil conditions and anode-cathode spacing values were employed. Typically, a $50\ \mu\text{m}$ nickel-plated titanium foil was used. In order to reduce the electron-beam energy deposition, a $50\ \mu\text{m}$ inconel foil was also employed in some of the experiments. Due to the higher atomic number of inconel compared to titanium, the scattering angle of the electrons passing through the foil is increased, resulting in a reduced energy deposition. Therefore, a combination of foils was adopted for further reduction of the energy deposition. It is possible to achieve a 40 percent energy reduction with an inconel foil, and a 65 percent energy reduction with a combination of both foils compared to the energy deposition value obtained using only a titanium foil. In addition, the anode-cathode spacing in the electron-beam diode could be changed in order to vary the current density available inside the laser cell.

Improved electron-beam energy deposition was achieved by means of an electron-beam backscattering reflector or so-called *concentrator* [9]. The concentrator was made of lead in order to obtain good backscattering of the electron beam. Its inner shape was concentric with the cavity optical axis surrounding the active volume as illustrated in Fig. 2. To avoid chemical reactions between lead and fluorine, the concentrator was nickel plated. The thickness of the nickel plating was about $1\ \mu\text{m}$, which is small compared to the typical penetration depth of 1 MeV electrons in nickel or lead. Therefore, the backscattering behavior of the device is governed by the high atomic number of lead and not by the surface material.

Current density values on the optical axis (2.3 cm from the foil) at an argon pressure of 6.5 atm were measured without the concentrator using a Faraday cup probe. The peak current density varied from ~ 100 to $\sim 290\ \text{A}/\text{cm}^2$, depending upon the foil material and the anode-cathode spacing. The energy deposition into the laser medium with the concentrator in place was measured on the optical axis using chlorostyrene film [10]. The deposition value was obtained by measuring the optical density of the irradiated film with an He-Ne laser. The dynamic range of these films extends over more than two orders of magnitude.

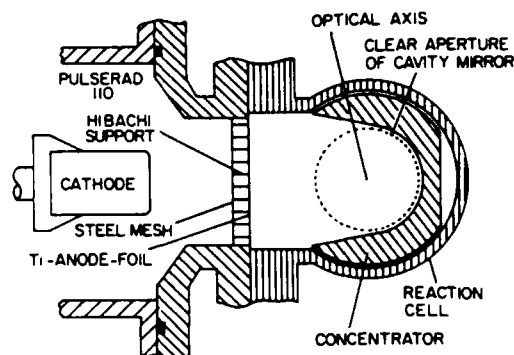


Fig. 2. Schematic representation of a transverse section of the electron-beam pumping region with the concentrator in place.

The average energy deposition density over the active pumping length along the optical axis, estimated to be $\sim 10\ \text{cm}$, ranged from ~ 37 to $\sim 112\ \text{J}/\text{l}$, depending upon which electron-beam coupling foil was used.

High-purity research grade laser gases (NF_3 , He-10 percent F_2 , Xe, Kr, and Ar) were used as source materials. The typical gas composition was 8 torr NF_3 , 1 torr F_2 , 8 torr Xe, 300 torr Kr, and 6.1 atm Ar, for a total pressure of $\sim 6.5\ \text{atm}$ [6], [7], [11]. Good mixing of the different gas components was achieved by rapid turbulent flow as each high-pressure gas component was introduced into the reaction cell. Each fresh gas mixture could be used for about ten shots without significant degradation of the laser performance. Nickel plating of the concentrator and the titanium foil considerably increased the lifetime of the laser gas mixture, and contributed to the reproducibility of the experiments. This will be of particular importance in scaled versions of this laser that require gas flow systems. The stainless steel reaction cell and the concentrator were well passivated by prolonged exposure to fluorine prior to any experiments.

B. Injection-Control System

The aforementioned timing uncertainty in earlier experiments between the injection laser pulse and firing of the electron beam was eliminated by replacing the 10 ns excimer-pumped dye laser used previously [6], with a long pulse (250 ns) coaxial flashlamp-pumped dye laser. A Phase-R dye laser system (DL-1200VT) having a spectral width of $\sim 0.6\ \text{nm}$ was used as the injection laser. Operated with an LD490 dye, the system can deliver an output pulse of $\sim 40\ \text{mJ}$ over the 470–500 nm wavelength range, in a 250 ns pulse (FWHM), with a beam diameter of 2.6 mm and beam divergence of $\sim 1.5\ \text{mrad}$. The long pulse duration of this laser ensured good temporal overlap of the injection signal and electron-beam firing. A 1 m focal length plano-convex lens was used to reduce the injection beam diameter from 2.6 to 1.5 mm so that most of the available dye laser pulse energy entered the unstable resonator located inside the reaction cell (Fig. 1). A beam splitter on the injection optical axis allowed observation of the backreflected beam from the laser cavity using a fast vacuum photodiode detector (Hamamatsu R1193U-03). Due to the low damage threshold of the optics coat-

ings used in the present investigation, the energy of the injected signal was limited to a maximum value of ~ 5 mJ (~ 0.3 J/cm²).

C. Diagnostics

The temporal evolution of the free-running laser (without injection), the dye laser throughput, and the injection-controlled XeF($C \rightarrow A$) laser output were monitored using a fast vacuum photodiode detector (ITT F4000(S5)). Neutral density filters were used to avoid saturation of the photodiode, and a color glass filter was used to define the spectral region of interest. Signals were recorded by a Tektronix R7912AD transient digitizer. The time resolution of the system was better than 2 ns. For an absolute energy measurement, this system was calibrated with the dye laser and a pyroelectric energy detector (Gentec ED-200). As a further check of the calibration procedure, the XeF($C \rightarrow A$) laser output energy was sometimes directly measured by the pyroelectric energy detector. With this system, we estimate the absolute accuracy of the measured laser energy to be ± 20 percent.

The temporally integrated, spectrally resolved laser output was recorded by an optical multichannel analyzer (OMAI), using a Jarrell-Ash 0.25 m spectrometer with a spectral resolution of about 0.45 nm. The temporal relationship of the dye laser and electron-beam pulse was monitored by a photodiode-storage oscilloscope combination (Fig. 1).

D. Cavity Optics

The optical cavity used in this study was a positive-branch confocal unstable, intracell resonator, consisting of a concave end mirror with an injection hole of 1.5 mm diameter and a coating having a high reflectivity in the blue-green region, and a convex output coupler (Fig. 1). The role of the cavity was to serve as a beam expanding telescope for a regenerative amplifier [5], [12]. The mirrors, having focal length of f_2 and $-f_1$, respectively, were separated by a distance $L = f_2 - f_1$. The cavity lengths used, $L = 12.5$ cm and $L = 18$ cm, correspond to electron-beam cathode lengths of 7.6 and 15.2 cm, respectively. The magnification of the unstable resonator is given by $M = f_2/f_1$. Various cavities were examined with magnifications of 1.05, 1.08, 1.15, and 1.23 for the 12.5 cm long cavity. A resonator with $M = 1.15$ yielded optimum laser output energy under conditions of high excitation and injection, and was adopted as a standard value. The output coupler was a meniscus lens of zero refraction power having a highly reflective coating spot on the convex side with a diameter $d = 1.4$ cm for $L = 12.5$ cm and $d = 1.5$ cm for $L = 18$ cm. The active region was a cylindrical volume defined by the electron-beam pumping length (~ 10 cm) and a clear aperture having a diameter $d \times M$, i.e., ~ 0.02 l for typical operating conditions.

E. Gain Measurement

The experimental arrangement for measuring the gain was similar to that shown in Fig. 1. However, in this case,

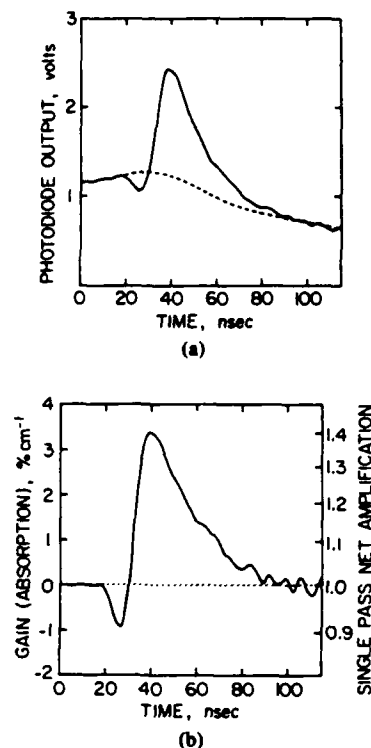


Fig. 3. Temporal evolution of the transmitted probe laser pulse at 478.6 nm (a), and of the XeF($C \rightarrow A$) net gain profile (b). The mixture was comprised of 8 torr NF₃, 1 torr F₂, 8 torr Xe, 300 torr Kr, and 6.1 atm Ar, and the average energy deposition of the electron beam for this condition was 95 J/l. The dashed line in Fig. 3(a) refers to the transmitted probe laser when the electron beam is not fired.

the dye laser was used as a probe laser. The laser intensity was attenuated appropriately for small-signal gain measurement, and then increased in order to investigate gain saturation, while 1 m focal length lens in Fig. 1 was taken out to avoid early gain saturation. The probe beam diameter at the cell was 4 mm. For these experiments, the concave end mirror was removed and the output coupler was replaced with a flat total reflector creating a double path for the probe beam through the cell. The temporal profile of the backreflected probe laser was monitored using the fast vacuum photodiode.

During the dye laser pulse duration (250 ns, FWHM), gain occurs only when the electron beam is fired. Fig. 3(a) shows a typical temporal profile on the transmitted probe laser pulse measured with this arrangement, indicating a superposition of a portion of the total dye laser pulse and the laser absorption/gain characteristic. In order to interpret this profile, the temporal pulse shape of the dye laser has to be determined as shown by the dashed line in Fig. 3(a). By taking the logarithm of the ratio of the laser pulse with and without gain at various times, and dividing by twice the electron-beam pumping length, the temporal gain profile was obtained as shown in Fig. 3(b). Due to the uncertainty of the dashed line fitting in Fig. 3(a), the value of Fig. 3(b) has an uncertainty of $\sim \pm 0.2$ percent/cm. Although there is a slight uncertainty in the determination of the temporal pulse shape of the dye laser, this method permits flexible gain measurements at any wavelength of interest and at any intensity level.

III. EXPERIMENTAL RESULTS AND DISCUSSION

A. Electron-Beam Energy Deposition and Its Effect

In order to study the effect of the concentrator on electron-beam energy deposition, several parameters were investigated. The energy deposited into the laser gas mixture was determined with and without the concentrator. Laser gain and injection-controlled laser output measurements were also performed with and without the concentrator in place. Fig. 4 shows the electron-beam energy deposition measured using overlapping 7.0×1.6 cm chlorostyrene film strips [10]. Electron-beam energy deposition in the cell was measured on the optical axis for an argon pressure of 6.5 atm. This figure shows that the electron-beam deposition profile is not uniform along the optical axis, but strongly peaks at the center of the cell. Due to this inhomogeneity, the electron-beam energy deposition in the optical volume must be averaged. The procedure should include three-dimensional averaging, that is, along the cavity axis, along the vertical direction, and along the horizontal orientation of Fig. 2. By positioning the film strips at various locations in the active volume, it was found that the average value in the vertical plane including the optical axis represents the average energy deposition over the total volume. Thus, *average* energy deposition was determined in this manner.

The average length along the optical axis is taken to be 10 cm, which is the effective aperture length defined by the spacing between the cavity mirror holders. Consequently, the gain characteristic shown in Fig. 3 is the spatially *averaged* profile over the inhomogeneous pumping length. We estimate that the absolute gain coefficient may have a relative error of ~ 20 percent due to the uncertainty of this averaging procedure. Since the gain is a nonlinear function of the pumping energy, the gain spatial distribution will be different from that shown in Fig. 4. Indeed, both experiments and modeling show that, *for our conditions*, the gain saturates for pumping densities over 100 J/l. With the concentrator in position, the energy deposition in the center of the cell exceeds 100 J/l (Fig. 4). Thus, the spatial inhomogeneity of the gain profile is expected to be significantly less than that exhibited by the electron-beam pumping profile. For the specific conditions of Fig. 4, the average energy deposition densities over the 10 cm pumping length with and without the concentrator were 95 and 68 J/l, respectively.

1) *Gain*: The effect of the concentrator on the *peak* gain (Fig. 3) is shown in Fig. 5 as a function of the power density of the probe laser. Gain was measured on the optical axis at a wavelength of 478.6 nm for which the gain is close to its maximum value [6]. The error bar shown in the figure refers to shot-to-shot variations. At low injected powers, the peak gain coefficient is about 3.0 and 3.4 percent/cm without and with the concentrator, respectively, decreasing to values of about 2.6 and 3.0 percent/cm at higher injection powers. These data show an increase in peak gain of only ~ 15 percent, corresponding to an in-

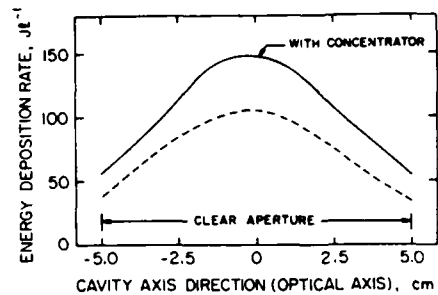


Fig. 4. Electron-beam energy deposition spatial profiles on the optical axis (2.3 cm from the foil) with and without the concentrator for an argon pressure of 6.5 atm. The electron-beam cathode length was 7.6 cm, and the coupling foil was $50 \mu\text{m}$ titanium. For this condition, the *average* energy deposition density was 68 and 95 J/l, without and with the concentrator.

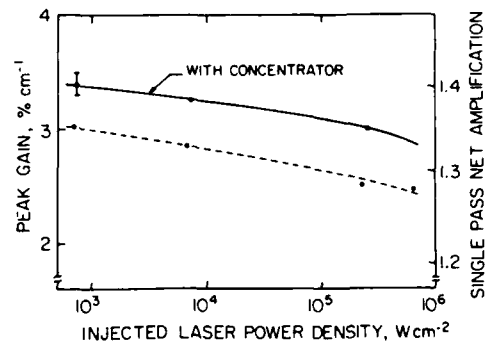


Fig. 5. Comparison of *peak* gain with and without the concentrator at a wavelength of 478.6 nm for a mixture comprised of 8 torr NF_3 , 1 torr F_2 , 8 torr Xe , 300 torr Kr , and 6.1 atm Ar . The solid line refers to the peak gain with the concentrator in place, corresponding to *average* energy deposition of 95 J/l, while the dashed line corresponds to 68 J/l (no concentrator).

crease in average energy deposition from 68 to 95 J/l, i.e., ~ 40 percent. This is a reflection of the onset of the gain saturation as the energy deposition of our 10 ns pulse approaches ~ 100 J/l. Kinetic modeling indicates that this effect is due primarily to electron quenching of $\text{XeF}(B, C)$, which becomes more important as the electron-beam pumping density, and therefore the electron density, increases.

2) *Laser Output Energy*: Fig. 6 shows the output energy of the injection-controlled $\text{XeF}(C \rightarrow A)$ laser as a function of the injection power. Injection input was defined by the power density at the 1.5 mm diameter hole of the concave cavity mirror. Also shown for comparison is the energy injected during the ~ 10 ns period when gain is rising (Fig. 3). At a 1 MW/cm² dye laser input level, the output energy increased by a factor of 4 when the concentrator was used, a reflection of the higher gain (Fig. 5). At the lower injection energy, the increase was even greater since the medium was not saturated. Since the effect of the concentrator was quite dramatic, resulting in a higher energy deposition, higher gain, and therefore larger $\text{XeF}(C \rightarrow A)$ laser output energy, the concentrator was utilized in all of the experiments reported below.

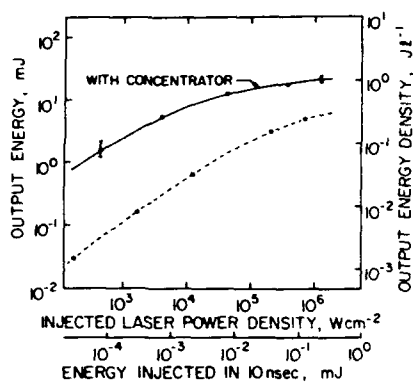


Fig. 6. XeF($C \rightarrow A$) output energy dependence on the injected dye laser power at 478.6 nm with the concentrator (solid line) and without the concentrator (dashed line) using a cavity magnification value of $M = 1.15$.

B. Pump Energy Variation

In order to optimize the intrinsic efficiency and absolute output energy of the laser, the relationship between the pumping power density and laser output must be understood. In order to study this, the electron-beam energy deposition was varied, mainly by altering the composition of the coupling foil as described in Section II-A. Gain and laser output at various injection energy levels were then studied as a function of pumping energy. Fig. 7 shows the dependence of the peak gain at 478.6 nm on electron-beam energy deposition for injection power densities of 350 W/cm^2 and 350 kW/cm^2 , the latter value approximately 10 percent of the saturation intensity. This figure shows the strong dependence of the peak gain on pumping energy, especially for the lower values of the latter. The peak gain tends toward saturation at the higher pumping level as was discussed previously.

The dependence of laser output and intrinsic efficiency on the electron-beam pumping level for a dye laser power density of 360 kW/cm^2 ($64 \mu\text{J}$ in 10 ns) is shown in Fig. 8. For these conditions, the cavity magnification was 1.15, and the injection wavelength was 478.6 nm. Fig. 8 shows typical laser amplification characteristics. Although a high injection power density is applied, there is a linear relationship between pumping power and laser output for low pumping powers, which saturates at higher pumping levels due to the peak gain saturation shown in Fig. 7. With regard to the intrinsic efficiency plotted in the figure, the spatially averaged excitation level of $\sim 90 \text{ J/l}$ was found to be optimum.

C. Geometric Scaling

In order to consider system scaling to achieve higher energy output, it is also important to understand the relationship between pumped volume and laser output. For scaling considerations, it is of particular importance to determine whether the laser output scales with active length and what is the optimum length for an XeF($C \rightarrow A$) amplifier. For this reason, a second pumping length was selected using a 15.2 cm long electron-beam cathode.

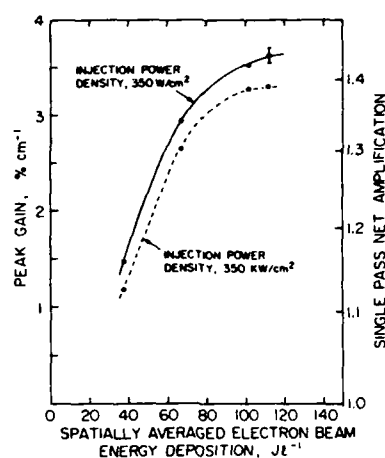


Fig. 7. Peak gain dependence on the electron-beam energy deposition at 478.6 nm for injection power density of 350 W/cm^2 (solid line, 440 nJ in 10 ns) and 350 kW/cm^2 (dashed line, $440 \mu\text{J}$ in 10 ns).

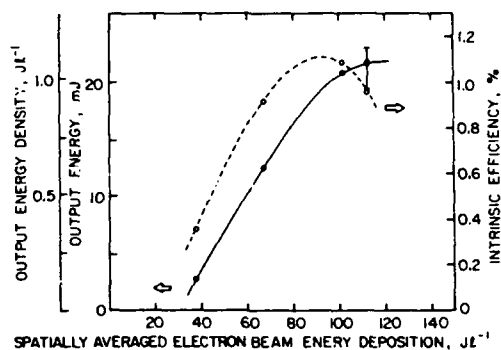


Fig. 8. Laser output and intrinsic efficiency dependence on the electron-beam pumping level at 478.6 nm using a cavity magnification value of $M = 1.15$. Injected laser power density is 360 kW/cm^2 ($64 \mu\text{J}$ in 10 ns). The solid line shows the output energy, while the dashed line represents the intrinsic efficiency.

The effective pumping length based on energy deposition measurements (Section III-A) was found to be 17.5 cm, and the average value of the energy deposition was 37 J/l , which was the same as the lowest pumping level obtained with the 10 cm pumping length. Increased energy deposition at this longer cathode length was impossible due to electron-beam machine design limitations. Injection-controlled laser experiments were conducted using an $M = 1.15$ cavity as a function of injection power density at 478.6 nm wavelength. Fig. 9 depicts the comparison of laser output characteristics for 10 and 17.5 cm pumping lengths for the same pumping level. The results are plotted in terms of the output energy densities as a function of the injection energy level in order to make a consistent comparison. Absolute energy outputs are also shown on the right side scales of the figure. At the low injection energies, the output energy density is almost one order of magnitude larger for the 17.5 cm pumping length, reflecting the exponential dependence of the small-signal amplification on length, whereas output energy density values approach each other with increasing injection power. This result indicates that with increased pumping length,

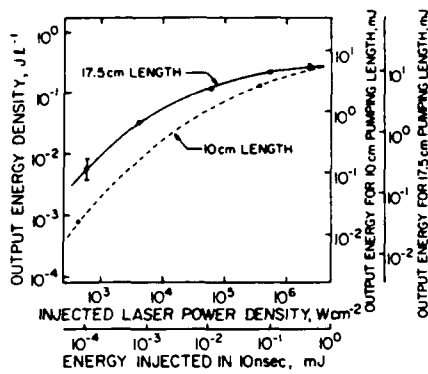


Fig. 9. Geometric scaling effect for a same electron-beam pumping level of 37 J/l; the injection wavelength was 478.6 nm and the cavity magnification was 1.15. The solid line represents the laser outputs for 17.5 cm pumping length, while the dashed line corresponds to a 10 cm pumping length.

the output energy scales with the pumping length even for the saturated region. The relatively low output energy density value in the saturated region is simply due to the low electron-beam pumping level (37 J/l).

D. Wavelength Tuning

An investigation of wavelength tuning efficiency was conducted by measuring the peak gain and the laser output as a function of the dye laser injection intensities. The electron-beam cathode length and the cavity length were again set at 7.6 and 12.6 cm, respectively, for these experiments. The specific injection wavelengths were chosen to correspond to either the gain maxima or the absorption valleys that are always apparent in the free-running XeF(C → A) laser spectrum as shown in Fig. 10. The shape of the free-running laser spectrum is governed by the coating bandwidth of the cavity mirrors used in this investigation (470–500 nm), by wide-band absorption due primarily to photoionization of excited Xe atoms [1], and by discrete narrow-band absorption which is due mainly to phototransitions of Xe, Ar, and Kr excited atoms [1], [13]. Because of the bandwidth limitation of the cavity optics coatings, the tuning range of the injection dye laser was restricted to wavelengths between 470 and 500 nm, a region where the gain is relatively insensitive to wavelength [6], except for specific wavelengths at which discrete absorption occurs.

1) *Gain*: Gain measurements were performed at two maxima and two valley wavelengths as a function of the probe beam intensity as shown in Fig. 11. The spatially averaged electron-beam pumping density was 95 J/l. Wavelengths of 478.6 and 486.8 nm correspond to the gain maxima positions, whereas those of 481.2 and 483.5 nm are valley positions (Fig. 10). Fig. 11 shows that with increasing injection power, the gain at the wavelength maximum locations decreases, whereas in the valley positions, the gain actually increases. As previously discussed, the measured gain is an average over a very inhomogeneous pumping power distribution (Fig. 4); therefore, these data have primarily qualitative significance. The decrease of the gain at 478.6 and 486.8 nm as

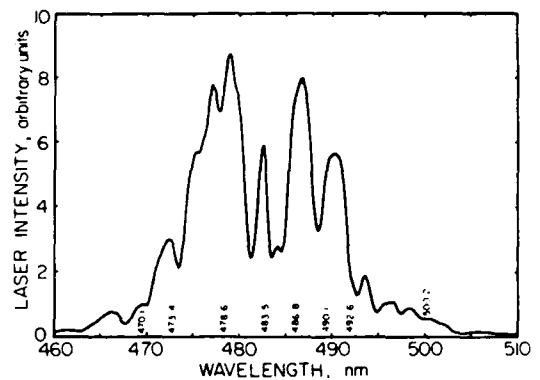


Fig. 10. Free-running XeF(C → A) laser spectrum. Specific wavelengths for the tuning experiments are indicated.

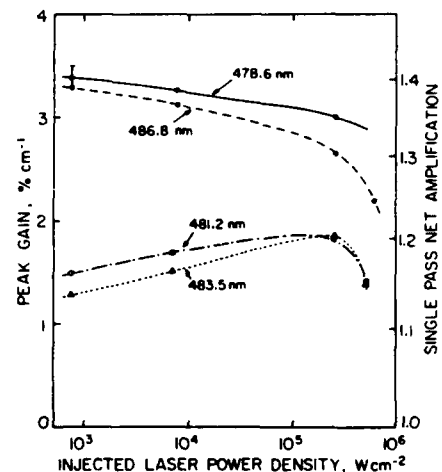


Fig. 11. Peak gain dependence on injected power density of the probe laser beam at various discrete wavelengths (Fig. 10); the electron-beam pumping energy was 95 J/l.

the injected power increases is most likely due to saturation of the gain over at least a portion of the gain length. At the 481.2 and 483.5 nm valleys where discrete absorption dominates, the increase in gain as the injected power increases suggests that absorber bleaching becomes important before the gain saturates.

2) *Laser Energy*: Presented in Fig. 12 are measured output energy characteristics as a function of wavelength for injection power density values of 430 W/cm² (76 nJ in 10 ns) and 360 kW/cm² (64 μJ in 10 ns). The spatially averaged electron-beam pumping level was 112 J/l. Each figure shows the superposition of the spectra of several separate injection-controlled laser shots. The line widths of the measured laser spectra were identical to those of the injected dye laser as previously reported [6]. Each spectrum shows relatively broad line width (0.75 nm). This is due to the convolution of the original dye laser line width (~0.6 nm) and the spectral resolution of the measuring system (~0.45 nm).

When a comparatively small power of 430 W/cm² was injected, the laser operated in the unsaturated region where the peak gain is high at gain maxima wavelength values and low at valley positions. Thus, the tuning data of Fig.

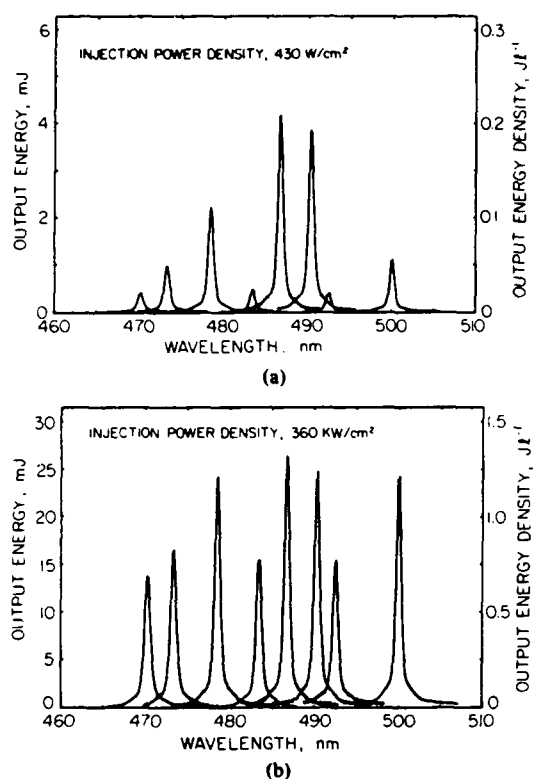


Fig. 12. Amplified XeF(C → A) laser output for various injection laser wavelengths and injection power densities of (a) 430 W/cm² (76 nJ in 10 ns), and (b) 360 kW/cm² (64 μJ in 10 ns).

12(a) exhibit characteristics qualitatively similar to those of the free-running spectrum. However, when a relatively high power was injected, 360 kW/cm², the tuned output shows a very significant change as depicted in Fig. 12(b). At the higher injection power level, the valleys become very much less pronounced, i.e., the wavelength tuning curve becomes flatter. This is apparently due to the bleaching of the absorbers which is in agreement with the gain measurements of Fig. 11. In fact, for low power injection, the output energy variation over a 30 nm region was a factor of 10. However, only a factor of 2 variation was observed with higher power injection.

For the conditions of Fig. 12(b), the *minimum* measured energy output of 14 mJ at 470.1 nm corresponds to an output energy density of 0.7 J/l, and an intrinsic efficiency of 0.6 percent, while the maximum measured energy output of 26 mJ at 486.8 nm corresponds to 1.3 J/l and 1.15 percent, respectively. It should be emphasized that these values refer to an injection power density of 360 kW/cm², and are not maximum values. When 1.1 MW/cm² was injected at a wavelength of 486.8 nm, which exhibited the maximum output at 360 kW/cm², an output energy of 33 mJ was obtained corresponding to an energy density of 1.6 J/l and an intrinsic efficiency of 1.5 percent.

IV. SUMMARY

The results of this investigation provide encouraging evidence that the electrically excited XeF(C → A) me-

dium has significant potential for the development of an *efficient* optical source that is *continuously* tunable throughout most of the blue-green spectral region. In addition, they provide the criteria for the efficient operation of this laser as a high-power excimer laser. Geometrical scaling confirms that the output energy scales with the pumping length.

Although relatively efficient (~1 percent) tuning has been demonstrated for wavelengths between 470 and 500 nm, XeF(C → A) amplifier performance has been limited in the present investigation by the combination of a relatively low damage threshold and the bandwidth of the cavity mirror coatings, a short active length (~10 cm), and an undesirably low value of cavity magnification ($M = 1.15$) which was required to compensate for the short active length and low stimulated emission cross section. However, it is clear that these factors are not fundamental limitations. For example, the present damage threshold of ~0.3 J/cm² is far below the current state of the art (few J/cm²) even if the cavity optics are exposed to fluorine-containing gas mixtures. Considering the relatively high gain and the absorber bleaching effect at the absorption valleys, significant improvement in laser performance throughout the entire blue-green region (~450–520 nm) should be possible by realizing improved resonator optics and by scaling of the laser medium excitation volume, assisted by magnetic field electron-beam confinement.

ACKNOWLEDGMENT

It is a pleasure to acknowledge the experimental assistance of J. R. Hooten and R. A. Chevillie of Rice University. The contribution of Dr. G. Marowsky of Max-Planck Institute, Göttingen, Germany, during the initial phase of the experiment is gratefully acknowledged, as well as discussions with Dr. G. McAllister of Maxwell Laboratories who introduced us to chlorostyrene film dosimetry, and with Dr. I. J. Bigio who advised us on various aspects of injection control.

REFERENCES

- [1] Y. Nachshon, F. K. Tittel, W. L. Wilson, Jr., and W. L. Nighan, "Efficient XeF(C → A) laser oscillation using electron-beam excitation," *J. Appl. Phys.*, vol. 56, pp. 36–48, 1984.
- [2] W. K. Bischel, D. J. Eckstrom, H. C. Walker, Jr., and R. A. Tilton, "Photolytically pumped XeF(C → A) laser studies," *J. Appl. Phys.*, vol. 52, pp. 4429–4434, 1981.
- [3] C. H. Fisher, R. E. Center, G. J. Mullaney, and J. P. McDaniel, "Multipass amplification and tuning of the blue-green XeF(C → A) laser," *Appl. Phys. Lett.*, vol. 35, pp. 901–903, 1979.
- [4] G. Marowsky, N. Nishida, F. K. Tittel, W. L. Wilson, Jr. and Y. Zhu, "Wideband tuning of the blue-green XeF(C → A) laser," *Appl. Phys. B.*, vol. 37, pp. 205–207, 1985.
- [5] G. Marowsky, N. Nishida, H. Stiegler, F. K. Tittel, W. L. Wilson, Jr., Y. Zhu, and W. L. Nighan, "Efficient narrow spectral output in the blue-green region from an injection-controlled electron-beam excited XeF(C → A) laser," *Appl. Phys. Lett.*, vol. 47, pp. 657–660, 1985.
- [6] F. K. Tittel, G. Marowsky, W. L. Nighan, Y. Zhu, R. Sauerbrey, and W. L. Wilson, Jr., "Injection-controlled tuning of an electron-beam excited XeF(C → A) laser," *IEEE J. Quantum Electron.*, vol. QE-22, pp. 2168–2173, 1986.
- [7] W. L. Nighan, R. Sauerbrey, Y. Zhu, F. K. Tittel, and W. L. Wilson, Jr., "Kinetically tailored properties of electron-beam excited

- XeF($C \rightarrow A$) and XeF($B \rightarrow X$) laser media using an Ar-Kr buffer," *IEEE J. Quantum Electron.*, vol. QE-23, pp. 253-261, 1987.
- [8] Y. Nachshon and F. K. Tittel, "A new blue-green XeF($C \rightarrow A$) excimer laser amplifier concept," *Appl. Phys. B*, vol. 35, pp. 227-231, 1984.
- [9] R. Sauerbrey, Y. Zhu, P. Millar, F. K. Tittel, and W. L. Wilson, Jr., "Improved laser pumping by intense electron beams via a back-scattering reflector," *J. Appl. Phys.*, vol. 61, pp. 4740-4743, 1987.
- [10] W. P. Bishop, K. C. Humpherys, and P. T. Randtke, "Poly(halo)styrene thin-film dosimeters for high doses," *Rev. Sci. Instrum.*, vol. 44, pp. 443-452, 1973.
- [11] W. L. Nighan, F. K. Tittel, W. L. Wilson, Jr., N. Nishida, Y. Zhu, and R. Sauerbrey, "Synthesis of rare gas-halide mixtures resulting in efficient XeF($C \rightarrow A$) laser oscillation," *Appl. Phys. Lett.*, vol. 45, pp. 947-949, 1984.
- [12] I. J. Bigio and M. Slatkine, "Injection locking unstable resonator excimer lasers," *IEEE J. Quantum Electron.*, vol. QE-19, pp. 1426-1436, 1983.
- [13] H. Horiguchi, R. S. F. Chang, and D. W. Setser, "Radiative lifetimes and two-body collisional deactivation rate constants in Ar for Xe($5p^36p$), Xe($5p^36p$) and Xe($5p^37p$) states," *J. Chem. Phys.*, vol. 75, pp. 1207-1218, 1981.

Injection-Controlled Tuning of an Electron-Beam Excited XeF($C \rightarrow A$) Laser

FRANK K. TITTEL, FELLOW, IEEE, GERD MAROWSKY, WILLIAM L. NIGHAN, SENIOR MEMBER, IEEE, YUNPING ZHU, STUDENT MEMBER, IEEE, ROLAND A. SAUERBREY, MEMBER, IEEE, AND WILLIAM L. WILSON, JR., MEMBER, IEEE

Abstract—Efficient, ultra-narrow spectral output from an electron-beam excited XeF($C \rightarrow A$) laser medium has been achieved by injection-controlled tuning. Using a pulsed dye laser as the injection source, amplified output pulses tunable between 435 and 535 nm and having a spectral width of 0.001 nm were obtained. For a 482.5 nm injection wavelength that is well matched to the XeF($C \rightarrow A$) gain maximum, output energy density and intrinsic efficiency values of approximately 8 J/l and 6 percent were achieved.

I. INTRODUCTION

THE XeF($C \rightarrow A$) excimer transition is unique among those of the rare gas halide class because of its blue-green wavelength and exceptionally broad-band fluorescence spectrum. Free running laser oscillators operating on the XeF($C \rightarrow A$) transition typically exhibit broad laser spectra (~ 20 nm) centered near 485 nm [1]. The XeF($C \rightarrow A$) laser has also been wavelength tuned from about 450 to 510 nm with a spectral width on the order of a few nanometers, albeit with very low efficiency [2]–[4]. However, recent developments indicate that the electrically excited XeF($C \rightarrow A$) medium has considerable potential for development as an *efficient* optical source that is tunable throughout the entire blue-green region of the spectrum.

This conclusion is based primarily on three factors. 1) Short-pulse, high-energy electron beam (e beam) excitation of multicomponent mixtures tailored specifically to minimize transient absorption has resulted in a broad-band, free-running laser oscillator output having energy density and efficiency values comparable to those of the UV XeF($B \rightarrow X$) transition [1], [5]. 2) Using the same medium as an amplifier, a 482.5 nm output pulse having a spectral width of only 0.01 nm was obtained using dye laser injection control [6]. Moreover, the narrowed spectral output was obtained at energy density and intrinsic

efficiency levels of approximately 3 J/l and ~ 2.5 percent, respectively. 3) Our recent measurements have shown that the e -beam excited XeF($C \rightarrow A$) medium exhibits relatively high peak gain (> 2 percent $\cdot \text{cm}^{-1}$) throughout the entire 450–515 nm wavelength region, indicating that efficient tuning over a broad spectral range should be possible. In this paper, we report on our first efforts to capitalize on these characteristics by injection control of an XeF($C \rightarrow A$) amplifier. The injection source used was a dye laser tunable throughout the entire blue-green region and having a spectral width of only 0.001 nm. Injection of the dye laser pulse through a small hole in one mirror of an unstable resonator served to rapidly expand the seed beam, ensuring efficient use of the active volume [6], [7]. This technique has resulted in amplified output pulses that preserve the spectral width of the injected pulse, with energy densities exceeding 0.2 J/l throughout the entire 459–505 nm region. For an injection wavelength of 482.5 nm, a wavelength coinciding with the region of maximum gain, output pulses corresponding to an extraction energy density of approximately 8 J/l were demonstrated, indicative of an intrinsic efficiency of about 6 percent.

The details of the experimental arrangement and related diagnostics are described in Section II. In Section III, the factors affecting the net gain are summarized with particular emphasis on the importance of Kr addition to the laser mixture. Experimental results are presented in Section IV, along with a discussion of prospects for further improvement in XeF($C \rightarrow A$) laser performance.

II. EXPERIMENT

A. Electron Beam System and Reaction Cell

The experimental apparatus used in this work is illustrated in Fig. 1. A Physics International Pulserad 110 electron beam generator was used to transversely excite high-pressure gas mixtures. In order to obtain a uniform e -beam distribution and to increase the lifetime of the foil separating the low- and high-pressure regions of the cell, a stainless steel wire mesh was mounted between the e -beam cathode and the foil. The electron beam energy was 1 MeV, and the excitation pulse duration was 10 ns (FWHM), producing a pump energy density of ~ 135 J/l, as measured by a calorimeter and Faraday cup probe.

The stainless steel reaction cell was carefully passi-

Manuscript received May 12, 1986. This work was supported by the Office of Naval Research, the National Science Foundation, and the Robert A. Welch Foundation.

F. K. Tittel, Y. Zhu, R. A. Sauerbrey, and W. L. Wilson, Jr. are with the Department of Electrical and Computer Engineering, Rice University, Houston TX 77251.

G. Marowsky is with Abteilung Laserphysik, Max-Planck Institut für biophysikalische Chemie, D-3400 Goettingen, Federal Republic of Germany.

W. L. Nighan is with United Technologies Research Center, East Hartford, CT 06108.

IEEE Log Number 8610417.

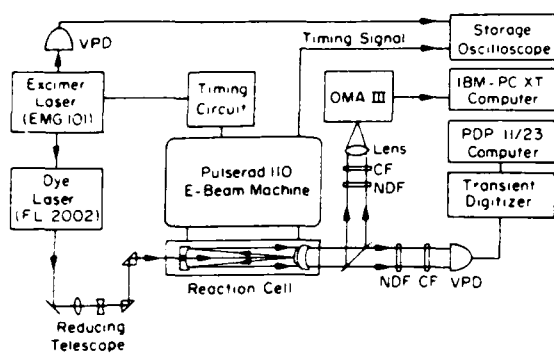


Fig. 1. Schematic illustration of the experimental apparatus, showing in particular the unstable cavity optics inside the reaction cell, the tunable injection laser source, and the timing and data acquisition systems. OMA = optical multichannel analyzer. VPD = vacuum photodiode. CF = color glass filter. NDF = neutral density filter.

vated by prolonged exposure to F_2 . High-purity gas mixtures comprised of NF_3 , F_2 , Xe, Kr, and Ar were used [1], [5], [6]. Good gas mixing of the components was found to be essential, and was obtained using turbulent flow of the high-pressure gas components into the reaction cell. Each fresh gas mixture could be used for about ten shots before performance degradation became significant.

B. Injection Control System

An excimer-pumped dye laser system (Lambda Physik Model EMG 101E/FL2002) having a bandwidth of $\sim 5 \times 10^{-3}$ nm was used to provide injection control [6]. Use of an intracavity etalon resulted in significant additional bandwidth reduction to 9×10^{-4} nm. This seed oscillator delivered an output of up to 8 mJ in a 10 ns pulse (FWHM), tunable from 430 to 550 nm using Coumarin dyes 2, 102, and 307. A telescope was used to reduce the injection beam diameter so that most of the available dye laser pulse energy entered the unstable cavity of the *e*-beam pumped cell (Fig. 1). Due to the loss of dye laser energy caused by the beam-forming optics, the maximum injected energy was limited to ~ 1.5 mJ in these experiments.

The temporal evolution of the free-running laser, the dye laser, and the injection-controlled XeF(C → A) laser output were monitored by a fast vacuum photodiode detector [ITT-F4000 (S5)]. Neutral density filters were used to avoid saturation of the photodiode, and color glasses were used to define the spectral region of interest. Signals were recorded by a Tektronix R7912 transient digitizer. The time resolution of the entire system was better than 2 ns. The temporally integrated, spectrally resolved laser signal was recorded by an optical multichannel analyzer (OMA III), using a Jarrell-Ash 0.25 m spectrometer having a spectral resolution of about 0.3 nm. Additionally, the temporal relationship of the dye laser and *e*-beam pulse was monitored by a storage oscilloscope. The timing relationship between the dye laser and *e* beam was adjusted by timing circuits so that the volume-filling pass of the injected dye laser pulse overlapped the rise of the XeF(C → A) temporal gain profile.

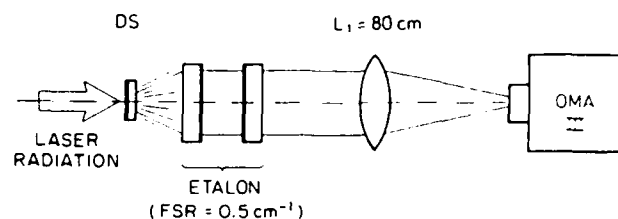


Fig. 2. Schematic illustration of the experimental arrangement used for the measurement of bandwidth. DS = diffusing screen.

C. Cavity Optics

The optical cavity used in these studies was a positive-branch confocal unstable, intracell resonator, consisting of a concave end mirror with an injection hole of 1.5 mm diameter and a coating having a high reflectivity in the blue-green region, and a convex output coupler (Fig. 1). The mirrors, having focal lengths of f_2 and $-f_1$, respectively, were separated by a distance $L = f_2 - f_1$, typically about 12 cm for our conditions, with the magnification given by the relation $M = f_2/f_1$. The output coupler was a meniscus lens of zero refraction power having a highly reflective coated spot on the convex side with a diameter d of 1.4 cm. With this arrangement, the output coupler could be placed in a conventional mirror holder and aligned externally. The active region was a cylindrical volume defined by the *e*-beam pumping length (10 cm) and the clear aperture having a diameter $d \times M$ cm.

Because the out coupling of the unstable cavities used was substantially greater than the value found to be optimum for a stable cavity (~ 5 percent), and since the injection hole also constitutes a large loss, significant self-oscillation (injected or not) was not possible for our conditions. Rather, in the present experiment, the role of the cavity was to serve as a beam-expanding telescope of a regenerative amplifier [6], [7]. Various cavities were examined having magnifications of 1.05, 1.08, 1.14, and 1.23, respectively. Although such small values of magnification result in a considerable sensitivity to alignment [8], they provide the long amplification path (several hundred cm) required for efficient use of the XeF(C → A) gain medium.

D. Bandwidth Measurement

In order to determine the spectral width of the dye laser injection pulse and of the amplified output pulse, a Fabry-Perot monitor etalon with adjustable spacing was used as illustrated in Fig. 2. Part of the amplified output was focused on a diffusing screen (DS) which served to homogeneously illuminate an air-gap etalon of adjustable spacing. By means of a long-focal-length lens ($L_1 = 80$ cm), a section of the emerging fringe pattern was imaged onto the entrance window of the OMA vidicon. Fig. 3 shows an example of a typical plot of an OMA III spectrum. Fine alignment of the setup was performed using the 488 nm line of a collinear Ar-ion laser, and after removal of the attenuators, with the throughput of the tunable dye laser radiation itself. By throughput, we mean the output

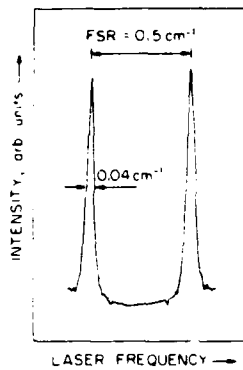


Fig. 3. Fabry-Perot etalon interferogram of a typical amplified output as observed using the OMA III vidicon.

of the injected dye laser signal after multiple reflections through the unstable resonator in the absence of e -beam pumping.

Using a free spectral range (FSR) of 0.5 cm^{-1} , the ultimate resolving power of the entire arrangement for line-width measurements was 0.01 cm^{-1} or 0.00024 nm at a wavelength of 485 nm . This resolution conveniently allowed a determination of the linewidth of the injected dye laser radiation: 0.2 cm^{-1} (grating tuned) or 0.04 cm^{-1} (grating tuned + intracavity etalon of 1 cm^{-1} FSR). Using this procedure, the e -beam pumped multipass amplifier output was found to have essentially the same spectral width as that of the injected dye laser pulse.

III. TEMPORAL GAIN PROFILE

Short-pulse, high-energy e -beam excitation of the $\text{XeF}(C \rightarrow A)$ medium is characterized by a period of strong transient absorption during the excitation pulse, followed by the development of net gain in the afterglow regime [1], [5]. In early work, the combination of a relatively short gain duration ($< 50 \text{ ns}$) and a relatively low value of the peak gain ($< 1 \text{ percent} \cdot \text{cm}^{-1}$) limited the energy and efficiency of the electrically excited $\text{XeF}(C \rightarrow A)$ laser to unacceptably low levels. However, in recent years, multicomponent mixtures have been developed that result in significant reduction in the transient absorption, thereby permitting much higher peak gain values ($\sim 2\text{--}3 \text{ percent} \cdot \text{cm}^{-1}$), with a dramatic improvement in laser performance [1], [5], [9], [10].

A. Mixtures Containing Krypton

The addition of Kr to $\text{XeF}(C \rightarrow A)$ laser mixtures has been found to result in a significantly improved gain profile when e -beam excitation is used [5], [10]. Presented in Fig. 4 is the measured temporal evolution of the net gain for representative $\text{XeF}(C \rightarrow A)$ laser mixtures with and without Kr. The fractional concentrations of each constituent of the Ar-Xe-NF₃-F₂ mixture are optimized and result in broad-band extraction energy density values typically in the $1.0\text{--}1.5 \text{ J/l}$ range when a free-running stable resonator is used [1], [5]. However, Fig. 4 vividly illustrates the significant reduction in the initial absorption and the increase in peak gain when Kr is added to the

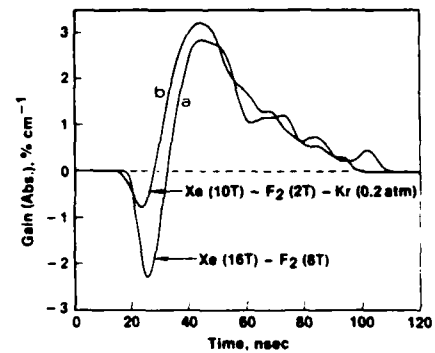


Fig. 4. Temporal evolution of the $\text{XeF}(C \rightarrow A)$ net gain profile measured at 488 nm using an Ar-ion probe laser for mixtures comprised of 6.5 atm Ar , 16 torr Xe , 8 torr NF_3 , and 8 torr F_2 (a), and 6.5 atm Ar , 10 torr Xe , 8 torr NF_3 , 2 torr F_2 , and 150 torr Kr (b).

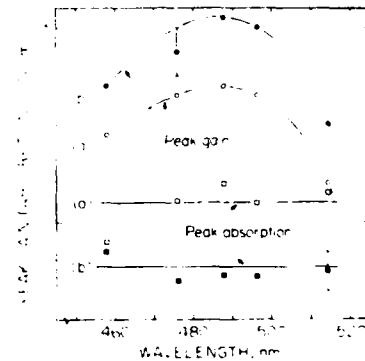


Fig. 5. Wavelength dependence of the peak values of gain and initial absorption for mixtures comprised of 6.5 atm Ar , 16 torr Xe , 8 torr NF_3 , and 8 torr F_2 (a), and 6.5 atm Ar , 10 torr Xe , 8 torr NF_3 , 2 torr F_2 , and 300 torr Kr (b).

mixture and all constituent fractional concentrations are reoptimized. The improved gain profile typical of Kr-containing mixtures has been found to increase the broad-band output energy and intrinsic efficiency of a stable, free-running oscillator to levels comparable to those of the UV $\text{XeF}(B \rightarrow X)$ transition [5]. The wavelength dependence of the peak values of gain and initial absorption for mixtures with and without Kr are presented in Fig. 5. These results are typical of Kr partial pressures in the $150\text{--}600 \text{ torr}$ range, and show that the peak gain is increased significantly and the initial absorption is decreased throughout the entire wavelength range of interest.

In our initial work on injection control [6], an optimized Ar-Xe-NF₃-F₂ mixture typical of the conditions of Figs. 4 and 5 was used. However, for the experiments reported herein, an optimized Kr-containing mixture was utilized. Of course, the higher value of peak gain typical of Kr mixtures results in greater amplification of the injected dye laser pulse. As important, however, is the fact that with Kr present in the mixture, the initial absorption of the injected pulse is greatly reduced (Fig. 4), thereby increasing the energy available for amplification. For this reason, the presence of Kr in the mixture has an even greater beneficial effect when the $\text{XeF}(C \rightarrow A)$ medium is used as an amplifier than when used as a free-running oscillator [5]. Additionally, for the conditions of Figs. 4 and

5, the concentration of Kr₂F is very large [10]. Since the Kr₂F excimer is an absorber of UV radiation, its presence significantly reduces the possibility of competitive oscillation on the XeF(B → X) transition [10].

IV. EXPERIMENTAL RESULTS AND DISCUSSION

A. Timing Considerations

The approximate temporal relationship among the injected dye laser pulse, the *e*-beam excitation pulse, the amplified output pulse, and the free-running broad-band XeF(C → A) laser oscillator output are shown in Fig. 6. Figs. 4 and 6 show that the duration of the dye laser pulse and the gain risetime are both on the order of 10–20 ns, a time nearly the same as that required for the injected pulse to fill the cavity. For this reason, control of the timing of the dye laser pulse with respect to the firing of the *e* beam was found to be a difficult and critical aspect of the present experiment. The problem was further complicated by the fact that a short period of initial absorption accompanies the *e*-beam firing (Fig. 4), although at a much reduced level when using mixtures containing Kr as described previously.

Presented in Fig. 7 is the dependence of the amplified 482.5 nm pulse energy on the delay time between the injection of a 1 mJ dye laser pulse and the firing of the *e* beam. This figure shows that for a magnification *M* of 1.08, for which approximately 86 percent of the dye laser energy is reflected back out through the injection hole, the temporal window corresponding to optimum timing is only 10–15 ns. For an *M* value of 1.05, the window was slightly larger, reflecting the fact that the transit time of the dye laser pulse through the cavity increases as *M* decreases, thereby relaxing the timing constraint somewhat. For the same reason, the optimum temporal window was reduced to about 5 ns for an *M* value of 1.23.

B. Magnification Effects

In addition to a significant dependence on timing, the amplified output pulse energy also exhibited a strong dependence on cavity magnification for the specific conditions of our experiment. Fig. 8 shows the dependence of the 482.5 nm output energy on *M* for near optimum timing (Fig. 7) and a 1 mJ injection pulse energy. As *M* is reduced from 1.23, the output energy increases, a reflection of the increase in cavity feedback for the lower *M* values. However, as *M* approaches unity, nearly all the injected dye laser energy is reflected back out through the 1.5 mm diameter injection hole. Indeed, Fig. 8 shows that the output energy decreases rapidly as the magnification is reduced to 1.05. Additionally, optical alignment was found to be very difficult using the *M* = 1.05 cavity [8].

C. Output Energy and Efficiency

For the conditions of Figs. 7 and 8, the *e*-beam energy deposition was measured and found to be approximately 135 J/l, a value consistent with calculated and measured values of medium properties [1]. Since the active volume defined by the mirror spacing and magnification values varied from 16.8 to 20.4 cm³ for our conditions, the max-

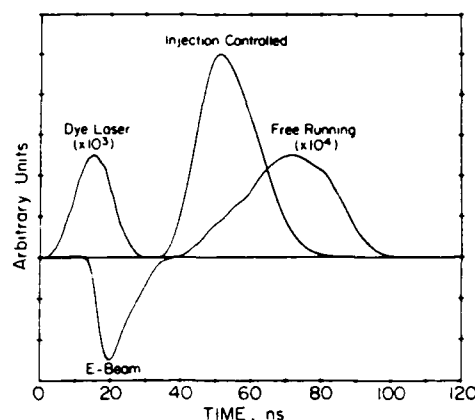


Fig. 6. Temporal relationships of the dye laser, the *e*-beam excitation pulse, the amplified XeF(C → A) output, and the broad-band and XeF(C → A) output with the system operating as a free-running oscillator.

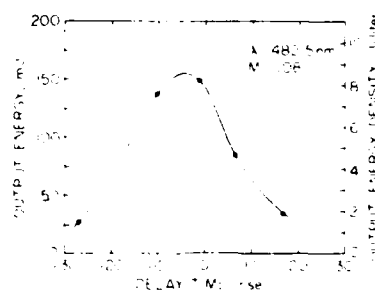


Fig. 7. Dependence of the amplified XeF(C → A) output energy on the delay time between a 482.5 nm dye laser pulse and firing of the *e* beam. The energy of the dye laser pulse entering the cavity was 1 mJ, approximately 86 percent of which was reflected back out through the injection hole. The mixture was comprised of 6.5 atm Ar, 8 torr Xe, 8 torr NF₃, 1 torr F₂, and 300 torr Kr.

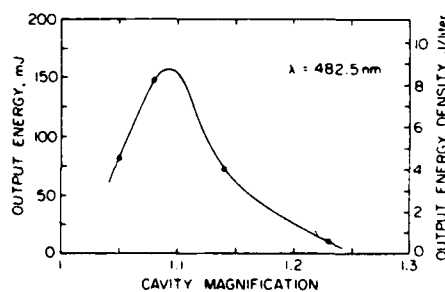


Fig. 8. Dependence of the 482.5 nm amplified output pulse on cavity magnification for optimum timing and conditions otherwise similar to those of Fig. 7.

imum 149 mJ output obtained at 482.5 nm corresponds to an energy density of ~8 J/l and an intrinsic efficiency of approximately 6 percent. On a volumetric basis, these values are actually higher than those typical of room temperature XeF(B → X) laser operation, and are comparable to XeF(B → X) performance at the 450 K temperature found to be optimum for that laser [11], [12]. This is rather surprising in view of the fact that the C → A quantum efficiency is ~25 percent less than that of the B → X transition. However, because of the strongly repulsive nature of the XeF(A) state, the C → A laser does not suffer from lower level population buildup as is the case with

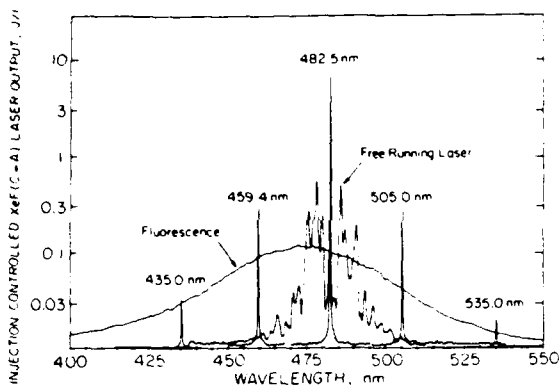


Fig. 9. Qualitative comparison of superimposed time integrated spectra of the XeF($C \rightarrow A$) fluorescence, the injection-controlled output of five separate shots at several wavelengths, and a typical free-running oscillator spectrum, all for representative conditions.

the $B \rightarrow X$ laser. Additionally, the 6.5 atm Ar-Kr buffer mixture used in the present work results in $B-C$ state mixing and vibrational relaxation times of approximately 0.1 ns [10], [13], which are very much less than those typical of optimum $B \rightarrow X$ laser mixtures using Ne as the buffer at pressure of ~ 3 atm [11], [12]. Since both lower level buildup and slow vibrational relaxation adversely affect XeF($B \rightarrow X$) laser energy and efficiency [11], [14], apparently the XeF($C \rightarrow A$) medium has advantages in this regard, provided the level of broad-band transient absorption is controlled kinetically and the characteristically slow build up of optical flux that usually limits oscillator performance is overcome by using the $C \rightarrow A$ medium as an amplifier.

D. Wavelength Tuning

In order to determine the range within which the XeF($C \rightarrow A$) medium can be efficiently tuned, the wavelength of the injected pulse was varied from 435 to 535 nm. Fig. 9 provides an illustrative comparison of the spectra of several injection-controlled shots and a free-running oscillator spectrum, along with the XeF($C \rightarrow A$) fluorescence spectrum. Because of the large cavity loss described previously, the maximum free-running output energy was always less than 0.1 mJ for our conditions. However, several mJ of amplified output were obtained for injection wavelengths as low as 459.4 nm and as high as 505 nm. In fact, amplification of the injected signal was observed for wavelengths as low as 435 nm and as high as 535 nm.

Presented in Fig. 10 is the measured output energy as a function of wavelength for several different cavities, along with a typical free-running spectrum for comparison. The specific injection wavelengths were chosen to correspond to the peaks and absorption valleys that are always apparent in the free-running XeF($C \rightarrow A$) laser spectrum. This figure shows that the wavelength dependence of the minima observed in the amplified output correlates reasonably well with the locations of the absorption valleys in the free-running spectrum. The discrete absorption is due primarily to phototransitions from Xe(3P_2 , 3P_1) atoms to higher Rydberg levels [1], [15].

While all the points shown in Fig. 10 correspond to

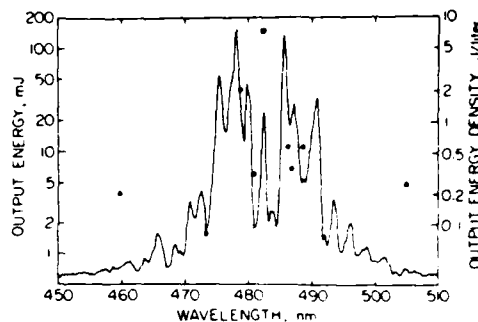


Fig. 10. Measured amplified XeF($C \rightarrow A$) output energy for selected wavelengths for an injected dye laser pulse of approximately 1 mJ, along with a typical free-running spectrum, the intensity of the latter in arbitrary units for comparison. The cavity M values were 1.05 (\blacktriangle), 1.08 (\blacksquare), and 1.14 (\bullet) (see Fig. 8).

near optimum timing between the dye pulse injection and e -beam firing (Fig. 7), only the 482.5 nm point was obtained using optimum cavity magnification (Fig. 8). Additionally, the measured dye laser throughput for a bare cavity was occasionally less than expected on the basis of the cavity magnification value, a condition found to be caused by significant mirror surface deterioration under certain conditions. For these reasons, we feel that, with the exception of the 482.5 nm value, the measured amplified output energies of Fig. 10 represent lower limits. Correcting the values of Fig. 10 for differences in cavity magnification (Fig. 8) and for the estimated effect of mirror surface deterioration suggests that, except for wavelengths coinciding with discrete absorption transitions, output energy density values > 1 J/l should be attainable throughout the entire blue-green region of the spectrum.

V. SUMMARY

The results of this investigation provide encouraging evidence that the electrically excited XeF($C \rightarrow A$) medium has significant potential for development as an efficient optical source of high brightness that is tunable throughout a large portion of the blue-green spectral region. Moreover, the usually high values of extraction energy density and of intrinsic efficiency that were obtained for an injection wavelength matched to the maximum gain suggest that the XeF($C \rightarrow A$) medium may have the potential to rival its UV rare gas-halide counterparts for certain selected applications requiring high energy and efficiency.

Although relatively efficient (> 0.1 percent) tuning has been demonstrated for wavelengths as low as 459.4 nm and as high as 505 nm, XeF($C \rightarrow A$) amplifier performance has been limited in the present investigation by the combination of a short active length (~ 10 cm), undesirably low values of cavity magnification (< 1.3) required to compensate for the former, and a critical sensitivity to timing. However, it is clear that these factors do not represent fundamental limitations. Considering that the gain of the e -beam excited XeF($C \rightarrow A$) medium is relatively high (> 2 percent $\cdot \text{cm}^{-1}$) over a 100 nm bandwidth centered at 480 nm, significant improvement in performance

should be forthcoming as a result of pumping geometries which are better suited to optimization of the laser cavity.

ACKNOWLEDGMENT

It is a pleasure to acknowledge the experimental assistance of J. Kinross-Wright and J. Hooton of Rice University, and the helpful comments of Dr. I. J. Bigio of Los Alamos National Laboratory.

REFERENCES

- [1] Y. Nachshon, F. K. Tittel, W. L. Wilson, Jr., and W. L. Nighan, "Efficient XeF(C \rightarrow A) laser oscillation using electron-beam excitation," *J. Appl. Phys.*, vol. 56, pp. 36-48, 1984.
- [2] W. K. Bischel, D. J. Eckstrom, H. C. Walker, Jr., and R. A. Tilton, "Photolytically pumped XeF(C \rightarrow A) laser studies," *J. Appl. Phys.*, vol. 52, pp. 4429-4434, 1981.
- [3] C. H. Fisher, R. E. Center, G. J. Mullaney, and J. P. McDaniel, "Multipass amplification and tuning of the blue-green XeF(C \rightarrow A) laser," *Appl. Phys. Lett.*, vol. 35, pp. 901-903, 1979.
- [4] G. Marowsky, N. Nishida, F. K. Tittel, W. L. Wilson, and Y. Zhu, "Wideband tuning of the blue-green XeF(C \rightarrow A) laser," *Appl. Phys. B*, vol. 37, pp. 205-207, 1985.
- [5] W. L. Nighan, F. K. Tittel, W. L. Wilson, Jr., N. Nishida, Y. Zhu, and R. Sauerbrey, "Synthesis of rare gas-halide mixtures resulting in efficient XeF(C \rightarrow A) laser oscillation," *Appl. Phys. Lett.*, vol. 45, pp. 947-949, 1984.
- [6] G. Marowsky, N. Nishida, H. Stiegler, F. K. Tittel, W. L. Wilson, Jr., Y. Zhu, and W. L. Nighan, "Efficient narrow spectral output in the blue-green region from an injection-controlled electron-beam excited XeF(C \rightarrow A) laser," *Appl. Phys. Lett.*, vol. 47, pp. 657-660, 1985.
- [7] I. J. Bigio and M. Slatkine, "Injection locking unstable resonator excimer lasers," *IEEE J. Quantum Electron.*, vol. QE-19, pp. 1426-1436, 1983.
- [8] W. F. Krupke and W. R. Sooy, "Properties of an unstable confocal resonator CO₂ laser system," *IEEE J. Quantum Electron.*, vol. QE-5, pp. 575-586, 1969.
- [9] W. L. Nighan, Y. Nachshon, F. K. Tittel, and W. L. Wilson, Jr., "Optimization of electrically excited XeF(C \rightarrow A) laser performance," *Appl. Phys. Lett.*, vol. 42, pp. 1006-1008, 1983.
- [10] W. L. Nighan, R. A. Sauerbrey, Y. Zhu, F. K. Tittel, and W. L. Wilson, Jr., "Kinetically tailored properties of electron-beam excited XeF(C \rightarrow A) laser media using Ar-Kr buffer mixtures," submitted to *IEEE J. Quantum Electron.*
- [11] J. C. Isia, J. A. Mangano, J. H. Jacob, and M. Rokni, "Improvement in XeF laser efficiency of elevated temperatures," *Appl. Phys. Lett.*, vol. 34, pp. 208-210, 1979.
- [12] A. E. Mandl and H. A. Hyman, "XeF laser performance for F₂ and NF₃ fuels," *IEEE J. Quantum Electron.*, vol. QE-22, pp. 349-359, 1986.
- [13] H. C. Brashears, Jr. and D. W. Setser "Transfer and quenching rate constants for XeF(B) and XeF(C) states in low vibrational levels," *J. Chem. Phys.*, vol. 76, pp. 4932-4946, 1982.
- [14] M. Rokni and J. H. Jacob, "Rare gas-halide lasers," ch. 10 in *Applied Atomic Collision Physics; Volume 3: Gas Lasers*, H. S. W. Massey, E. W. McDaniel, and B. Bederson, Eds. New York: Academic, 1982.
- [15] H. Horiguchi, R. S. F. Chang, and D. W. Setser, "Radiative lifetimes and two-body collisional deactivation rate constants in Ar for Xe(5p³6p), Xe(5p³6p) and Xe(5p³7p) states," *J. Chem. Phys.*, vol. 75, pp. 1207-1218, 1981.

Efficient narrow spectral output in the blue-green region from an injection-controlled electron-beam excited XeF ($C \rightarrow A$) laser

G. Marowsky

Max-Planck Institute für Biophysikalische Chemie, Abteilung Laserphysik, D-3400 Göttingen, Federal Republic of West Germany

N. Nishida, H. Stiegler, F. K. Tittel, W. L. Wilson, Jr., and Y. Zhu

Electrical and Computer Engineering Department, Rice University, Houston, Texas 77251-1892

William L. Nighan

United Technologies Research Center, East Hartford, Connecticut 06108

(Received 17 June 1985; accepted for publication 15 July 1985)

Efficient, narrow spectral output has been achieved by injection control of an electron-beam excited XeF ($C \rightarrow A$) laser medium using a 482-nm dye laser pulse having a spectral width of 0.01 nm. The energy density and intrinsic efficiency characteristic of the amplified output beam were 3 J/l and approximately 2.5%, respectively, and the spectral width was on the order of that of the injected pulse.

In recent years narrow bandwidth (≤ 0.01 nm), tunable laser operation has been demonstrated by injection locking electrically excited rare gas-halide lasers such as KrF (248 nm)¹ and XeF (351 nm),^{1,2} and HgBr (502 nm).³ Additionally, the UV output of lasers such as XeCl (308 nm) has been

Raman converted to several specific wavelengths in the visible region, also with narrow spectral width.⁴ Although the high efficiency ($> 1\%$) typical of these lasers operating as free-running oscillators was preserved in the narrow wavelength-tuned output, their tuning *range* is limited to about 1

nm. In contrast, the very broadband XeF ($C \rightarrow A$) laser, centered in the blue-green region at 485 nm, has been tuned continuously from about 450 to 510 nm with a spectral width on the order of a few nanometers, using either intracavity optical elements^{5,6} or dye laser pulse injection.⁷ However, in these experiments both the free-running and tuned laser output were extremely inefficient ($\ll 1\%$).

Recently, very significant improvement in the performance of an electron-beam (e -beam) excited XeF ($C \rightarrow A$) laser has been achieved by selective tailoring of the gas mixture so as to minimize transient absorption.⁸⁻¹⁰ Use of multicomponent gas mixtures comprised either of Ar-Xe-F₂-NF₃ (Refs. 8 and 9) or of Ar-Kr-Xe-F₂-NF₃ (Ref. 10) has resulted in laser pulse energy density values in the 1.5–3.0 J/l range with an intrinsic efficiency of approximately 1.5%, a performance level which, for the first time, is comparable to that typical of the $B \rightarrow X$ rare gas-halide and mercury-halide lasers. In these studies the free-running XeF ($C \rightarrow A$) laser output was centered at 480 nm with a bandwidth of ~ 25 nm (FWHM). However, measurements^{9,10} showed that the gain extended over a much larger spectral range and exhibited a relatively weak dependence on wavelength. These results indicate that it should be possible to tune the XeF ($C \rightarrow A$) laser continuously throughout the entire blue-green region, with narrow spectral width and with an efficiency typical of that demonstrated in the free-running mode. In this letter we report efficient (~ 2.0 – 3.0%), narrow spectral output ($\Delta\lambda \sim 0.01$ nm) from an XeF ($C \rightarrow A$) laser medium by amplification of an injected dye laser pulse.

Transverse laser excitation was provided by an e -beam with an electron energy of 1 MeV and a pulse duration of 10 ns (FWHM). The e -beam current density at the center of the optical axis was ~ 200 A cm⁻², as measured with a Faraday probe. Specific details of the experimental arrangement and related diagnostic apparatus are described in Ref. 9. For the present purposes the gas mixture was composed of 6.5 atm Ar, 16 Torr Xe, 8 Torr F₂, and 8 Torr NF₃. Good mixing of the component gases and thorough fluorine passivation of the stainless steel reaction cell were found to be absolutely essential in order to ensure reliable laser performance. The source of the injected radiation was a narrow bandwidth excimer-pumped dye laser system (Lambda-Physik models EMG 100 and FL 2002). This reference oscillator arrangement delivered up to 12 mJ in a 10 ns pulse, tunable from 440 to 540 nm using Coumarin dyes 47, 102, and 307. The spectral width of the seed pulse was 0.01 nm as measured with a monitoring étalon.

The collimated dye laser pulse was injected through a small hole (2 mm diameter) in the concave back mirror of an intracell positive branch confocal unstable resonator¹ as illustrated in Fig. 1. Two different resonators were used having radii of curvature for the concave mirrors of either 1.5 or 2.0 m, and for the corresponding smaller convex mirrors of either 1.22 or 1.75 m; the mirror separation was about 13.0 cm, depending on the specific resonator. The concave mirrors were covered with a broadband coating that was totally reflective from 440 to 530 nm, while the coating on the convex output reflector (a meniscus lens) was limited to a diameter of 1.4 cm. The thin outer annular region of the output

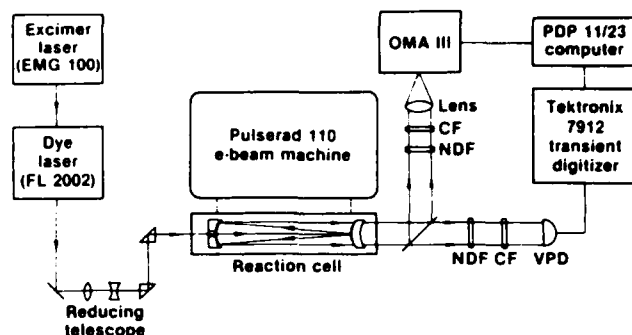


FIG. 1. Schematic illustration of experimental arrangement. NDF = neutral density filter, CF = color-glass filter, VPD = vacuum photodiode.

mirrors was AR coated on both sides. These elements resulted in cavity magnification (M) values of 1.23 and 1.14, corresponding to output coupling of 34 and 24%, respectively, values that are very much higher than the $\sim 5\%$ previously found to be optimum for a free-running stable resonator.^{9,10} Since oscillation in this type of unstable resonator builds up most readily in the "lossless" paraxial region,¹ and since (for these small magnifications) the injection hole constitutes a large loss ($\sim 70\%$) to the paraxial volume, significant self-oscillation (injected or not) is not possible. Indeed, the output energy obtained by operating these resonators as free-running oscillators was three to four orders of magnitude lower than that obtained using an optimized stable resonator under otherwise similar conditions.¹⁰ Thus, in this case the primary role of the cavity is to serve as the beam-expanding telescope of a regenerative amplifier. Hence the term *injection controlled* is used instead of injection locked.

The temporal relationships among the injected 482-nm dye laser pulse, the e -beam excitation pulse, the XeF ($C \rightarrow A$) laser output at 482 nm, and the free-running broadband XeF ($C \rightarrow A$) laser output are shown in Fig. 2. Also shown for

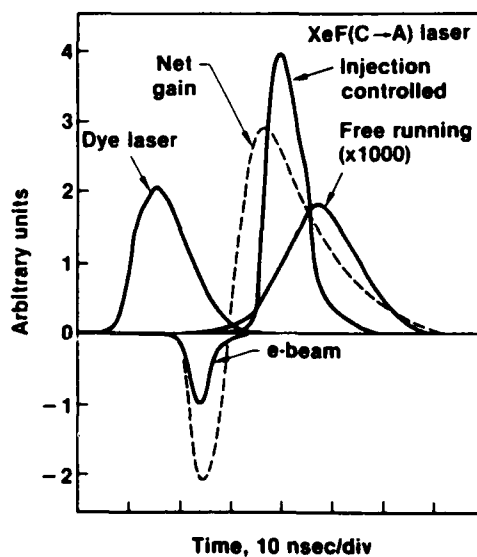


FIG. 2. Approximate temporal relationships among the 482-nm injected dye laser pulse at the cavity input hole, the e -beam excitation pulse, the 482-nm XeF ($C \rightarrow A$) laser output at the cavity exit, and the broadband free-running XeF ($C \rightarrow A$) laser output. Also shown is the typical temporal evolution of the zero field net gain at 488 nm. For the present mixture, 6.5 atm Ar, 16 Torr Xe, 8 Torr NF₃, and 8 Torr F₂, the peak gain is $\sim 2.75\%$ cm⁻¹ (Ref. 10).

illustrative purposes is the temporal evolution of the *net* gain at 488 nm. The causes of the strong initial absorption occurring during the *e*-beam excitation pulse have been identified and are explained in detail elsewhere.^{9,10} Because of the low magnification, it takes ~ 10 round trips through the ~ 13 -cm-long cavity before the injected dye laser pulse expands to fill the active cavity volume, requiring a time of ~ 10 ns. Thus, the duration of the injected pulse, the rise time and the duration of the gain, and the cavity fill time are all about the same. For this reason, the timing of the dye laser pulse with respect to the firing of the *e*-beam was found to be quite critical and had to be controlled to within a few nanoseconds in order to obtain repeatable results.

Figure 3 shows the dependence of the XeF ($C \rightarrow A$) output pulse energy on the energy of the injected dye laser pulse for the $M = 1.23$ cavity. Because of the low magnification, in the *absence* of *e*-beam excitation 60 to 70% of the dye laser energy is reflected back out through the 2-mm-diam hole in the concave mirror. The fraction of the input pulse that escapes through the hole when the *e*-beam is fired is likely to be somewhat lower due to spatial nonuniformity of the gain medium. Thus, the input energy shown in Fig. 3 represents an upper limit to the actual intracavity value, and the output-input ratio that can be inferred from the data is therefore a lower limit. The linear dependence of the output pulse energy on dye laser input energy for a three order of magnitude variation of the latter indicates that the cavity/medium combination is acting as a multipass amplifier for the present conditions and that the gain is not significantly saturated until high input energies are reached. Such behavior is consistent with the very low output obtained with the resonator operating as a free-running oscillator. However, saturation of the gain medium appears to occur for input pulse energies above approximately 0.1 mJ. The 20-mJ maximum output for the $M = 1.23$ cavity corresponds to an energy density of 1 J/l and an intrinsic energy utilization efficiency of approxi-

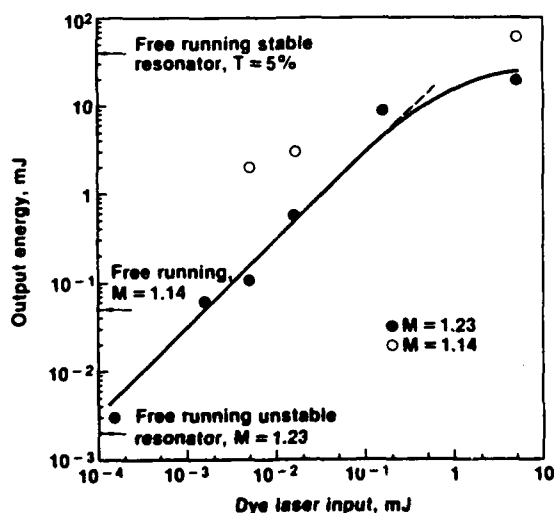


FIG. 3. XeF ($C \rightarrow A$) output pulse energy dependence on the injected dye laser energy, both at 482 nm, measured using a calibrated vacuum photodiode detector. The gas mixture was comprised of 6.5 atm Ar, 16 Torr Xe, 8 Torr NF_3 , and 8 Torr F_2 ; and volumetric *e*-beam energy deposition was ~ 100 J/l (Ref. 9). Laser output levels obtained with unstable and stable (optimized) free-running oscillators are indicated.

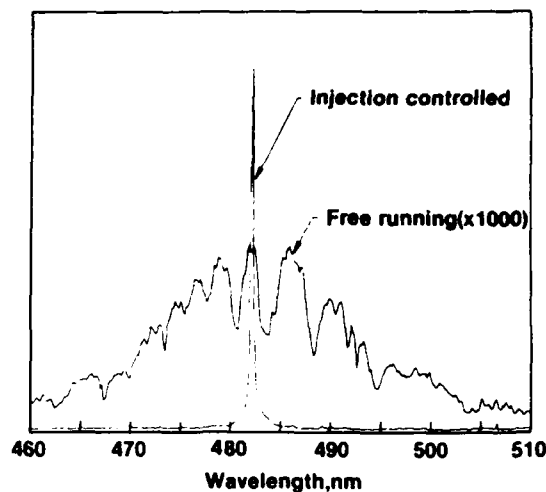


FIG. 4. XeF ($C \rightarrow A$) spectra for the free-running and injection-controlled conditions of Fig. 3. The resolution limit of the measurement system was 0.5 nm.

mately 1%, based on an active volume of 20 cm^3 and an *e*-beam energy deposition of $\sim 100 \text{ J/l}$.⁹ For the same conditions the $M = 1.14$ cavity resulted in an output energy an order of magnitude higher than the $M = 1.23$ cavity when the input energy was < 0.01 mJ, with a maximum output of over 60 mJ at saturation, corresponding to energy density and intrinsic efficiency values of 3 J/l and approximately 2.5%, respectively.¹¹ For the net gain typical of these conditions (Fig. 2) the significantly increased output obtained using the $M = 1.14$ cavity compared to that of the $M = 1.23$ cavity is consistent with the $\sim 50\%$ longer amplification path length of the former.

Presented in Fig. 4 is the broadband XeF ($C \rightarrow A$) spectrum typical of the unstable (or stable^{9,10}) resonators operating as free-running oscillators, compared with that of the injection-controlled XeF ($C \rightarrow A$) amplifier. The indicated ~ 0.5 -nm width of the amplified 482-nm pulse reflects the resolution limit of our present measurement system. Preliminary evaluation of the spectral characteristics of the narrowed XeF ($C \rightarrow A$) output indicates that the spectral width is nearly the same as that of the dye laser input, i.e., $\Delta\lambda \sim 0.01$ nm. In these experiments the dye laser output was tuned so as to coincide with a maximum in the free-running laser spectrum (Fig. 4). However, tuning the input a few nanometers to the location of an absorption valley resulted in no significant changes in the output. Although the broadband laser spectrum of a free-running oscillator (stable or unstable) typically is limited to the 465–495-nm range within which the gain is a maximum, measurements show^{9,10} that the net gain is reduced from its maximum at ~ 485 nm by only $\sim 20\%$ for wavelengths as low as 460 nm and as high as 510 nm, indicating that continuous tuning over a broad range with high-energy output should be possible.

This investigation has shown that simultaneous narrow spectral output and efficient energy extraction can be obtained using an XeF ($C \rightarrow A$) laser medium to amplify an injected dye laser pulse. These results indicate that *efficient*, narrow spectral output should be attainable throughout the entire blue-green region using an injection-controlled, elec-

trically excited XeF ($C \rightarrow A$) medium, with the medium serving either as an amplifier as in the present investigation or as an injection-locked oscillator. However, longer gain lengths will be required for true efficient oscillator operation of an unstable cavity.

It is a pleasure to acknowledge the helpful comments of our colleagues: Dr. R. Sauerbrey of Rice University and Dr. I. J. Bigio of Los Alamos National Laboratory. In addition, the authors wish to thank J. Hooten for his valuable technical assistance. This work was supported in part by the Office of Naval Research, the National Science Foundation, and the Robert A. Welch Foundation.

¹I. J. Bigio and M. Slatkine, *IEEE J. Quantum Electron.* **QE-19**, 1426 (1983).

²J. B. West, H. Komine, and E. A. Stappaerts, *J. Appl. Phys.* **52**, 5383 (1981).

³T. Shay, F. Hanson, D. Gookin, and E. J. Schimitschek, *Appl. Phys. Lett.*

39, 783 (1981).

⁴R. Burnham and N. Djeu, *Opt. Lett.* **3**, 215 (1978).

⁵W. K. Bischel, D. J. Eckstrom, H. C. Walker, Jr., and R. A. Tilton, *J. Appl. Phys.* **52**, 4429 (1981).

⁶J. Liegel, F. K. Tittel, and W. L. Wilson, Jr., *Appl. Phys. Lett.* **39**, 369 (1981).

⁷C. H. Fisher, R. E. Center, G. J. Mullaney, and J. P. McDaniel, *Appl. Phys. Lett.* **35**, 901 (1979).

⁸W. L. Nighan, Y. Nachshon, F. K. Tittel, and W. L. Wilson, Jr., *Appl. Phys. Lett.* **42**, 1006 (1983).

⁹Y. Nachshon, F. K. Tittel, W. L. Wilson, Jr., and W. L. Nighan, *J. Appl. Phys.* **56**, 36 (1984).

¹⁰W. L. Nighan, F. K. Tittel, W. L. Wilson, Jr., N. Nishida, Y. Zhu, and R. Sauerbrey, *App. Phys. Lett.* **45**, 947 (1984).

¹¹In the work reported herein only Ar-Xe-NF₃-F₂ mixtures were used. Five component mixtures containing Kr require nearly an order of magnitude less F₂ for optimum performance, a factor which complicates the passivation procedure for the present apparatus. Nonetheless, the magnitude of the net gain is significantly larger and its duration longer for Kr-containing mixtures than is the case for the mixture used in the present work (Ref. 10). This indicates that much higher levels of output energy/efficiency should be attainable with no increase in either the energy of the injected input pulse or the e-beam excitation pulse.

Simultaneous Multiwavelength Operation of a Commercial Rare Gas Halide Laser

R. A. SAUERBREY, W. L. NIGHAN, F. K. TITTEL, W. L. WILSON, JR., AND J. KINROSS-WRIGHT

Abstract—Simultaneous dual wavelength operation of a commercial-discharge excited rare gas halide excimer laser is reported for the first time. A combined energy output in excess of 20 mJ was obtained for the 193 and 248 nm ArF and KrF $B \rightarrow X$ transitions oscillating simultaneously, and also for the 248 and 351 nm KrF and XeF transitions. Analysis indicates that significantly higher dual wavelength energies should be possible.

INTRODUCTION

FOR applications in areas such as spectroscopy, optical diagnostics, materials processing, and medicine, it may be useful to have the capability of operating a *single* rare gas halide excimer laser system at two or more wavelengths. In this letter, we report the first demonstration of relatively efficient, simultaneous oscillation of two UV rare gas halide transitions in a commercial excimer laser.

In a previous investigation, it was shown that an electron-beam excited medium that had been optimized for efficient blue/green XeF($C \rightarrow A$) laser oscillation also exhibited strong net gain on the UV $B \rightarrow X$ transition, and that simultaneous laser oscillation on both transitions was possible [1]. Subsequently, relatively efficient (~ 0.25 percent), simultaneous UV/visible XeF laser oscillation was achieved through use of an optimized dual wavelength resonator along with addition of Kr to the gas mixture [2], [3]. In that work, the intensity of the 248 nm KrF($B \rightarrow X$) fluorescence was observed to be comparable to that of the 351 nm XeF($B \rightarrow X$) fluorescence under conditions for which the dual XeF $B \rightarrow X$ and $C \rightarrow A$ laser output energies were equal. Since the kinetics of the $B \rightarrow X$ transitions of KrF and XeF are actually less competitive than those of the XeF $B \rightarrow X$ and $C \rightarrow A$ transitions, this observation suggested that efficient, simultaneous multiple wavelength oscillation on $B \rightarrow X$ rare gas halide transitions should be possible using appropriate gas mixtures in a commercial-discharge excited excimer laser.

EXPERIMENTAL APPARATUS AND PROCEDURE

In order to investigate the possibility of simultaneous "dual wavelength" operation, we used an unmodified commercial excimer laser. This laser has a discharge

Manuscript received September 16, 1985; revised October 8, 1985. This work was supported by the Office of Naval Research, the National Science Foundation, and the Robert A. Welch Foundation.

R. A. Sauerbrey, F. K. Tittel, W. L. Wilson, Jr., and J. Kinross-Wright are with the Department of Electrical and Computer Engineering, Rice University, Houston, TX 77251.

W. L. Nighan is with United Technologies Research Center, East Hartford, CT 06108.

IEEE Log Number 8406662.

length of 50 cm, an interelectrode spacing of 2.6 cm, and an active discharge volume of approximately 0.12 l. The optical resonator consists of a MgF₂ coated aluminum high-reflectivity mirror and a CaF₂ window that serves as the output coupler. The distance between the window and the mirror is 75 cm. The laser was operated with a discharge voltage of 30 kV and a repetition frequency in the 3–10 s⁻¹ range. Laser gases were mixed inside the laser cavity which had been thoroughly passivated through several months' use with mixtures containing only fluorides. Gas pressures were measured with the built-in manometer of the laser. In order to obtain accurate gas pressure measurement when mixture constituents with partial pressure below 50 mbar were required, the low partial pressure gases were prediluted in helium, the recommended buffer gas for rare gas fluoride laser operation. For each change in gas mixture, a new fill was used.

The total output energy of the laser was measured by means of two calibrated Gentec pyroelectric energy meters (Models ED 200 and ED 500). A quartz flat served as a beam splitter to guide part of the laser output to a vacuum photodiode. Interference and color glass filters were used for spectral selection of the laser transitions. Quartz neutral-density filters served as attenuators for the laser beam. This arrangement permitted an accurate determination of the total laser energy without regard to wavelength, as well as independent laser energy and temporal pulse shape measurements for each UV laser transition.

The total energy output of our laser operating on each of the rare gas fluoride $B \rightarrow X$ transitions individually was (90 ± 20) mJ for ArF (193 nm), (250 ± 40) mJ for KrF (248 nm), and (80 ± 20) mJ for XeF (351 nm). These values were obtained using the optimum *three*-component gas mixtures recommended by the manufacturer. The maximum energy values for KrF and XeF are in accord with the manufacturer's specifications, whereas the measured ArF output is approximately half of the optimum energy output for this laser. The 193 nm ArF laser transition is by far the most sensitive of the rare gas fluorides to gradual deterioration of system components through normal use [4]. Therefore, considering the age and prior history of the laser used in this investigation, the reduced ArF laser energy level is not unusual.

RESULTS AND ANALYSIS

In order to obtain dual wavelength oscillation on the KrF and XeF transitions, xenon was added gradually to the

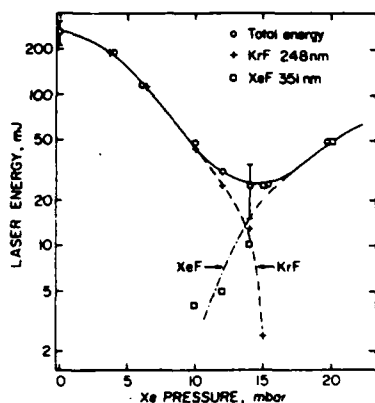


Fig. 1. Total UV laser energy and KrF and XeF laser energies as a function of Xe pressure for a mixture comprised of 6 mbar F_2 , 150 mbar Kr and He at an initial total pressure of 2.5 bar. In the absence of Xe, this mixture is optimized for KrF laser oscillation alone. The discharge voltage was 30 kV.

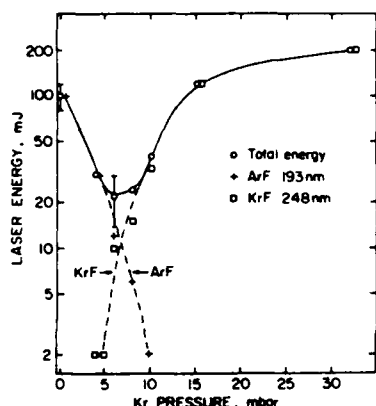


Fig. 2. Total UV laser energy and ArF and KrF laser energies as a function of Kr pressure for a mixture comprised of 7.5 mbar F_2 , 350 mbar Ar and He at an initial total pressure of 2.2 bar. In the absence of Kr, this mixture is optimized for ArF laser oscillation alone. The discharge voltage was 30 kV.

three-component He-Kr- F_2 mixture that had been optimized for 248 nm KrF laser oscillation alone. A similar experiment was carried out starting with a mixture optimized for 193 nm ArF oscillation; in this case, Kr was added gradually to the optimum He-Ar- F_2 mixture. The results of these experiments are shown in Figs. 1 and 2.

As xenon is added to the mixture optimized for KrF laser oscillation, the total laser output energy decreases to a value about one tenth the initial value typical of KrF alone. A minimum is established for a xenon pressure of about 14 mbar, above which the total energy increases (Fig. 1). The spectrally resolved data show that initially the KrF laser energy decreases with increasing xenon pressure. For xenon pressures between 10 and 15 mbar, both the 248 nm KrF and the 351 nm XeF lasers exhibit laser action simultaneously. At a xenon pressure of ~14 mbar, the energy of each laser is 10-15 mJ, resulting in a total combined energy of about (25 ± 10) mJ, corresponding to an overall efficiency of ~0.2 percent based on the energy stored in the capacitors. For xenon pressures above 15 mbar, the laser operates only on the 351 nm XeF tran-

sition, achieving an output energy at 20 mbar that approaches the maximum value that can be obtained using the optimized three-component XeF laser mixture. Since no effort was made to optimize the fractional concentrations of Kr, Xe, or F_2 in the four-component mixture of Fig. 1, it seems likely that higher dual laser energy could be achieved with mixture reoptimization and/or that the output from a four-component mixture optimized for XeF oscillation alone might actually be higher than that obtainable using the recommended three-component mixture.

Dual KrF and XeF laser oscillation was also demonstrated [5] using another laser of the same type that previously had been operated for several months using an XeCl gas fill. The dependence of the total laser energy on Xe pressure was found to be essentially the same as that shown in Fig. 1, but not until the system had been operated with rare gas fluoride mixtures for nearly a week. Thus, the relatively lengthy fluorine passivation procedure that is typical of conversion from chloride to fluoride operation for lasers of this general type is exceptionally important for the reduced laser energy levels characteristic of dual UV wavelength operation.

Behavior generally similar to that of Fig. 1 was also observed for the dual ArF and KrF laser experiments (Fig. 2). Starting with a mixture optimized for ArF laser oscillation alone, upon addition of Kr, the total laser energy decreases from its initial level characteristic of ArF (but below specification as described previously). In this case, the minimum in total laser energy is reached at a Kr pressure of ~7 mbar. At this point, the combined ArF and XeF laser energies are equal and the total output of ~25 mJ is almost exactly the same as that of the KrF and XeF lasers, even though the initial ArF laser energy was much lower than that of the KrF laser (Fig. 1). For Kr pressures higher than 7 mbar, the KrF laser takes over, reaching an energy level at 30 torr for this nonoptimized four-component mixture that, at ~200 mJ, is practically equivalent to that typical of the optimized three-component KrF mixture, once again suggesting that an optimized four-component mixture might yield a higher KrF laser energy than a three-component mixture.

Attempts to demonstrate simultaneous ArF and XeF oscillation were not successful. Addition of even small amounts of Xe (~1 mbar) to the optimized ArF mixture resulted in a sharp decrease from the already subspecification initial level for ArF alone. However, further increases in Xe pressure did result in XeF laser oscillation.

For the conditions in Figs. 1 and 2, the laser pulsewidth decreased gradually as the third rare gas was added to produce dual UV laser action. When xenon was added to the optimized three-component KrF mixture, the KrF pulsewidth decreased from 20 ns to about 9 ns at the total energy minimum occurring for a Xe pressure of ~14 mbar (Fig. 1). For this xenon pressure, the XeF laser pulsewidth was about 8 ns and increased gradually to about 15 ns with increasing xenon pressure. Thus, the relative decrease in the total laser peak power accompanying dual laser operation is only about half the relative decrease in the total

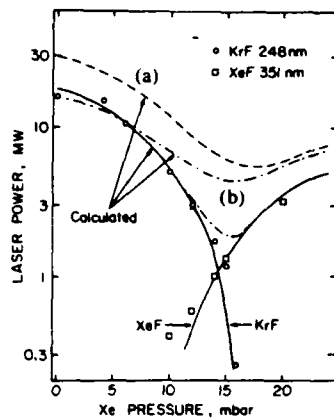


Fig. 3. KrF and XeF laser power corresponding to the conditions of Fig. 1. The solid lines are the result of calculations based on the medium/resonator properties typical of the laser used in this investigation following the procedure described in the text. The possible effects of increasing the length of the active medium by 50 percent (a) or of replacing the CaF_2 output window with a mirror having a reflectivity of 20 percent (b) are also shown.

laser energy. The peak powers for the KrF and the XeF dual laser corresponding to the condition of Fig. 1 are shown in Fig. 3. For the conditions of combined laser action, the pulses from both lasers overlapped temporarily.

In order to evaluate the prospects for improved dual wavelength laser performance, we have developed an approximate analysis relating KrF and XeF laser gain in a rare gas fluoride medium containing both Kr and Xe. When combined with Schindler's theory [6] of optical power extraction, modified to account for laser oscillation at two wavelengths, this approach permits us to relate laser power to experimental resonator variables such as length and output coupling, and to KrF/XeF medium properties such as saturation intensity, small-signal gain, and absorption loss. The total pumping density was distributed between production of KrF and XeF by defining the fractional pumping power density contributing to XeF formation as δ_x . Within the framework of our analysis, it is easily shown that the KrF small-signal gain coefficients are then related in the following way:

$$g_{\text{XeF}} = g_{\text{XeF}_0} \delta_x$$

$$g_{\text{KrF}} = g_{\text{KrF}_0} (1 - \delta_x)$$

where g_{XeF_0} and g_{KrF_0} are the gain coefficient for either an XeF or KrF laser *alone*. Assuming that the primary transfer reactions from the KrF chain to the XeF chain are linear in Xe pressure, the variable δ_x is then simply proportional to Xe pressure.

For the present purposes, medium properties typical of discharge-excited KrF and XeF lasers similar to ours were used in the analysis [7], [8]. Fig. 3 presents measured and computed values of dual KrF and XeF laser power corresponding to the conditions of Fig. 1. Using the resonator parameters of our laser and guided by the experimental data reported by Gower and co-workers [7], [8], values of KrF medium properties were selected so as to ensure agreement between measured and computed KrF laser

power with *no* Xe in the mixture, i.e., the left boundary of Fig. 3. Using those specific values of KrF gain, absorption, and saturation intensity, a complementary set of XeF medium properties was chosen [9]. The constant of proportionality relating the fractional XeF power density δ_x to Xe pressure was then selected so as to ensure agreement between measured and computed dual laser power for the Xe pressure at which the KrF and XeF laser power are equal, i.e., a Xe pressure of 14 mbar. With this information, the laser power for KrF and XeF could be determined for all Xe pressures over the range of interest. The solid lines in Fig. 3 clearly show that the self-consistent set of KrF and XeF variables so determined is capable of reproducing the qualitative and quantitative variation of dual laser power that we have observed.

Using the set of variables resulting in the solid lines shown in Fig. 3, the calculation was then repeated for a discharge length 50 percent larger than that of the laser used in this investigation [Fig. 3(a)]. At the end points (Xe pressure 0 or ~ 25 mbar), the respective KrF and XeF laser powers increase by approximately 50 percent, as should be the case since the laser medium is nearly saturated with either KrF or XeF operating alone. However, for Xe pressures typical of the minimum dual laser power for which the medium is far from saturation, a 50 percent increase in discharge length results in a factor of three increase in laser power. Fig. 3(b) illustrates the effect of replacing the CaF_2 output window ($R < 10$ percent) with a mirror having a 20 percent reflectivity at both laser wavelengths. In this case, the minimum dual laser output is increased by more than a factor of two. These illustrative results suggest that dual laser powers substantially in excess of those demonstrated in this investigation should be attainable.

SUMMARY

We have demonstrated that an unmodified commercial excimer laser is capable of simultaneously producing relatively high-energy laser oscillation on two different UV rare gas halide transitions by way of an appropriate choice of mixture composition. Furthermore, analysis indicates that with relatively minor changes in discharge and/or resonator properties, dual wavelength laser energy/efficiency levels comparable to those typical of a single wavelength rare gas halide laser should be possible.

ACKNOWLEDGMENT

The authors appreciate the cooperation of J. J. Hinchey and R. E. Cutting of United Technologies Research Center.

REFERENCES

- [1] R. Sauerbrey, Y. Zhu, F. K. Tittel, W. L. Wilson, Jr., N. Nishida, F. Emmert, and W. L. Nighan, "Simultaneous UV visible laser oscillation on the $B \rightarrow X$ and $C \rightarrow A$ XeF excimer transitions," *IEEE J. Quantum Electron.*, vol. QE-21, pp. 418-420, 1985.
- [2] R. Sauerbrey, F. K. Tittel, W. L. Wilson, Jr., Y. Zhu, N. Nishida, and W. L. Nighan, "Efficient simultaneous multiwavelength UV/visible operation of excimer lasers," presented at CLEO 1985, Baltimore, MD, post-deadline paper.

- [3] W. L. Nighan, F. K. Tittel, W. L. Wilson, Jr., N. Nishida, Y. Zhu, and R. Sauerbrey, "Synthesis of rare gas-halide mixtures resulting in efficient XeF($C \rightarrow A$) laser oscillation," *Appl. Phys. Lett.*, vol. 45, pp. 947-949, 1984.
- [4] B. Klimt, Lambda Physik, private communication.
- [5] J. J. Hitchen and R. E. Cutting, United Technol. Res. Cen. private communication.
- [6] G. M. Schindler, "Optimum output efficiency of homogeneously broadened lasers with constant loss," *IEEE J. Quantum Electron.*, vol. QE-16, pp. 546-550, 1980.
- [7] M. C. Gower and C. B. Edwards, "Gain and absorption measurements in a discharge excited KrF laser," *Opt. Commun.*, vol. 40, pp. 369-372, 1982.
- [8] M. C. Gower, R. Exberger, P. D. Rowley, and K. W. Billmann, "Measurements of kinetic processes in a self-sustained discharge XeF laser," *Appl. Phys. Lett.*, vol. 33, pp. 65-67, 1978.
- [9] The parameters used in the illustrative examples of Fig. 3 were, for KrF and XeF, respectively, saturation intensity $2.5 \text{ MW} \cdot \text{cm}^{-2}$ and $1.1 \text{ MW} \cdot \text{cm}^{-2}$, small-signal gain coefficient $8 \text{ percent} \cdot \text{cm}^{-1}$ and $5.5 \text{ percent} \cdot \text{cm}^{-1}$, and unsaturated absorption coefficient $0.6 \text{ percent} \cdot \text{cm}^{-1}$ for both. The reflectance of the high-reflectivity mirror was taken as 80 percent for both wavelengths. Although these variables do not constitute a unique set, they do represent a physically reasonable, self-consistent set that, within the framework of our illustrative analysis, is capable of reproducing the observed experimental dual wavelength output. For this reason, the curves of Fig. 3 illustrating the effect of changes in discharge length and/or output window are felt to provide a reasonable first-order estimate of the potential for improving dual laser performance.

Simultaneous UV/Visible Laser Oscillation on the $B \rightarrow X$ and $C \rightarrow A$ XeF Excimer Transitions

ROLAND SAUERBREY, YUNPING ZHU, FRANK K. TITTEL, WILLIAM L. WILSON, JR., N. NISHIDA, F. EMMERT, AND WILLIAM L. NIGHAN

Abstract—Simultaneous laser oscillation from the 351 nm XeF($B \rightarrow X$) transition and the broad-band XeF($C \rightarrow A$) transition centered near 475 nm has been demonstrated using intense, short-pulse electron-beam excitation of high-pressure gas mixtures. Analysis of the causes of transient absorption suggests that it may be possible to obtain efficient UV/visible laser oscillation from each of the XeF excimer transitions excited in the same medium.

INTRODUCTION

XENON fluoride is the only diatomic rare gas-halide molecule exhibiting two lasing transitions. Laser oscillation occurs on the $B(\frac{1}{2})-X(\frac{1}{2})$ transition in the near ultraviolet at 351 nm, and on the broad-band tunable $C(\frac{3}{2})-A(\frac{3}{2})$ transition in the visible centered near 475 nm. Electrically excited lasers operating on the $B \rightarrow X$ transition have been under investigation for several years, and are capable of very efficient (~ 2 -5 percent) generation of high-power UV radiation [1]. Recently, efficient (> 1 percent) operation of the XeF($C \rightarrow A$) laser with an energy output in excess of 3 J/l was also demonstrated [2], [3]. For a variety of applications such as frequency mixing or multistep photoexcitation, it might be of interest to have an efficient laser source that is capable of emitting intense UV and tunable visible radiation simultaneously. In this letter, the feasibility of simultaneous operation of the XeF($B \rightarrow X$) and ($C \rightarrow A$) laser transitions in the same apparatus is reported for the first time.

EXPERIMENTAL APPARATUS AND PROCEDURE

A gas mixture comprised of 8 torr F_2 , 8 torr NF_3 , 16 torr Xe, and 6.5 atm Ar was excited by an intense electron beam (1 MeV, 250 A \cdot cm $^{-2}$, 10 ns FWHM), conditions previously found to be compatible with efficient XeF ($C \rightarrow A$) laser operation [2]. In order to investigate the possibility of simultaneous laser oscillation on both XeF excimer transitions, a dual-wavelength resonator was constructed using broad-band mirrors that were available in our laboratory. The basic de-

Manuscript received November 7, 1984; revised January 11, 1985. This work was supported in part by the Office of Naval Research, the National Science Foundation, and the Robert A. Welch Foundation. The work of R. Sauerbrey was supported by the Deutsche Forschungsgemeinschaft.

R. Sauerbrey, Y. Zhu, F. K. Tittel, W. L. Wilson, Jr., and N. Nishida are with the Department of Electrical and Computer Engineering, Rice University, Houston, TX 77251.

F. Emmert is with the Physikalisches Institut der Universität Würzburg, D-8700, Würzburg, West Germany.

W. L. Nighan is with United Technologies Research Center, East Hartford, CT 06108.

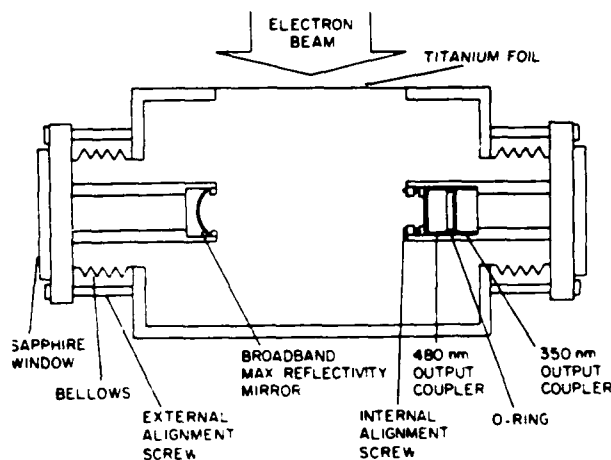


Fig. 1. Dual wavelength resonator configuration for the simultaneous operation of the XeF ($B \rightarrow X$) and XeF ($C \rightarrow A$) lasers.

sign of this resonator is shown in Fig. 1. A curved mirror with more than 99 percent reflectivity between 350 and 490 nm was used as the full reflector. Two flat output couplers were mounted as shown. The broad-band $C \rightarrow A$ output coupler had a reflectivity of 98 percent at a wavelength of 510 ± 30 nm and a transmissivity of 90 percent for 351 nm radiation, while the $B \rightarrow X$ output mirror had a reflectivity of 83 percent for the UV radiation and 60 percent transmissivity in the visible region. Between these two mirrors, a viton O-ring was inserted and, by means of a set of three adjustment screws, the $C \rightarrow A$ mirror was aligned so as to be parallel to the $B \rightarrow X$ mirror. Alignment was performed before the mirrors were installed in the reaction cell. Both mirror holders could then be aligned externally as described in [2]. The dual-wavelength resonator so constructed had relatively small intracavity losses for the $C \rightarrow A$ transition, while those for the $B \rightarrow X$ transition were quite high. However, the gain of the narrow-band UV bound-bound transition is considerably larger than that of the $C \rightarrow A$ transition, since the $B \rightarrow X$ stimulated emission cross section is about 30 times larger than that of the $C \rightarrow A$ transition.

RESULTS AND ANALYSIS

Although the gas mixture was far from optimum for $B \rightarrow X$ laser oscillation [1], and the $C \rightarrow A$ resonator was not optimized, laser oscillation on both transitions was routinely observed. Presented in Figs. 2 and 3 are the temporal and spectral characteristics of the UV and blue/green XeF $B \rightarrow X$ and $C \rightarrow A$ laser pulses obtained using the dual, coincident UV/visible cavity configuration illustrated in Fig. 1. As described

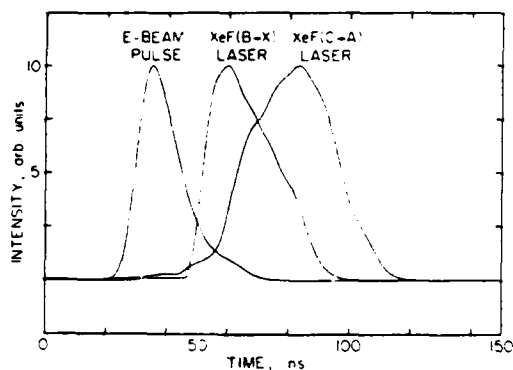


Fig. 2. Temporal evolution of the e -beam pulse and the XeF($B \rightarrow X$) and XeF($C \rightarrow A$) laser pulses for a mixture comprised of 6.5 atm Ar, 16 torr Xe, 8 torr F_2 , and 8 torr NF_3 .

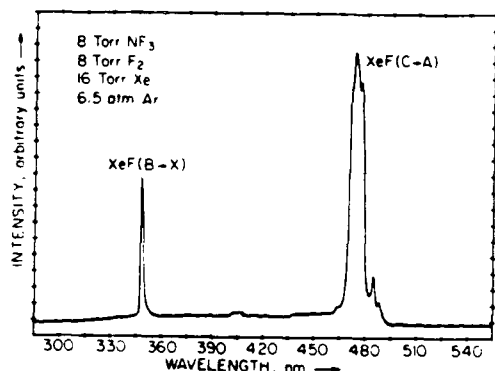


Fig. 3. Time integrated spectrum of the XeF $B \rightarrow X$ laser at 351 nm and $C \rightarrow A$ laser centered near 475 nm.

previously [2], the e -beam pulse results in the production of broad-band absorbing species, and therefore, the laser pulses appear in the afterglow regime (Fig. 2). The net effect of transient absorption is most severe for the $C \rightarrow A$ transition due to the fact that its cross section for stimulated emission is relatively small ($\sim 10^{-17} \text{ cm}^2$) [4]. Thus, the onset of the $C \rightarrow A$ laser pulse is delayed for a longer time than that of the $B \rightarrow X$ pulse.

The laser spectrum (Fig. 3) shows both the narrow $B \rightarrow X$ emission at 351 nm and the broad-band $C \rightarrow A$ emission centered near 475 nm. The laser wavelength and spectral width for the $C \rightarrow A$ transition are mainly determined by the specific properties of the end reflector and output coupler. For the present nonoptimized dual-wavelength resonator, the laser pulse energy levels were relatively low; $\sim 0.01 \text{ J/l}$ was obtained from the $C \rightarrow A$ transition and $\sim 0.05 \text{ J/l}$ for the $B \rightarrow X$ transition. However, for these specific conditions, $C \rightarrow A$ laser pulse energy in excess of 1.0 J/l has been routinely obtained using an optimized resonator [3].

Presented in Fig. 4 is the temporal evolution of the various contributions to the gain and absorption at 351 and 475 nm, computed for the conditions of Figs. 2 and 3 following the procedures described in detail in [2]. The *net* gain shown for the blue-green $C \rightarrow A$ transition is in very good agreement with experimental observations [2], [3]. We have not measured the gain/absorption in the UV region. However, the results

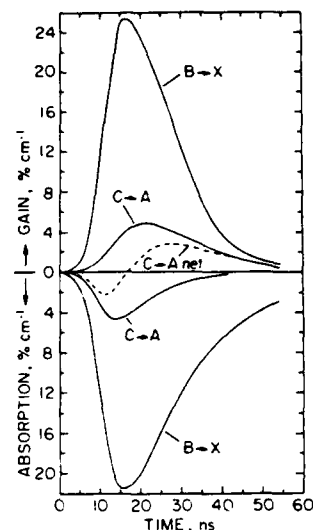


Fig. 4. Contributions to the XeF($B \rightarrow X$) and XeF($C \rightarrow A$) gain and absorption at 351 and 475 nm, respectively, computed for the conditions of Figs. 2 and 3 following the procedures described in [2].

of Fig. 4 show that the computed *net* gain for the UV $B \rightarrow X$ transition (~ 4 percent cm^{-1} maximum at ~ 15 - 20 ns) is the difference between two much larger gain-absorption values. For these specific mixture conditions, which have been optimized for blue-green $C \rightarrow A$ laser oscillation, the calculations show that absorption in the UV is dominated (>75 percent) by Ar_2F photodissociation [5]. Krypton has been found to be an effective quenching species for Ar_2F [6]. Moreover, subsequent to the completion of this work, it was found that the addition of Kr at partial pressures in the 0.5-1.0 atm range results in an increased rate of XeF(B, C) formation and in a decrease in absorption in the visible region, the combined effect of which is a significant increase in *net* gain for the $C \rightarrow A$ transition [3]. For these reasons, mixtures containing Kr might exhibit higher levels of net gain for *both* the $B \rightarrow X$ and $C \rightarrow A$ transitions than those indicated in Fig. 4. This suggests that significantly higher $B \rightarrow X/C \rightarrow A$ dual laser output may be possible.

SUMMARY

We have demonstrated that an e -beam excited medium that has been optimized for efficient blue/green XeF($C \rightarrow A$) laser oscillation also exhibits strong net gain for the UV $B \rightarrow X$ transition, and that simultaneous laser oscillation on both transitions is possible. Further, our results show that the presence of a strong $B \rightarrow X$ flux has relatively little effect on $C \rightarrow A$ gain. These findings suggest that with an optimum resonator design and/or with additional mixture refinement, efficient (≥ 1 percent) UV/visible laser oscillation from *each* of the XeF excimer transitions excited in the same medium may be possible.

REFERENCES

- [1] J. C. Hsia, J. A. Mangano, J. H. Jacob, and M. Rokni, "Improvement in XeF laser efficiency at elevated temperatures," *Appl. Phys. Lett.*, vol. 34, pp. 208-210, 1979.
- [2] Y. Nachshon, F. K. Tittel, W. L. Wilson, Jr., and W. L. Nighan,

- "Efficient XeF($C \rightarrow A$) laser oscillation using electron beam excitation," *J. Appl. Phys.*, vol. 56, pp. 36-48, 1984.
- [3] W. L. Nighan, F. K. Tittel, W. L. Wilson, Jr., N. Nishida, Y. Zhu, and R. Sauerbrey, "Synthesis of rare gas-halide mixtures resulting in efficient XeF($C \rightarrow A$) laser oscillation," *Appl. Phys. Lett.*, vol. 45 pp. 947-949, 1984.
- [4] W. K. Bischel, D. J. Eckstrom, H. C. Walters, Jr., and R. A. Tilton, "Photolytically pumped XeF($C \rightarrow A$) laser studies," *J. Appl. Phys.*, vol. 52, pp. 4429-4434, 1981.
- [5] W. R. Wadt and P. J. Hay, "Electronic states of Ar₂F and Kr₂F," *J. Chem. Phys.* vol. 68, pp. 3850-3863, 1978. In the present work, the Ar₂F photoabsorption cross section at 351 nm was taken as 1.7×10^{-17} cm², a value typical of Ar₂⁺. See H. H. Michels, R. H. Hobbs, and L. A. Wright, *J. Chem. Phys.*, vol. 71, p. 5053, 1978.
- [6] R. Sauerbrey, F. K. Tittel, W. L. Wilson, Jr., and Y. Zhu, "The displacement reactions of the triatomic rare gas-halide excimers," *J. Chem. Phys.*, to be published.

III. PATENTS

Two-Halogen Donor Mixture for XeF(C→A) Laser, U. S. Patent 4,660,210 issued April 21, 1987. Inventors: W. L. Nighan, F. K. Tittel and W. L. Wilson, Jr.

Multi-Component Buffer Gas Mixture for XeF(C→A) Laser, U.S. Patent 4,646,311, issued February 24, 1987. Inventors: W. L. Nighan, F. K. Tittel and W. L. Wilson, Jr.

Multiple Wavelength Excimer Laser, U. S. Patent (to be issued, March 1989).
Inventors: W. L. Nighan, F. K. Tittel and R. A. Sauerbrey.

APRIL 1984

REPORTS DISTRIBUTION LIST FOR ONR PHYSICS DIVISION OFFICE
UNCLASSIFIED CONTRACTS

Director Defense Advanced Research Projects Agency Attn: Technical Library 1400 Wilson Blvd. Arlington, Virginia 22209	1 copy
Office of Naval Research Physics Division Office (Code 412) 800 North Quincy Street Arlington, Virginia 22217	2 copies
Office of Naval Research Director, Technology (Code 200) 800 North Quincy Street Arlington, Virginia 22217	1 copy
Naval Research Laboratory Department of the Navy Attn: Technical Library Washington, DC 20375	1 copy
Office of the Director of Defense Research and Engineering Information Office Library Branch The Pentagon Washington, DC 20301	1 copy
U.S. Army Research Office Box 1211 Research Triangle Park North Carolina 27709	2 copies
Defense Technical Information Center Cameron Station Alexandria, Virginia 22314	12 copies
Director, National Bureau of Standards Attn: Technical Library Washington, DC 20234	1 copy
Director U.S. Army Engineering Research and Development Laboratories Attn: Technical Documents Center Fort Belvoir, Virginia 22060	1 copy
ODDR&E Advisory Group on Electron Devices 201 Varick Street New York, New York 10014	1 copy

Air Force Office of Scientific Research Department of the Air Force Bolling AFB, DC 22209	1 copy
Air Force Weapons Laboratory Technical Library Kirtland Air Force Base Albuquerque, New Mexico 87117	1 copy
Air Force Avionics Laboratory Air Force Systems Command Technical Library Wright-Patterson Air Force Base Dayton, Ohio 45433	1 copy
Lawrence Livermore Laboratory Attn: Dr. W. F. Krupke University of California P.O. Box 808 Livermore, California 94550	1 copy
Harry Diamond Laboratories Technical Library 2800 Powder Mill Road Adelphi, Maryland 20783	1 copy
Naval Air Development Center Attn: Technical Library Johnsville Warminster, Pennsylvania 18974	1 copy
Naval Weapons Center Technical Library (Code 753) China Lake, California 93555	1 copy
Naval Underwater Systems Center Technical Center New London, Connecticut 06320	1 copy
Commandant of the Marine Corps Scientific Advisor (Code RD-1) Washington, DC 20380	1 copy
Naval Ordnance Station Technical Library Indian Head, Maryland 20640	1 copy
Naval Postgraduate School Technical Library (Code 0212) Monterey, California 93940	1 copy
Naval Missile Center Technical Library (Code 5632.2) Point Mugu, California 93010	1 copy

Naval Ordnance Station Technical Library Louisville, Kentucky 40214	1 copy
Commanding Officer Naval Ocean Research & Development Activity Technical Library NSTL Station, Mississippi 39529	1 copy
Naval Explosive Ordnance Disposal Facility Technical Library Indian Head, Maryland 20640	1 copy
Naval Ocean Systems Center Technical Library San Diego, California 92152	1 copy
Naval Surface Weapons Center Technical Library Silver Spring, Maryland 20910	1 copy
Naval Ship Research and Development Center Central Library (Code L42 and L43) Bethesda, Maryland 20084	1 copy
Naval Avionics Facility Technical Library Indianapolis, Indiana 46218	1 copy